OAK RIDGE NATIONAL LABORATORY
operated by
UNION CARBIDE CORPORATION
NUCLEAR DIVISION
for the
U.S. ATOMIC ENERGY COMMISSION

ORNL - TM - 2204

ON THE FEASIBILITY OF POWER BY NUCLEAR FUSION

D. J. Rose

ORNL-TM-2204

Contract No. W-7405-eng-26

THERMONUCLEAR DIVISION

ON THE FEASIBILITY OF POWER BY NUCLEAR FUSION

D. J. Rose

MAY 1968

OAK RIDGE NATIONAL LABORATORY
Oak Ridge, Tennessee
operated by
UNION CARBIDE CORPORATION
for the
U. S. ATOMIC ENERGY COMMISSION

CONTENTS

ON THE FEASIBILITY OF POWER BY NUCLEAR FUSION

D. J. Rose

ABSTRACT

Power from nuclear fusion will be feasible if certain plasma physics and engineering problems can be solved simultaneously: Equilibrium plasma properties discussed here are the thermalization rates between ions, electrons, and fusion α-particles; fuel burnup fractions for given electron and ion temperatures, given injection or heating energies, and specified plasma environmental conditions. The effect of the presence of α-particles and of unequal particle temperatures on plasma pressure and reaction rate are calculated. Typical operating conditions for a variety of plasmas typical of open or closed magnetic confinement systems are shown. New solutions to outstanding engineering problems are indicated, viz: a cellular niobium vacuum wall, cooled with lithium or fused salt; a beryllium or BeO pebble-bed moderator, with added graphite; magnetic stress supports of titanium. Many subsidiary problems are discussed. It is shown that fusion systems with output in the order of 10,000 electric megawatts may be economically attractive; cost of the fusion system "core" lies between $10 and $20/kwe, depending upon circumstances. The desired operating parameters in an open-ended fusion system may be achieved if the plasma pressure is a substantial fraction of the magnetic pressure, but not otherwise, and the task will be difficult. Closed magnetic field configurations will be more attractive, provided stability and system size problems can be satisfactorily resolved. The relevance of these studies to present fusion research is indicated.

1. INTRODUCTION

1.1 Preamble and Plan of Work

Useful power obtained from nuclear fusion requires the solution of many problems. Important ones are, in no particular order:

(1) Plasma confinement and stability. This includes understanding of the weak turbulence or imperfect confinement liable to be found in a real device, plus practical understanding of how to prevent gross loss of confinement. It also includes knowledge of the effect of velocity anisotropies, plasma size, unequal electron and ion energy distributions, and other things. Thus we have described the usual field of fusion plasma physics.

(2) Moderation of 14 MeV neutrons and regeneration of tritium, with favorable breeding ratio (for a D-T fusion system).

(3) Practical development of more complex and less expensive magnetic confinement systems than have existed hitherto.

(4) Development of a vacuum wall for such a system, resistant to radiation damage over a useful economic life, permitting very high heat transfer (using cooling schemes compatible with the presence of large magnetic fields and permitting good tritium breeding).

(5) Development of plasma injection and pumping techniques adequate to the very large tasks to be set before us.

(6) Recovery of tritium safely and efficiently from the entire system.

(7) Doing all this to produce electric power cheaply enough to compete with other anticipated energy sources.

These are large tasks, and require some amplification before we are through. In the past, much attention has (rightly) been given to the physics of the problem, and very little to the economics.

To provide some basis for later judgment about fusion feasibility, and to set some practical tone to these studies, consider first the economic question in simple terms.

Whether the fusion system produces electricity direct at some overall capital cost $/kwe (dollars/kilowatt of electricity), or nuclear heat, that requires further conversion, at some lesser cost is of secondary importance. Most essential is that the system be at least competitive with breeder reactors by about the year 2000, which is the earliest date that any real fusion system would go into operation. Predicted power costs are in the range 3 mills/kwh, which is the interest charge on $150/kwe, at the industrial money rate 14%, and operation 7000 hr /yr. But the capital cost must be less than this, for operating and fuel costs have not been included.

By inclination, we limit this study to D-T systems that produce nuclear heat, believing little in the feasibility of direct conversion at very high efficiency. Cost of secondary heat exchangers, turbines, generators, and some other auxiliaries will not be considered because they are similar to those in conventional plants. Thus the study covers devices analogous to a breeder reactor core plus some of its auxiliaries. For such an equivalent core, cost should lie in the range $40 to $50/kwe, to compete.*

---

*Costs here and later are 1968 dollars.

At this stage, such costs are not firm, and are rough guidelines only. There are some advantages to fusion, whose economic value could be assessed in a study more comprehensive than this:

(1) Little radioactive contamination or waste disposal, more a nuisance than a substantial cost.

(2) The possibility of very short tritium doubling time -- perhaps one year. This problem is analogous to the doubling time problem for breeding fissionable material, where the shortest estimates are several years.

(3) As a corollary to (2), the possibility of a very plentiful neutron economy.

(4) Minimal hazards, and no continuing nuclear heat source when the device is shut down. This lowers costs, makes siting easier, and may reduce electric transmission costs.

System size will enter critically into our calculations. By the year 2000, 10^3 Mwe will be a modest plant, and 10^4 Mwe or larger will be reasonable, provided waste heat can be handled. These numbers are fortunate ones for fusion, because our examples will tend to show that fusion systems will be economically feasible only in very large sizes.

This study proceeds over several stages. First, comes a listing and summary of previous work, at the end of Chapter 1. Next, we work on the plasma problem, in several stages through Chapters 2 and 3, assuming pro tem that adequate plasma confinement can be achieved. Perhaps surprisingly, such basic things as the reaction parameter proper for use in a real fusion plasma must be calculated; this is the quantity too simply characterized as $\langle\sigma v\rangle/T^2$; the facts that electrons and ions

do not have the same temperature, and that the presence of He^4 affects the burning rate at constant β complicates the situation. After that, a simple approximate plasma theory is developed, which takes into account electron and/or ion injection (with or without energy), various electron radiation possibilities, and fractional fuel burnup desired. The theory then predicts such things as equilibrium electron and ion temperatures, radiation coming from the plasma, disposition of the He^4 fusion product energy, and so forth. All the questions must be answered in some self-consistent way, just so that we can choose reasonable plasma parameters when it comes time to calculate examples. It will turn out that the plasma conditions are not always those hitherto thought to be optimal.

The cost of a fusion system is the cost of the device needed to make the plasma and extract the energy. Thus with reasonable plasma conditions in mind, we turn to the system design. In Chapter 4 comes the magnetic field structure, surely the most speculative of all components. Nothing profound is developed about the topic; but some general rules known to the art and restated here permit a simple approximate cost formula to be derived. New ideas are presented about magnet structural support.

Next, in Chapter 5 comes a brief discussion about where the arts of vacuum wall design, fusion moderator design, etc., are headed. Here the continuing work of A. P. Fraas and D. Steiner of ORNL is presented in abstract. Detailed and realistic studies of a number of configurations are at this moment (April 1968) being analyzed by Fraas and Steiner, to whom go many thanks. Their initial work appears in Appendices III and IV.

Given the building blocks here described — magnet, vacuum wall, moderator, plus a neutron shield for the magnet, and perhaps a few smaller items, we can make a cost estimate for the core of the system, in the final chapter of this report. Along with the costs comes the actual system size, and we find that the cost $/kwe depends on size in ways that cannot be ignored. One important reason is that the vacuum region that holds the plasma is free; only the surrounding material costs money, and it tends to cost some amount per unit area. Thus up to various limits determined largely by thermal loading of the vacuum wall, we win the advantage by going to larger size.

The introduction of size in this way brings us back to the first of our problems: plasma confinement, because confinement time τ is a function of size. This is true in either open or closed magnetic systems; even in open ones, losses via fluctuations induced by gradients, etc., must be reduced to the order of or less than the Coulomb scattering loss; and in closed systems, the anomalous diffusion loss is expected to decrease with increasing size. Expectedly, the most desirable size is large; unexpectedly, the magnetic field strength (at least in the middle of the device) may not be very high. At least for closed magnetic systems, the confinement problem may not be as serious as some have imagined.

Many of the calculations to be done are relatively "model-free" in the sense that magnetic field costs some amount per meter^2 of vacuum wall; moderator and the vacuum wall itself can be similarly priced. Also, the general principles of electron-ion-He^4 thermalization, plasma heating, radiation, and so forth do not apply just to one type of device. Thus much is contained here applicable to closed or open systems, pulsed or

steady-state. Nevertheless, we must choose realistic examples. After all, who will build a closed magnetic system to opeate at an ion temperature of 80 keV if 15 keV, with its better reaction parameter, is possible? And who will build an open magnetic system at 15 keV, knowing that the ions cannot be contained? We are naturally led to consider both types, partly (but not altogether) separately. At this stage of our study, more specific examples of each type are not required, but the study itself will suggest some directions to go.

The systems will all be steady-state, not through firm conviction that pulsed systems are unfeasible, but through the firm conviction that introducing an additional important parameter — time — into all the considerations is beyond our immediate capability. Nevertheless, many of the analyses and methods to be given can be applied to pulsed systems, and surely cannot be ignored; on the other hand, we do not speculate here upon what else must be built into adequate models.

1.2. Summary of Work Hitherto

This section is an annotated bibliography on fusion feasibility. We recall the work of Spitzer et al.,[1] of the Danish Risö group[2,3] in 1958, and of Post and the Danish groups in 1960,[4] but choose to discuss things in a different and more specific way.

A number of studies can be identified as pertaining more to open-ended or closed confinement systems, and some are of general nature. Consider first open systems. In an early report,[5] Post takes up the main problem of injection, mirror loss, circulating power, and so forth, and considers in some detail the crucial and vexing problem of

obtaining a satisfactory power balance in any open-ended system. A second summary of the situation in 1962 is also given by Post.[6]

This scattering-out problem has received much specific attention, starting with unpublished work by Judd, MacDonald, and Rosenbluth (1955), who calculated end-loss using a Fokker-Planck formulation. Then came calculations by MacDonald, Rosenbluth, and Chuck,[7] and by Bing and Roberts[8] along the same line. At the same time, A. N. Kaufman in an unpublished report from UCRL pointed out that the plasma potential in a mirror device would be expected to run positive, because of preferential electron scattering-out. Thus the ion loss is enhanced because of acceleration into the loss cone, and the effective mirror ratio is more like the logarithm of the actual magnetic mirror ratio. These lugubrious matters have been considerably explored by BenDaniel.[9] BenDaniel and Allis,[10] and by Kelley[11] (who proposes that the enhanced loss might be eliminated), and quite recently in papers presented at a topical conference.[12] At that conference, B. McNamara confirms previous estimates of particle energies and loss rates made by Fowler and Rankin,[13] and calculates further the time development of potentials, particle energies, losses, etc., during the initial stages of non-steady magnetic mirror operation; he concludes, from an auxiliary and short feasibility calculation, that fusion power via open-ended confinement is a chancy business. Post and others have speculated on the energy cost of stabilizing the plasma against microinstabilities; others upon stopping mirror losses by using rf power, and such exotic things. In addition, Fowler and Rankin[13] make more estimates of circulating power, confirm that the important ratio

$$Q = \frac{\text{fusion power}}{\text{circulating power}}$$

scales only as $\log_{10} R$, and so forth.

Because of these difficulties, optimism about achieving an open-ended, low-β fusion system is not shared by all. For instance, Sivukhin[14] reviews the situation and concludes that the probability of success is very low. We do not take any such view ab initio. The plasma loss in any real system will be serious, may be fatal, but certainly the problem is not yet well enough analyzed.

Closed systems have been analyzed also, chiefly by Mills.[15-17] Here the problems have seemed more straightforward but really are not so simple. The problem here is plasma confinement in average min-B magnetic configurations. If — a very large if — adequate confinement is achieved, then the main problems seem to be the applied science and engineering ones. Mills, especially in reference 17, presents a number of basic and important ideas about confinement time, fuel burnup, costs, and over-all requirements.

Let us now turn to less model-oriented aspects of the problem. Valuable fusion and other cross sections are given by Wandel et al.;[18] they also give (as do Spitzer and others) plasma thermalization and relaxation formulas. The difficulty with these exponential integral formulations for relaxation rates is that we do not want them just as end results; rather, they appear as variable coefficients in yet more complex equations. Thus simpler approximations (adequate for present purposes) written by Rose and Clark[19] (hereafter R & C) will be used. Similar stratagems of approximation will be required to include synchrotron radiation, whose very magnitude is found as the summation over an infinite series of Bessel functions, the arguments of which pertain to a relativistic electron momentum distribution.

One of the first studies concerned with what we call the nuclear engineering aspects of proposed fusion reactors appears in Chapter 13 of R & C. Parts

of it will be used here, in places indicated. The first relatively comprehensive studies of the vacuum wall, moderating region, coil shield, tritium breeding ratio, and energy deposition were made by Impink,[20] Homeyer,[21] and Lontai[22] in three theses. Their work lies near enough to our interests to require a brief summary here. Figure 1.1 shows their general configuration, which is self-explanatory. The vacuum wall diameter was taken as 2 meters, the device was imagined to be a long cylinder, and length was unspecified. A 50-lethargy-group code was devised to calculate the fate of 14-MeV fusion neutrons incident upon the vacuum walls from the plasma. The code was written for plane, cylindrical, and spherical geometry, and several calculational schemes were used and checked one against the other. Relevant nuclear cross sections were calculated, when they did not appear in the literature.

Table 1.1 summarizes some of Impink's results, for tritium breeding and neutron leakage out of the moderator region. In all cases, the magnet shield (Fig. 1.1) was 56 cm thick, and consisted of 30 cm Pb-B-H_2O, 20 cm LiH, and 6 cm Pb. The first three columns of Table 1.1 describe the vacuum wall, wall coolant, and moderator analyzed. The first row is a "standard"; including the magnet shield, we see that the total blanket thickness of the "standard" configuration is 120 cm. For this, the breeding ratio T/n was 1.16. In subsequent rows, the effect of varying the parameters on T/n and leakage is seen. The principal difficulty with using a fused salt moderator is the presence of fluorine, which (a) has much inelastic scattering, thus preventing beneficial $Be^9(n,2n)2\alpha$ reactions, (b) generates copious gamma rays, which shine back upon the vacuum wall and give high unwanted heat deposition there. Note that: (1) increasing the fluorine relative

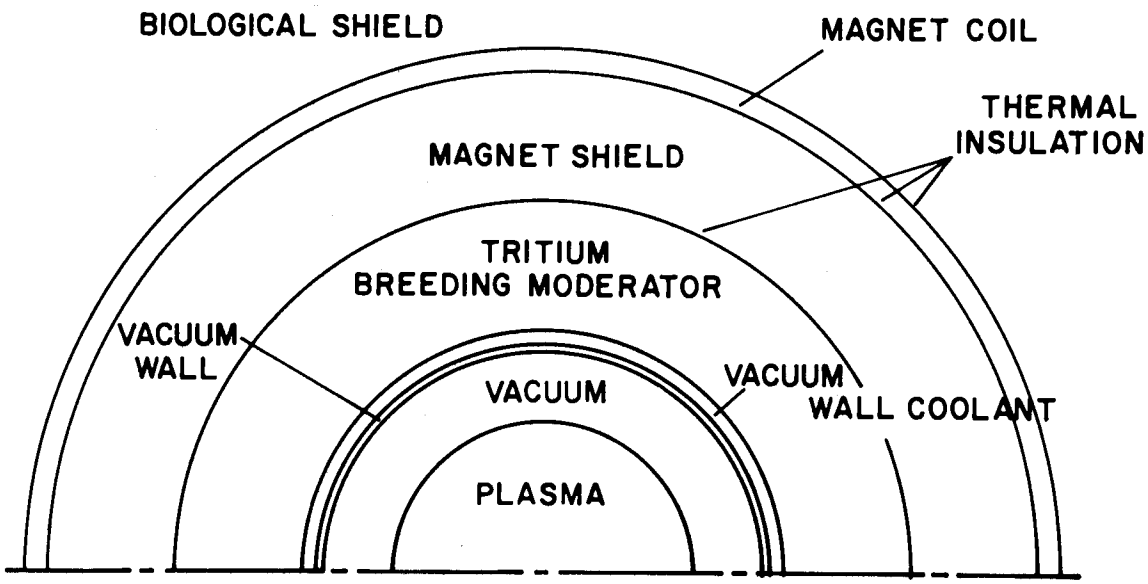

Fig. 1.1. Configuration of a Conceptual Steady-State D-T Fusion System.

Table 1.1

Tritium Breeding Calculations by Impink[20]

Vacuum Wall	Wall Coolant	Moderator	Tritium Neutron	Leakage
Mo 2 cm	Li_2 Be F_4 (Natural isotopic) 6.25 cm	75% Li_2 BeF_4 25% graphite 56 cm	1.17	0.042
0 cm Mo			1.07	0.052
1 cm Mo			1.14	0.047
3 cm Mo			1.16	0.041
1 cm Ni			1.00	0.045
	20% enr. Li^6	Natural	1.20	0.053
	50% enr. Li^6	50% enr. Li^6	1.22	0.027
	Li Be F_3	Li Be F_3	1.12	0.060
	Li NO_2	Li NO_2	0.82	0.11
8 cm Pb(!)	3.75 cm	36 cm only	1.45	0.19
		+5 cm Be	1.35	0.016
1 cm Ni		+10 cm Be	1.37	0.013
		+9 cm BeO	1.20	-

concentration decreases T/n; (2) the Mo (n,2n) reactions are useful up to the point where the neutron spectrum is seriously degraded by Mo collisions; (3) heavy metals with large (n,2n) cross sections are good to have, and can even overcome the disadvantageously high leakage from a thinner moderator; (4) Be is very useful, but BeO is much less useful, because of bad inelastic scattering from O at high energy; (5) both O and N have similar drawbacks; (6) enriching Li^6 decreases leakage, but may not be worth the cost.

Independent T/n calculations have been made by Bell[23] at Los Alamos. Where he and Impink calculate the same configuration, both obtain the same tritium yield within 1%. Thus there is confidence in both calculations. For Li-Be (no F) moderators, Bell calculates T/n = 1.5 - 1.9, depending upon circumstances, and T/n > 1.5 seems quite feasible.

The addition of U^{238} to the moderator, to breed plutonium, has been shown by Lontai to result in a power gain of about 2 via U^{238} fast fission and other direct mechanisms, in a fused salt moderator. This is interesting, but may not be worth the effort, in view of the complication of a large added fission product inventory. A more likely road to follow would be to add U^{238} (or thorium) to a very high T/n moderator, where much more fast fission might be coaxed from the system, and Pu (or U^{233}) made for burning in fission reactors. This fuel breeding may have small economic value, because the cost of fission fuel is low: it is the reactor that costs the money. If the bred material were burned <u>in situ</u>, things would be better; but again difficulties ensue: for example, the time to build up an equilibrium inventory of Pu^{239} or U^{233} may exceed the reactor lifetime. It seems clear that the idea of Cohen[24] to multiply the energy from a small fusion system by a factor $\sim$ 30 by surrounding the

plasma by pure uranium is a considerable over-optimism. Nevertheless, sufficient power amplification may be obtained to turn economically uninteresting systems into interesting ones; we will not consider further in this report the use of fissionable material, but recommend the topic to a later generation of workers.

Several chemical problems have received attention, in addition to work done by Homeyer.[21] Potentially serious is holdup of tritium in the moderator, and recovery of tritium from various surcharged components. Work has been done on this topic by Strehlow and Richardson,[25] and by Kirslis,[26] both at Oak Ridge National Laboratory. In summary, the problem appears serious, requires work, but should be solvable. Extracting tritium from LiT in Li has been considered by Johnson.[27]

Beyond all this, there are a number of specific feasibility studies. One made by Rose et al for the U.S.A.E.C. in 1963 was not published, but received substantial circulation. R & C, Homeyer, and Mills, already quoted, address themselves to the problem. An unpublished report[29] from the General Electric Company contains uncritical analyses, which are used to show that fusion is unfeasible. The recent report by Carruthers, Davenport, and Mitchell[30] includes costs of major components (wall, moderator, magnet, pumps, etc.), chooses the configuration given by Homeyer, and adduces favorable over-all costs vis-a-vis breeders. This last conclusion of Carruthers et al., seems to depend upon achieving confinement attainable only in a torus; in addition, the capital cost of their system is higher and money interest rate lower (8%) than United States custom would have it.

There are few feasibility estimates that pertain to pulsed systems. The principal one to date is by Ribe et al.[31] who consider a small (20 cm

diameter) highly stressed θ-pinch, in a Cu-Be or Cu-Zr coil, with Li-Be moderator outside. Another unpublished thesis by Dunn[32] analyzes (and shows feasible) a large slow-pulsed system, somewhat resembling a pulsed version of the one shown in Fig. 1.1.

Several related topics require brief comment. For any steady-state fusion system, superconducting magnets appear mandatory. Originally seen as a fusion-related problem, superconducting magnet science and technology are developing satisfactorily on their own. Radiation damage of the vacuum wall of a fusion device by 14-MeV neutrons is a subject of serious speculation, very little is known, and the required total flux 10^{22} - 10^{23} NVT of 14-MeV neutrons cannot at present be found by any scheme. The vacuum pump problem of a fusion reactor will require some novel solution.

Thus ends this account of the present state of the art.

2. FUSION REACTION PARAMETERS

2.1. Alpha Pressure Neglected

The fusion rate for a 50% D - 50% T plasma is

$$R = n_D n_T \langle\sigma v\rangle = n_i^2 \langle\sigma v\rangle/4 \qquad (2.1)$$

where $n_i = n_D + n_T$ is the useful ion density. The values of $\langle\sigma v\rangle$ used in this report, taken from Mills[15] and other sources, are listed in the middle column of Table 2.1. Also shown are those quoted by Sivukhin;[14] ours are slightly lower at low T_i, but our peak at 70-80 keV is higher. The difference is small. Lack of complete ion thermalization probably affects $\langle\sigma v\rangle$ more than this, and furthermore in the direction of shifting Sivukhin's results (if they be more accurate for a Maxwellian distribution) in the direction of ours.

Reaction rates will be used in connection with the relative plasma pressure β, where*

$$\beta = \Sigma nkT/(B^2/2\mu_o) \quad . \qquad (2.2)$$

Thus for $n_e = n_i$, $T_e = T_i$,

$$n_i = \beta B^2/4\mu_o kT_i \quad , \qquad (2.3)$$

and the reaction rate is

$$R = \frac{\beta^2 B^4}{64\mu_o^2} \frac{\langle\sigma v\rangle}{(kT_i)^2} \quad . \qquad (2.4)$$

*MKS units, with frequent conversion of particle energy to keV, will be used throughout.

Table 2.1. Values of Fusion Reaction Rate $\langle \sigma v \rangle$

Ion Temperature (keV)	This Report $m^3/sec \times 10^{22}$	Sivukhin $m^3/sec \times 10^{22}$
10	1.08	-
12	1.64	-
14	2.27	-
16	2.94	-
18	3.60	-
20	4.22	4.54
25	5.71	-
30	6.75	6.72
35	7.65	-
40	8.15	7.92
45	8.60	-
50	9.00	8.27
60	9.40	8.48
70	9.55	8.54
80	9.60	8.54
90	9.40	8.45
100	8.80	8.36

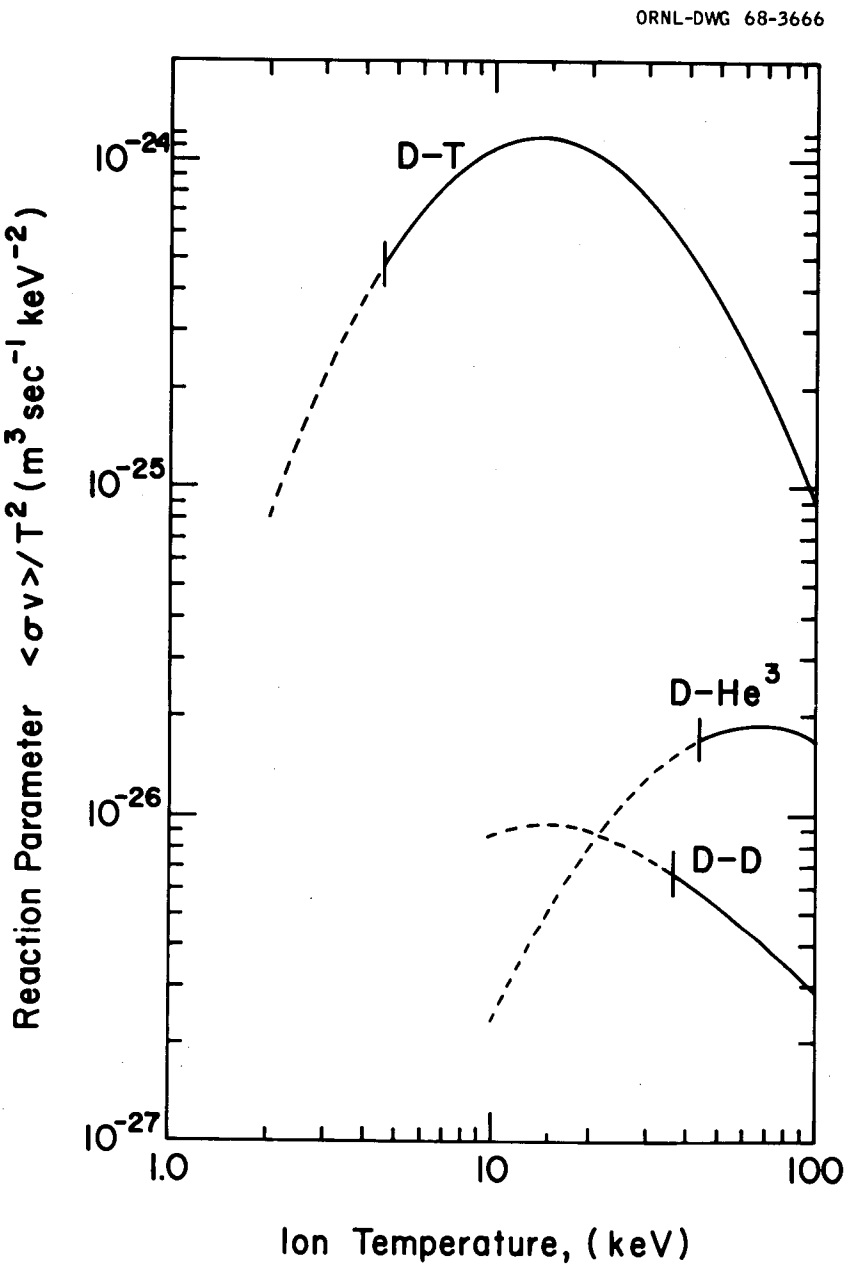

Fig. 2.1. The Reaction Parameter $\langle\sigma v\rangle/T^2$ for Nuclear Fusion Variations of Interest.

This reaction parameter $\langle\sigma v\rangle/T_i^2$ is the usual quantity appearing in the literature, and is plotted in Fig. 2.1. Similar parameters $\langle\sigma v\rangle/T_i^2$ for D-D and D-He^3 reactions are also shown; the D-D reactor is not analyzed quantitatively in this report. A fusion reactor must operate at a temperature high enough that fusion power exceeds bremsstrahlung loss — i.e., on the solid portion of each curve.

Our interest lies in more complicated cases. First, if $T_e \neq T_i$, but the alpha particle pressure p_α is zero, the plasma pressure is $n_i(kT_i + kT_e)$, whence the more general version of Eq. (2.4) is

$$R = \frac{\beta^2 B^4}{64 \mu_o^2} \left\{ \frac{4 \langle\sigma v(T_i)\rangle}{(kT_i + kT_e)^2} \right\} \quad . \tag{2.5}$$

The factor 4 is retained in the reaction parameter to agree with previous custom when $T_e = T_i$. The quantity is shown in Fig. 2.2, for the D-T reaction, for various values of T_e. Note that for any specified electron temperature $T_e > 0$, the "ideal" ion temperature T_i of maximum reaction rate always lies above the value ~ 14 keV determined by the criterion $\langle\sigma v\rangle/T_i^2 = \text{maximum}$. Note also that the penalty of high ion temperature is not so severe if T_e is kept lower.

These remarks are germaine to what will come later. To be sure, we will find that large temperature differences between electrons and ions cannot easily be maintained, because of electron-ion, electron-alpha, and ion-alpha thermalization. But that is no reason to limit the parametric discussion at present; we wish to explore trends. For example in an open-ended system T_e might be reduced by the existence of an added electron

ORNL-DWG 68-3672

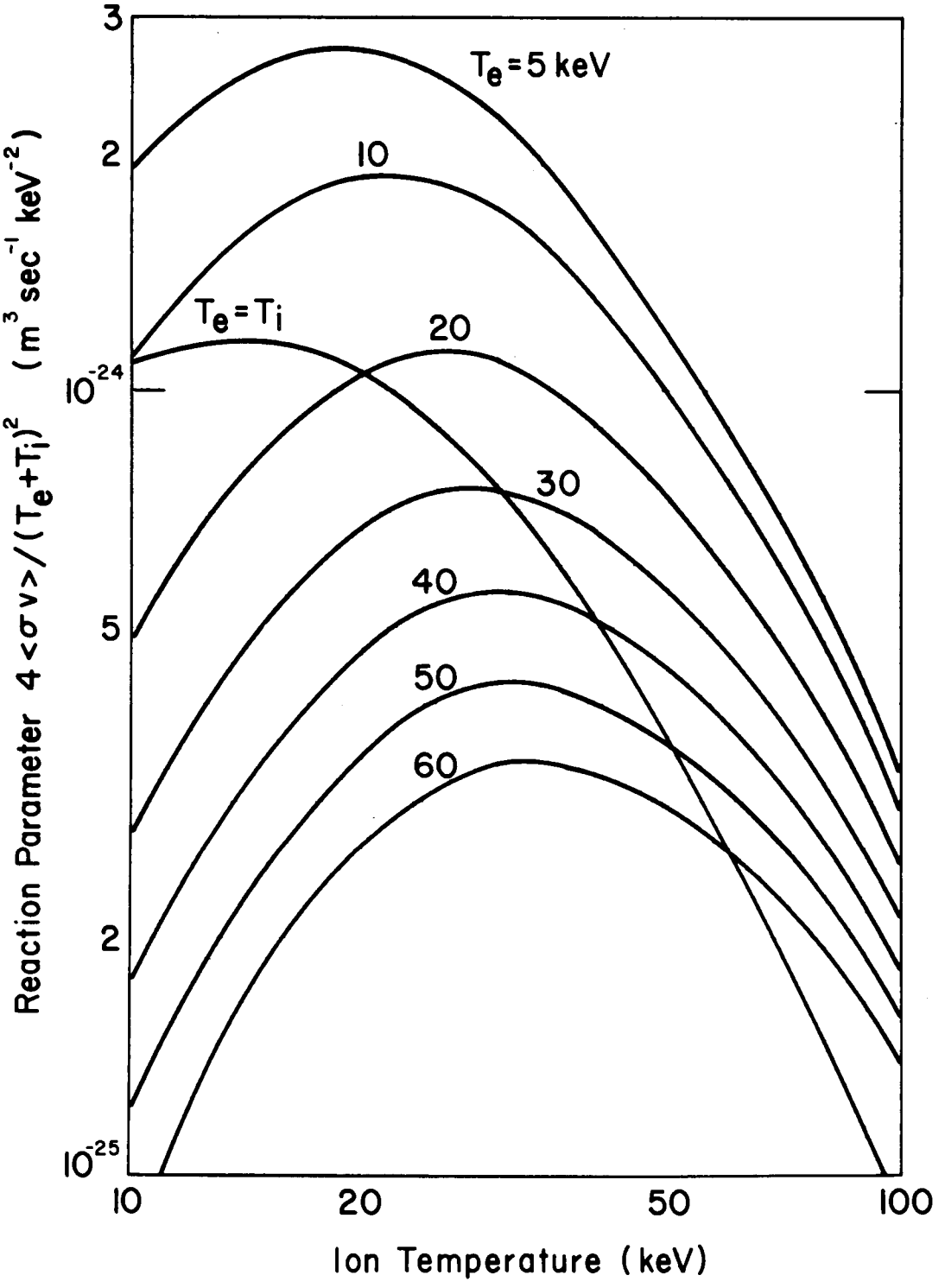

Fig. 2.2. Effective Reaction Parameter for Unequal Electron and Ion Temperatures, but no α-Particles.

throughput; four things happen:

(a) The burning rate increases at constant β.

(b) The bremsstrahlung plus synchrotron radiation heat load on the vacuum wall (which tends to limit the system power density) is reduced.

(c) The α-particle pressure is also reduced, thus preventing degradation of reaction rate at constant β — an effect we notice in the next section.

(d) The ion temperature is reduced, or additional ion heat must be supplied — a serious disadvantage, as will be seen in Chap. 3.

In a closed system, it may be possible to cool electrons selectively, e.g., by adding impurities; but any large additional electron throughput hardly seems possible. If no precautions are taken and confinement time is long, T_e might rise very considerably. The experience of the many calculations to follow shows that T_e does not rise above (say) 50-60 keV, under any reasonable circumstances because it is limited by synchrotron radiation. For example, if T_e = 50 keV, we see from Fig. 2.2 that the reaction parameter is a maximum at $T_i \sim 30$ keV.

2.2. Reaction Parameters, Including Alpha Pressure

The presence of He^4 in the plasma changes matters substantially. There is an unwanted pressure of α-particles, p_α, and also a heating of both electrons and ions. This latter effect can be either beneficial or deleterious, depending on circumstances. We require for this section the relative pressure p_α/p_i, and density n_α/n_i. In Chap. 3, the fate of the α's is determined, and we could (and most logically should) compute the quantities from those calculations. In fact a prior formulation appearing

in R & C, Section 13.4 was used. The result should be the same, but no detailed consistency check has been made.

Consider first the effect of the pressure p_α. The fusion rate is still given by Eq. (1.1) but the pressure balance now is

$$(n_i + 2n_\alpha)kT_e + n_i kT_i + p_\alpha = \beta B^2/2\mu_o \quad . \tag{2.6}$$

Setting $p_\alpha = p_i(p_\alpha/p_i)$ and $n_\alpha = n_i(n_\alpha/n_i)$ allows us to write a reaction rate equivalent to Eq. (2.4) or (2.5), which is

$$R = \frac{n_i^2 \langle \sigma v \rangle}{4}$$

$$= \frac{\beta^2 B^4}{64\mu_o^2} \frac{4\langle \sigma v(T_i)\rangle}{\left[kT_i\left(1 + \frac{p_\alpha}{p_i}\right) + kT_e\left(1 + \frac{2n_\alpha}{n_i}\right)\right]^2} \tag{2.7}$$

$$= \frac{\beta^2 B^4}{64\mu_o^2} P \quad . \tag{2.8}$$

This parameter P is the one of ultimate importance. The ratios p_α/p_i and n_α/n_i are chiefly functions of T_i and T_e, and are insensitive to circumstances of plasma confinement. The reason is that in cases of interest, the α's thermalize before escaping from the plasma: thus while slowing down and contributing appreciably to Eq. (2.7), they think they are in an infinite medium. Figure 2.3 shows the parameter P plotted vs T_i for various electron temperatures. Two curves from Fig. 2.2 are shown in comparison. Some presumably valid approximations have been made in calculating p_α and n_α (see R & C). The T_e = 10 and 15 keV contours have been inferred, using calculations for T_e = 20 keV,

and the fact that $p \sim 0$ as $T_e \rightarrow 0$ (the α's – and the ions too, unfortunately) lose energy promptly on cold electrons.

Note the inclusion of finite p_α reduces P, particularly where it is high: the reaction P produced p_α in the first place. Note also the peculiar effect of p_α in reducing T_i for maximum P, in the range below 40 keV. This is because increasing T_i to increase $\langle\sigma v\rangle$ now brings an additional penalty in p_α. Coincidentally, we can still find $P \approx 1.1 \times 10^{-24}$ m^2 sec^{-1} keV^{-2} corresponding to the maximum of Fig. 2.1 but now at $T_i \sim 20$ keV, $T_e \sim 15$ keV.

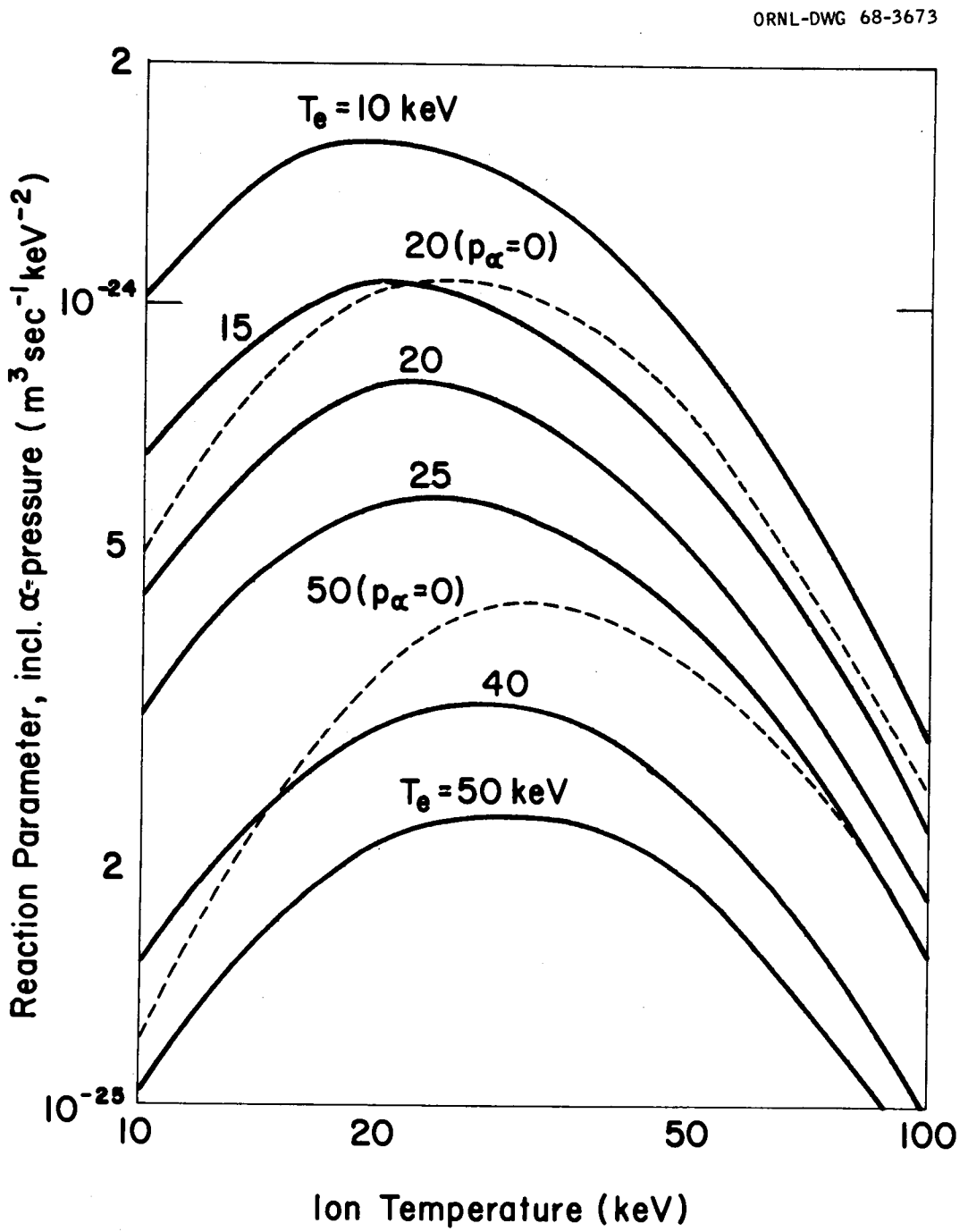

Fig. 2.3. Effective Reaction Parameter for Unequal Electron and Ion Temperatures, Including the Effect of α-Particles.

3. PLASMA THERMAL BALANCE

3.1. General Scheme

Much of the work in this chapter is similar to that in Chapter 13 of R & C.

Figure 3.1 shows a block diagram of the energy balance. Ions and electrons are injected with power w_{si} and w_{se} per unit volume respectively. This may be actual injection energy or heating in situ; the calculation cannot distinguish. Complete plasma heating of the injected fuel comes by setting $w_{si,e} = 0$.

The D + T ions are characterized by density n_i, energy U_i, corresponding temperature T_i, and confinement time τ_i; this latter is time against escape, and does not include losses via fusion. In escaping, they carry off power w_{Li} per unit volume. Ions are heated by fusion α-particles, and may be heated or cooled by electrons, depending on whether $T_e > T_i$ or not. We assume where necessary that the ion energy distribution is Maxwellian.

The electrons are similarly described, with $n_e = n_i \equiv n$, but (possibly) a confinement time τ_e different from τ_i. They are heated by the α's, and radiate bremsstrahlung w_x and synchrotron radiation w_c.

Turning now to the α-particles, born at energy $U_o = 3500$ keV, we set the density approximately zero, and have taken their pressure into account in developing the modified reaction parameter (in the previous chapter). The energy distribution $f(U_\alpha)$ is not Maxwellian; the quantities of main interest are the part $U_{\alpha e}$ of U_o delivered to electrons, the part $U_{\alpha i}$ to ions, and remaining in the α's as they escape. The α confinement time is set equal to τ_i, for convenience, although this may not really be so.

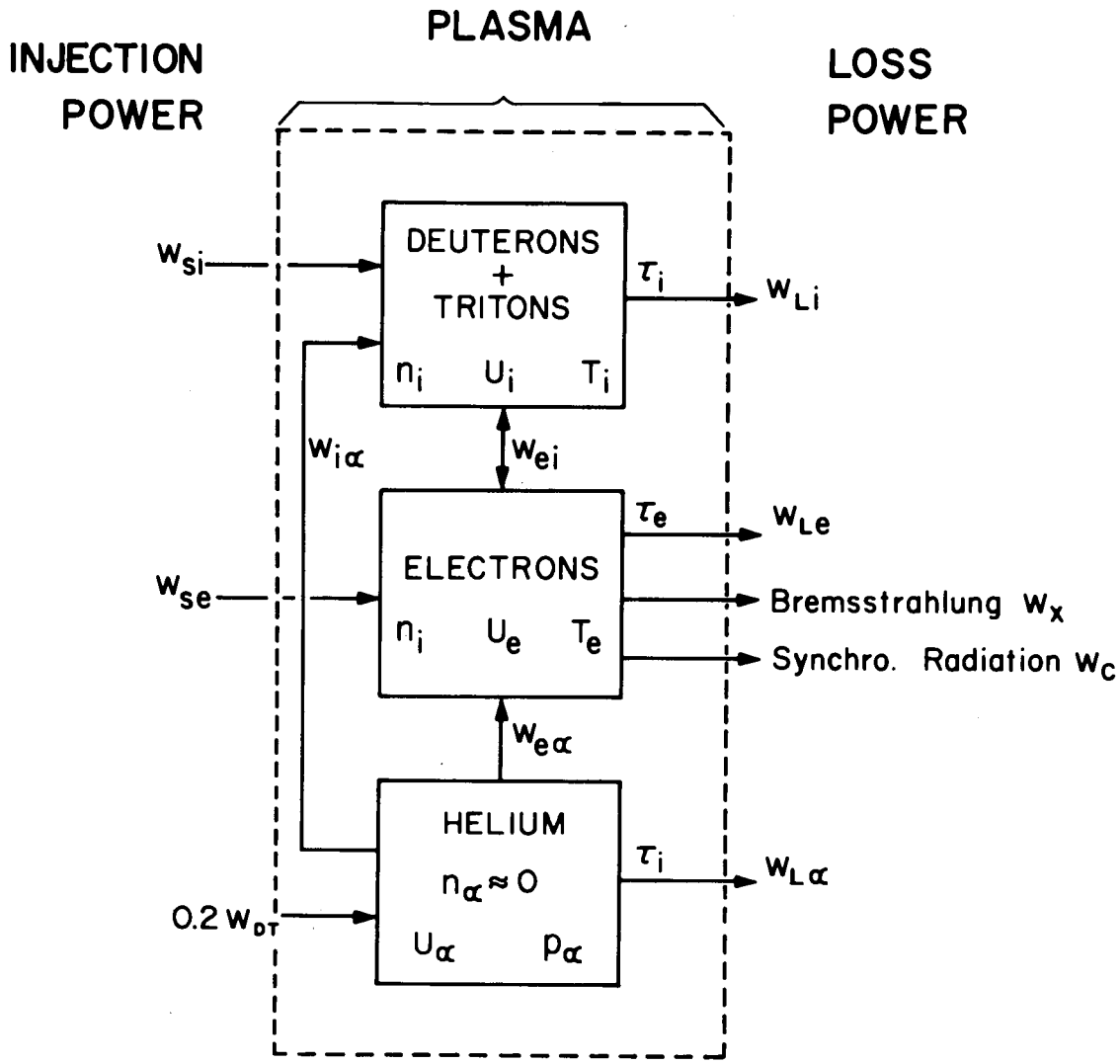

Fig. 3.1. Energy Flow Diagram for a D-T Fusion Plasma.

The solution of this problem in steady state requires that many approximations be used. For example, the exact forms of $w_{e\alpha}$, w_{ei}, etc., involve functions of exponential integrals, in which T_e, T_i and the densities appear in complex ways. The synchrotron radiation intensity is determined as a summation over a set of Bessel functions describing radiation at specific harmonics of ω_{ce}. All this must be simplified.

Even worse perhaps, the electron energy distribution may not be Maxwellian in small but critical ways. For instance, the slowing down of α's on electrons depends upon there being present the expected number of electrons with speed less than the α-speed — that is, less than 500 eV for α's of 3.5 MeV. Similarly for ion-electron thermalization, the principal interaction of 20 keV deuterons is with 5 eV electrons. Suppose the population is depleted or enhanced? We point out from time to time where much of the following analysis can be changed by such seemingly small things.

3.2. α-Energy Deposition

As a first step, helpful to what comes later, we work out how an α-particle slows down in the plasma, and divides its energy between strictly Maxwellian electrons and ions whose energy distribution is not important. A tractable expression for the rate of change of α-particle energy, U_α, is given by Eq. (13.28) of R & C, accurate enough for present needs. It is

$$\frac{dU_\alpha}{dt} = - \frac{Z_\alpha^2 e^4 n_i m_e^{1/2} \ell n\Lambda \, U_\alpha}{3\pi(2\pi)^{1/2} \epsilon_o^2 m_\alpha (kT_e)^{3/2}} \left[1 + \frac{3\sqrt{\pi} \, (m_\alpha kT_e)^{3/2}}{4 m_r m_e^{1/2} U_\alpha^{3/2}} \right] \tag{3.1a}$$

$$= - \frac{2.5 \, U_\alpha}{\tau_s} \left[1 + \gamma \left(\frac{U_o}{U_\alpha} \right)^{3/2} \right] \tag{3.1b}$$

$$= - \frac{2 \times 10^{-18} \, U_\alpha n_i}{T_e^{3/2}} \left[1 + 296 \left(\frac{T_e}{U_\alpha} \right)^{3/2} \right] . \tag{3.1c}$$

Here we have implicitly defined the quantities

$$\gamma = 0.00143\ T_e^{3/2} \quad , \tag{3.2}$$

$$n_i \tau_s = 1.25 \times 10^{18}\ T_e^{3/2} \quad . \tag{3.3}$$

Equations (3.1) start a custom to be followed here: expressing equations in physical symbols and/or in units for later calculation (T, U = keV, others MKS unless otherwise specified). The meaning of the quantities is as follows. m_r is α-ion reduced mass in Eq. (3.1a); the first term in the bracket represents loss to electrons, and the second is loss to ions. The characteristic time τ_s is the slowing down time for the (singly charged) ions, whose atomic weight is set equal to 2.5. Slowing down time for α's is $Z_\alpha^2\, m_i/m_\alpha = 2.5$ times as fast. In all numerical calculations, take $\ell n\Lambda = 20$.

Equation (3.1b) can be solved to yield

$$U_\alpha = U_o\ [(\gamma + 1)e^{-x} - \gamma]^{2/3} \tag{3.4}$$

where

$$x = \frac{15t}{4\tau_s} \quad . \tag{3.5}$$

The quantity x represents α-particle lifetime in the plasma.

By integrating appropriate parts of Eq. (3.1), using Eq. (3.4) for U_α, we can easily find the energy $U_{\alpha e}$ per α-particle going to the electrons:

$$\frac{U_{\alpha e}}{U_o} = \frac{2}{3}\int_o^\theta [(\gamma + 1)e^{-x} - \gamma]^{2/3}\, dx \quad . \tag{3.6}$$

We must be careful of the upper limit θ, which is

$$\theta = \text{lesser of} \left\{ \begin{array}{l} \phi_s = 15\tau_i/4\tau_s = 3 \times 10^{-18}\, n_i\tau_i/T_e^{3/2} \\ \phi = \ell n\, \dfrac{\gamma + 1}{\gamma} \end{array} \right\} \qquad (3.7)$$

The logarithmic upper limit represents the time at which U = 0 (the integral of Eq. (3.4) is zero), at which time the α's must disappear. However, if they are not confined so long, their true confinement time τ_i should be used. Eq. (3.5) is correct if $15\tau_i/4\tau_s \gg 1$, for the α's thermalize well before escaping; fortunately this circumstance obtains in many of our calculations. It is not quite correct otherwise; for we have, in effect, replaced a distribution function $f(U_\alpha)$ that runs from U_o to zero with continuous particle losses by a simple slowing-down function that has sudden disappearance at some lifetime and corresponding energy. Our error in that case underestimates slightly the ion heating, which becomes dominant at low U_α.

The fraction of U_o going to the ions is

$$\frac{U_{\alpha i}}{U_o} = \frac{2}{3}\int_o^\theta \frac{\gamma dx}{[(\gamma + 1)e^{-x} - \gamma]^{1/3}} \quad . \qquad (3.8)$$

The quantity $U_{\alpha e}/U_o$ is unity for $T_e \to 0$ and zero for $T_e \to \infty$. Figure 3.2 shows the relative disposition of energy, in case the α's thermalize completely; for $T_e < 33$ keV, the energy goes predominantly to electrons; and for $T_e > 33$ keV, to ions.

As said before, these results depend upon the presence of the proper low-energy part of the electron distribution. Enhancing the low-energy part would be similar to lowering T_e. Whether that is possible, in the

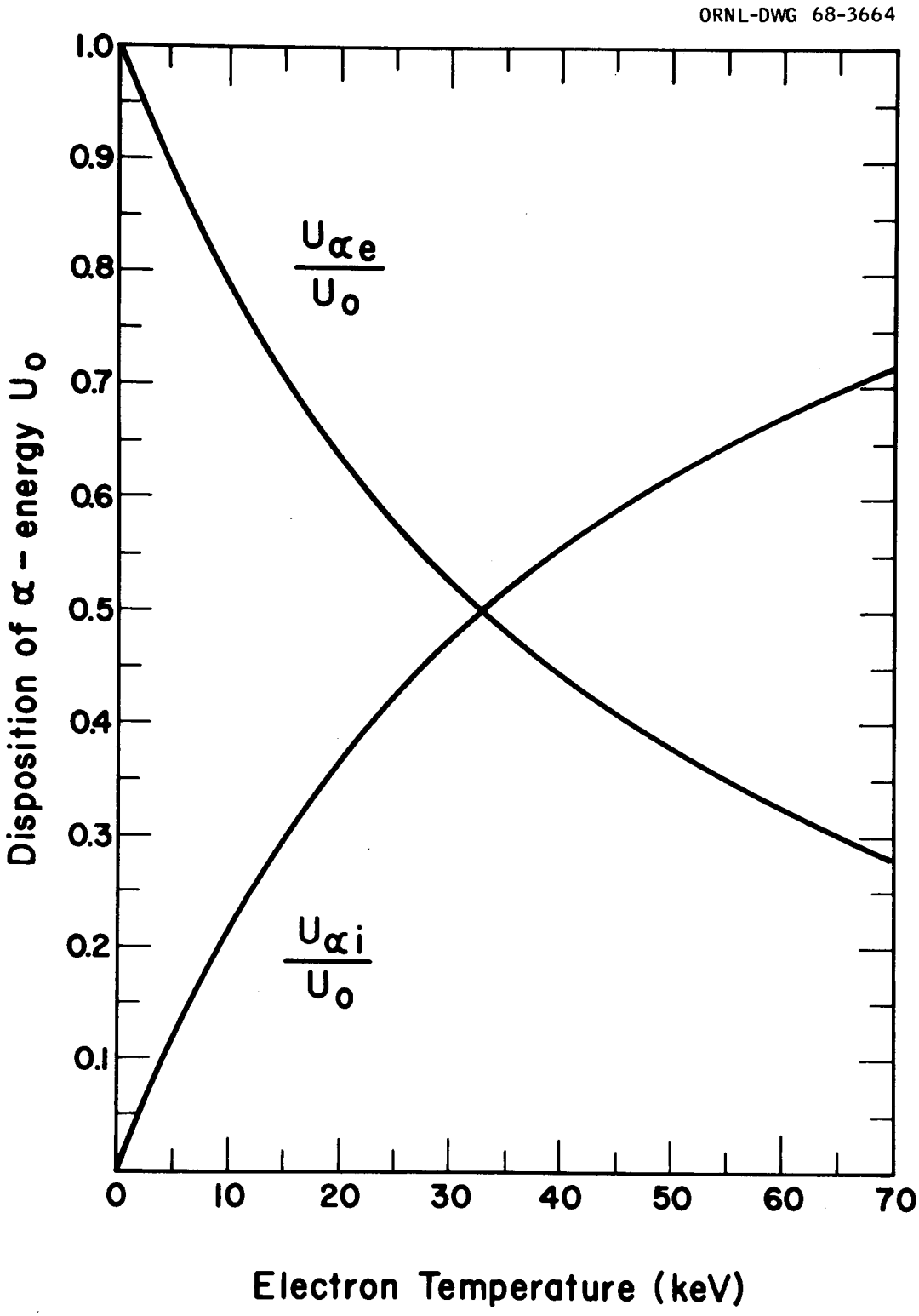

Fig. 3.2. Fraction of α-Particle Energy Given to Electrons ($U_{\alpha e}/U_o$) and to D-T Ions ($U_{\alpha i}/U_o$) vs Electron Temperature, if the α's are Fully Thermalized.

face of rapid electron-electron thermalization, has not been checked for the examples to be shown later. More likely is some depletion of the low energy electron population, by the α-heating itself. That reduces the α-electron energy transfer rate, hence increases the over-all α slowing down time. If the new slowing down time is still less than the confinement time, then [by Eq. (3.1)] a larger fraction of U_α appears in $U_{\alpha i}$; in general, that is beneficial. However, once the α slowing down time reaches the confinement time, the benefit stops; in fact, because $U_{\alpha i}$ receives its main contribution from lower energy α's, extending the α slowing down time beyond the confinement time generally reduces $U_{\alpha i}$ sharply. Thus we see the possibility (not to be worked out here) of adjusting conditions to have maximum $U_{\alpha i}$, by controlling the electron velocity distribution in detail.

3.3. Ion-Electron Thermalization

The ions at temperature T_i thermalize on electrons at the rate

$$\frac{dT_i}{dt} = -\frac{T_i}{\tau_s}\left(1 - \frac{T_e}{T_i}\right) \tag{3.9a}$$

$$= -\frac{8 \times 10^{-19}\, n_e T_i}{T_e^{3/2}}\left(1 - \frac{T_e}{T_i}\right) \tag{3.9b}$$

from R & C, Chap. 8 or 13. If $T_e > T_i$, ions gain energy. The same caveat applies here as for α-thermalization. A modest low energy electron deficiency will reduce the thermalization rate, for instance. This matter will be brought up again in Sec. 3.8, on open-ended systems.

3.4. Electron Radiative Loss

The normal electron bremsstrahlung loss is simple

$$w_x = 4.8 \times 10^{-37}\, n_i^2\, T_e^{1/2} \text{ watt/m}^3 \tag{3.10}$$

from Eq. (11.17) of R & C. In keV, this is

$$\frac{dT_e}{dt} = 2.0 \times 10^{-21}\, n_i T_e^{1/2} \quad . \tag{3.11}$$

In later sections, this bremsstrahlung rate will be modified (by adding heavy ions?) to alter plasma conditions beneficially.

The synchrotron radiation w_c is not so simple. From R & C, the energy loss rate per electron is

$$\frac{dT_e}{dt} = 0.26\, B^2\, T_e\left(1 + \frac{T_e}{204} \ \ldots\right) K_{\mathscr{L}} \tag{3.12}$$

if none of the radiation is reflected at the vacuum walls. Here, $K_{\mathscr{L}}$ is a complicated plasma transparency coefficient, being a function of T_e and of the mysterious quantity

$$\mathscr{L} = L\omega_p^2/c\omega_{ce} = cL\,\beta B\sqrt{\frac{k(T_e + T_i)}{e}} \quad . \tag{3.13}$$

Here, L is plasma size for an equivalent slab, perhaps equal to the radius for cylindrical geometry; β is here strictly speaking the ratio of plasma pressure to magnetic pressure, neglecting α's. But we ignore such fine distinctions here as required.

In general, 20 keV $< T_e <$ 50 keV, $10^3 < \mathscr{L} < 10^5$ for our plasmas, and we search for a simple approximation. A good one is

$$K_{\mathscr{L}} = 2.1 \times 10^{-3}\, T_e^{7/4}/\mathscr{L}^{1/2} \tag{3.14}$$

for T_e in keV. Figure 3.3 shows the quantity $K_{\mathscr{L}}$ vs T_e and $\mathscr{L}$ as given by

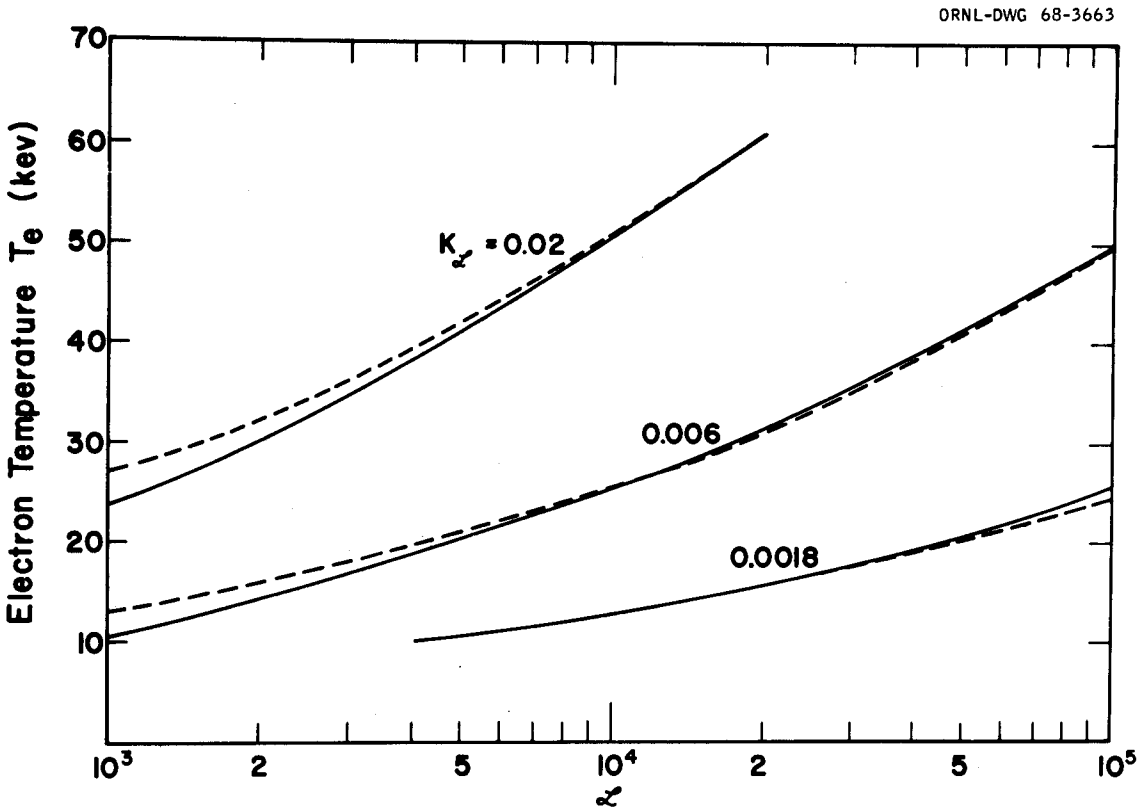

Fig. 3.3. Contours of Parameter $K_{\mathscr{L}}$, Used in Synchrotron Radiation Calculations (Solid Line) and the Analytic Approximation $K_{\mathscr{L}} = 2.1 \times 10^{-3} T_e^{7/4}/\mathscr{L}^{1/2}$ (Dashed).

R & C (the solid curve); and Eq. (3.14) (dashed). The approximation is much better than the applicability of the theory. It is the resulting approximate T_e^4 behavior in Eq. (3.12) that strongly inhibits T_e from rising.

The synchrotron radiation is partly reflected at the electrically conducting vacuum wall. This does not reduce w_c correspondingly, for T_e then rises until a new energy balance (with a new and higher frequency synchrotron spectrum) obtains. The matter is complicated, and discussed in R & C, Chap. 11. A reasonable procedure is to multiply the power loss calculated in Eq. (3.12) by a coefficient $C_2 < 1$. For a reflectivity Γ, we should choose

$$(1 - \Gamma) < C_2 < 1 \tag{3.15}$$

and will make in subsequent calculations various aesthetically pleasing choices.

The question arises whether, as $\beta \to 1$, the entire synchrotron radiation subsides, to be replaced by the much weaker radiation from the surface as electrons are reflected from the plasma magnetic sheath. Burkhardt[33] analyzes electron orbits at the boundary, shows that indeed a considerable reduction takes place, and that the power radiated per unit area is

$$S_c = 9.7 \times 10^{-32}\ n^{3/2}\ T_e^2\ \text{watt/m}^2 \tag{3.16}$$

in our units. The surface radiation represented by Eq. (3.16) is truly negligible in all our applications. On the other hand, achieving β close enough to unity to satisfy Burkhardt's analytic needs seems very improbable. All we can say at present is that synchrotron radiation from finite-β plasmas will be less per electron in the plasma, and we can adjust the parameter C_2 at will.

3.5. The Thermal Balance Equations

Developments of the previous sections, plus use of some adjustable parameters with physical meaning, permit our writing fairly simple energy balance equations for T_e and T_i.

Start with the particle balance for ions:

$$\frac{dn_i}{dt} = 0 = S_i - \frac{n_i^2\langle\sigma v\rangle}{2} - \frac{n_i}{\tau_i} \quad . \tag{3.17}$$

The source is S_i, two ions are lost (i.e., not $n_i^2\langle\sigma v\rangle/4$) per fusion, and the lifetime against geometric escape is τ_i. The fractional burnup is

$$f_b = \frac{S_i - L_i}{S_i} = \left[1 + \frac{2}{n\tau_i\langle\sigma v\rangle}\right]^{-1} \quad ; \tag{3.18}$$

here, and in what follows, $n_i \equiv n$. As in the Lawson criterion, of which this work is an enlargement, products $n\tau$ enter often, and we set

$$n\tau_i,\ n\tau_e,\ n\tau_s = h_i,\ h_e,\ h_s,\ \text{etc.} \tag{3.19}$$

Bearing in mind that total energy content per unit volume is $3n_i kT_i/2$ for the ions, we now write

$$\begin{aligned} d(3n_iT_i/2)/dt &= 0 \\ &= w_{i\alpha} + w_{Si} - w_{Li} - w_{ei} \\ &= \frac{n^2\langle\sigma v(T_i)\rangle\, U_{\alpha i}(h_i,T_e)}{4} + \left[\frac{n}{\tau_i} + \frac{n^2\langle\sigma v\rangle}{2}\right] V_i \\ &\quad - \frac{3T_i}{2}\left[\frac{n}{\tau_i} + \frac{n^2\langle\sigma v\rangle}{2}\right] - \frac{1.2 \times 10^{-18}\, n^2 T_i}{T_e^{3/2}}\left(1 - \frac{T_e}{T_i}\right) \quad . \end{aligned} \tag{3.20}$$

The first term on the RHS is α-energy given to ions, and the T_i, T_e, and h_i dependences are shown. The second term represents all the ion input

to the system, with an ion injection energy V_i. The third is all the ion loss (by geometric escape or by fusion) with energy $3T_i/2$ assigned; we neglect the reappearance of any part of T_i in the fusion products. The fourth term is from Eq. (3.9b). This equation can be put in the form

$$\langle\sigma v\rangle [U_{\alpha i} + 2V_i - 3T_i] - [6T_i - 4V_i]/h_i$$

$$- \frac{4.8 \times 10^{-18} T_i}{T_e^{3/2}} \left[1 - \frac{T_e}{T_i}\right] = 0 \quad . \tag{3.21}$$

For electron balance, collect Eqs. (3.6), (3.9b), (3.11), (3.12), (3.14), put in parameters to be described below, and find

$$\langle\sigma v\rangle [U_{\alpha e} + 2V_e - 3T_e] - [6T_e - 4V_e]/h_e$$

$$+ \frac{4.8 \times 10^{-18} T_i}{T_e^{3/2}} \left[1 - \frac{T_e}{T_i}\right] - 1.2 \times 10^{-20} C_1 T_e^{1/2}$$

$$- 2.41 \times 10^{-27} C_2 T_e^{11/4} (T_e + T_i)^{3/2} \left(1 + \frac{T_e}{204}\right)/D = 0 \quad . \tag{3.22}$$

Here, electrons are injected with energy V_e keV, two electrons with energy $3T_e/2$ are lost with each escaping α-particle, and electrons might additionally flow through or be better confined in the system with their own confinement time h_e. The third term is electron energy gain from electron-ion thermalization, and the fourth has the parameter C_1 for exploring the effect of changing bremsstrahlung. The last term is synchrotron radiation; recall that $C_2 < 1$ represents the effect of wall reflectivity and other things; the dimensional parameter

$$D = \beta^{3/2} (LB)^{1/2} (\text{weber/m})^{1/2} \tag{3.23}$$

appears from the manipulations at the end of Sec. 3.4. Unfortunately, the synchrotron radiation does not scale only with T_e, T_i, and the $n\tau$ products.

The two equations (3.21) and (3.22), with their constituent definitions, in principle together determine T_e and T_i self-consistently if the following quantities are specified ab initio:

Input ion and electron energies

Fractional burnup

Ratio of ion to electron confinement times h_i/h_e

Bremsstrahlung adjustment C_1

Synchrotron radiation reflection adjustment C_2

Size parameter D

In fact, the equations must be solved differently. It is easiest to substitute Eq. (3.21) into (3.22) to obtain

$$0 = \langle\sigma v\rangle \left[U_{\alpha e} + 2V_e - 3T_e\right]$$

$$- J\left(\frac{3T_e - 2V_e}{3T_i - 2V_i}\right)\left[\langle\sigma v\rangle(U_{\alpha i} + 2V_i - 3T_i) - K\right]$$

$$+ K - (WX) - (WC) \quad , \tag{3.24}$$

where

$$J = h_i/h_e \quad . \tag{3.25}$$

The quantities K (positive if $T_e < T_i$), (WX) and (WC) (both positive) are the last three terms of Eq. (3.22). The notation arises from that of Appendix I.

If the α's thermalize completely, i.e., $\theta = \phi$ in Eq. (3.7), Eq. (3.24) puts us in good shape. Then $n\tau$ appears only as h_i/h_e: we need decide only

on the ratio of ion and electron confinement times, specify (say) T_e and solve Eq. (3.24) for T_i. If a posteriori, one finds, alas, $\phi_s < \phi$, Eq. (3.24) is still a good starting point for trials with θ specified afresh.

The solution scheme is in Appendix I. Ratios (RK), (RX), (RC), (RSI) appearing therein are useful in seeing the ion-electron energy transfer, bremsstrahlung, synchrotron radiation, as fractions of fusion α-energy deposited to the electrons; and in seeing the ion injection energy as a fraction of total fusion α-energy. Also useful are the quantities

$$\begin{aligned} U_k &= K/\langle\sigma v\rangle \\ U_x &= (WX)/\langle\sigma v\rangle \\ U_c &= (WC)/\langle\sigma v\rangle \\ U_r &= U_x + U_c \end{aligned} \tag{3.26}$$

which are, respectively, the ion-to-electron energy transfer, total bremsstrahlung, total synchrotron radiation, and total radiation, per fusion event. The quantity U_r, a measure of the radiation load on the vacuum wall, appears often in the computed results to follow.

Some of the circumstances described by these equations are easy to see; consider Eq. (3.24) if the electrons did not radiate, if $\tau_e = \tau_i$, and if there were no injection energy, we see that $U_{\alpha e} = U_{\alpha i}$ (hence $T_e = 33$ keV, from Fig. 3.1), and $T_e = T_i$ is a solution. Is it the only solution for this value of T_e, in the sense of Eq. (3.24) being stable in the vicinity? It is, as follows. If T_i rises, T_e remaining constant, the sum of the $\langle\sigma v\rangle$ terms is positive both because $\langle\sigma v\rangle$ rises, and because $T_e/T_i < 1$. The net K term is also positive. Thus no solution is to be found that way. Similar conclusions follow if other variations are made, mutatis mutandis.

Electron radiation reinstated leads to lower T_e, hence a lower temperature at which $T_e = T_i$. Thus we predict that with radiation, there is a common temperature operating point, and corresponding unique fractional burnup f_b^*. At any larger f_b both T_e and T_i rise, but because now the ions are more readily heated, $T_i > T_e$. Similarly, if $f_b < f_b^*$, both T_e and T_i are less but $T_e > T_i$.

3.6. Plasma Heating of Fuel

Following the final remarks of the previous section, we can start discussing the results. By far the easiest to understand is the balance among particle temperatures, burnup, etc., if the electrons and ions are heated by the fusion α-particles in the plasma. Thus we set $V_i = V_e = 0$, and $J = 1$ in the previous equations, and must make some assumption about the magnitude of the synchrotron radiation, which appears in the quantity C_2/D of Eq. (3.22). For convenience set $D = 1$ and adjust C_2; the value $C_2 = 0$ corresponds to magical suppression of synchrotron radiation; $C_2 = 2.5$ corresponds to the maximum credible assumption (optically thin plasma, or low β, poorly reflecting walls, etc.). Thus we choose $C_2 = 0$, 0.08, 0.2, 1.0, 2.5, corresponding to various possibilities, and will in this section emphasize calculations for the intermediate case $C_2 = 0.2$. We set $C_1 = 1$ for normal bremsstrahlung.

Figure 3.4 shows equilibrium temperatures T_i and T_e versus f_b for the extreme assumptions $C_2 = 0$ or 2.5. The unattainable but useful reference point $T = 33$ keV, $f_b = 0.0536$ (corresponding to all radiation turned off) is shown by the isolated mark, and on other curves of similar nature to follow. In a few of the figures, we draw actual computed points, to illustrate the extent of the calculation.

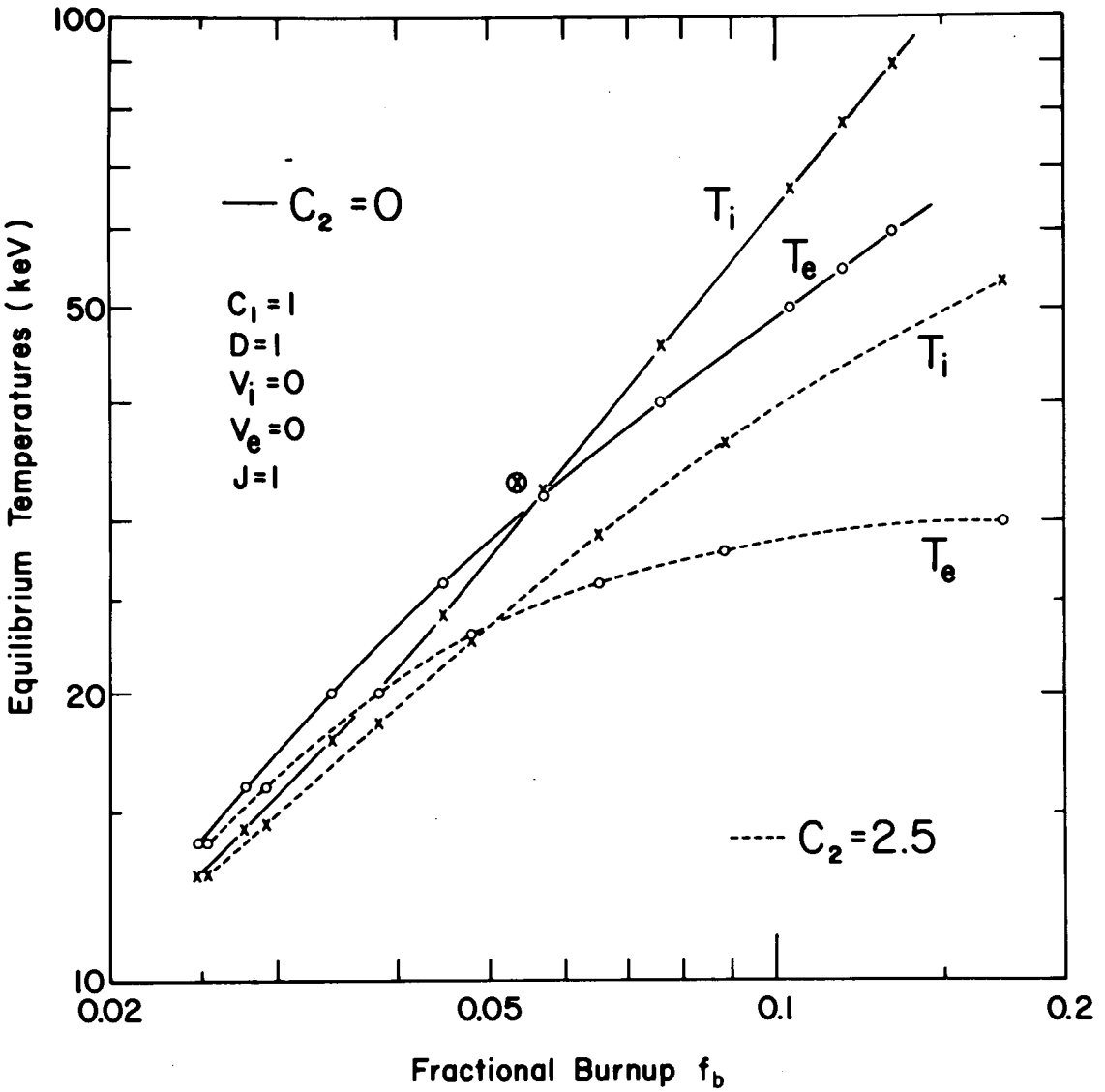

Fig. 3.4. Equilibrium Ion and Electron Temperatures vs Fractional Burnup in a Self-Heated Fusion Plasma. Assumptions of no synchrotron radiation ($C_2 = 0$) or much radiation ($C_2 = 2.5$) are shown.

In each case, the curves vary as expected. At low f_b, T is low, and because $U_{\alpha e} > U_{\alpha i}$, then $T_e > T_i$. However, because thermalization is rapid at low temperature, $T_e - T_i$ is not very large. At high burnup, say 0.1 or more, both species are heated more; but now $U_{\alpha e}$ has dropped (see Fig. 3.2) and $T_i > T_e$. Note the effect of easy synchrotron radiation escape: at low T_e, it is small, because w_c is small there. But at high f_b, T_e is forced down — e.g., at $f_b = 0.1$, from 49 keV to 28.7 keV. This leads to colder ions on <u>two</u> counts: direct ion-electron heat transfer, and also $U_{\alpha i}$ decreases as T_e is lowered. Thus we see in the figure, again at $f_b = 0.1$, T_i has been reduced from 64 keV to 39.5 keV, a <u>larger</u> drop than was suffered by the electrons.

With these results in mind, we now peruse some intermediate cases in more detail. Figures 3.5, 3.6, 3.8, and 3.9 show T_e, T_i, and the radiation load per fusion U_r versus f_b, for $C_2 = 0.08$, 0.2, 1.0, and 2.5.

Figures 3.6 and 3.7 go together. At low f_b, T_e and T_i are both low as we expect; and at higher f_b, synchrotron radiation limits T_e, hence also T_i. The total radiation curve U_r is interesting; at $f_b = 0.04$ it is a minimum, with only 170 keV/fusion absorbed on the vacuum wall. The number is low because at the low electron temperature (23.2 keV) radiation is low; the electrons gained energy from the α's, but carry it out with them as kinetic energy. At $f_b < 0.04$, the radiation/fusion rises because bremsstrahlung is becoming relatively more important (at yet lower f_b and temperatures, we could reach the so-called ignition temperature at which fusion energy equaled bremsstrahlung). At $f_b > 0.04$, T_e increases, and synchrotron radiation increases rapidly.

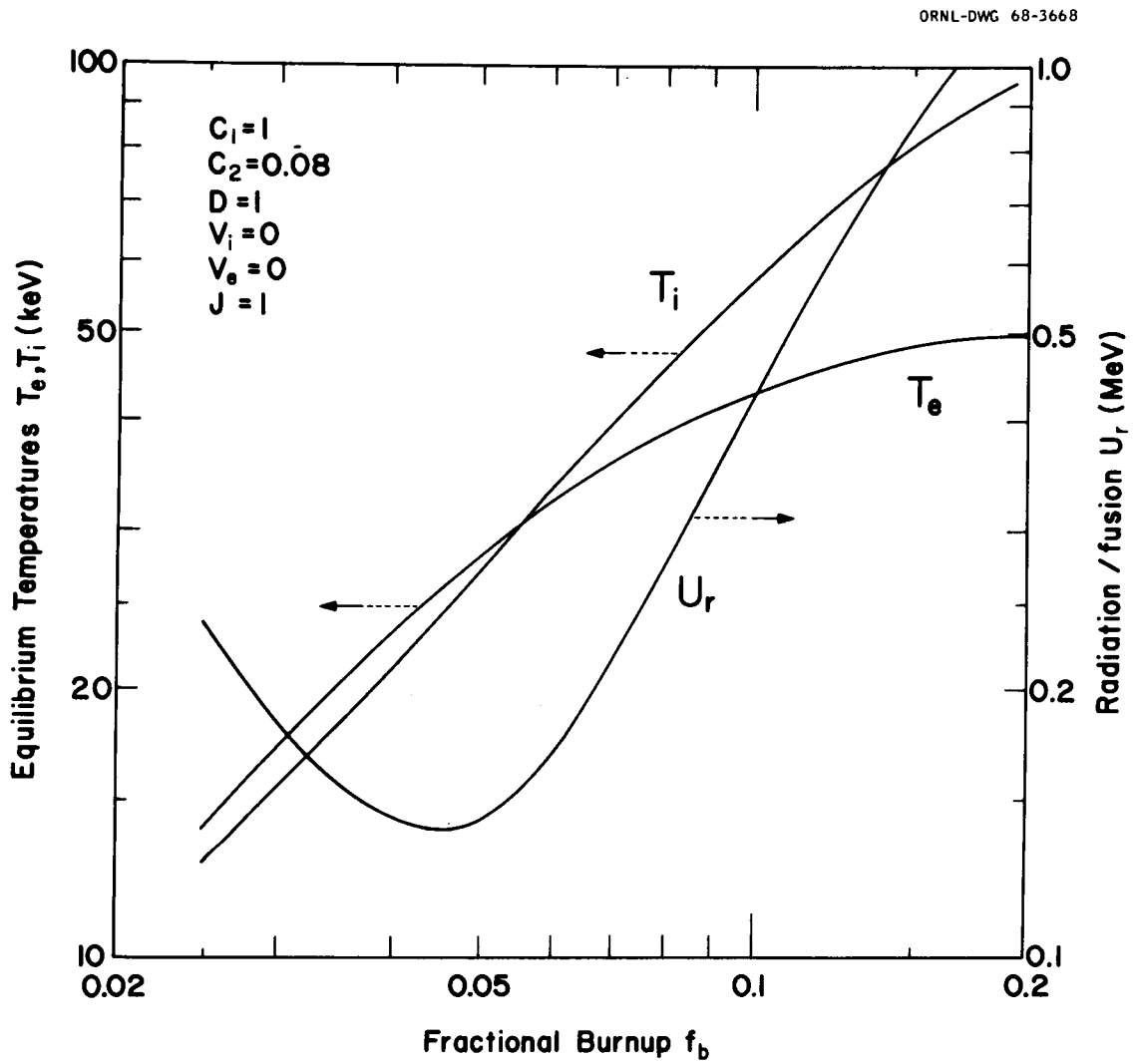

Fig. 3.5. Ion and Electron Temperatures and Vacuum Wall Radiation Load Per Fusion vs Fractional Burnup in a Self-Heated Fusion Plasma. Small synchrotron radiation (C_2 = 0.08, D = 1).

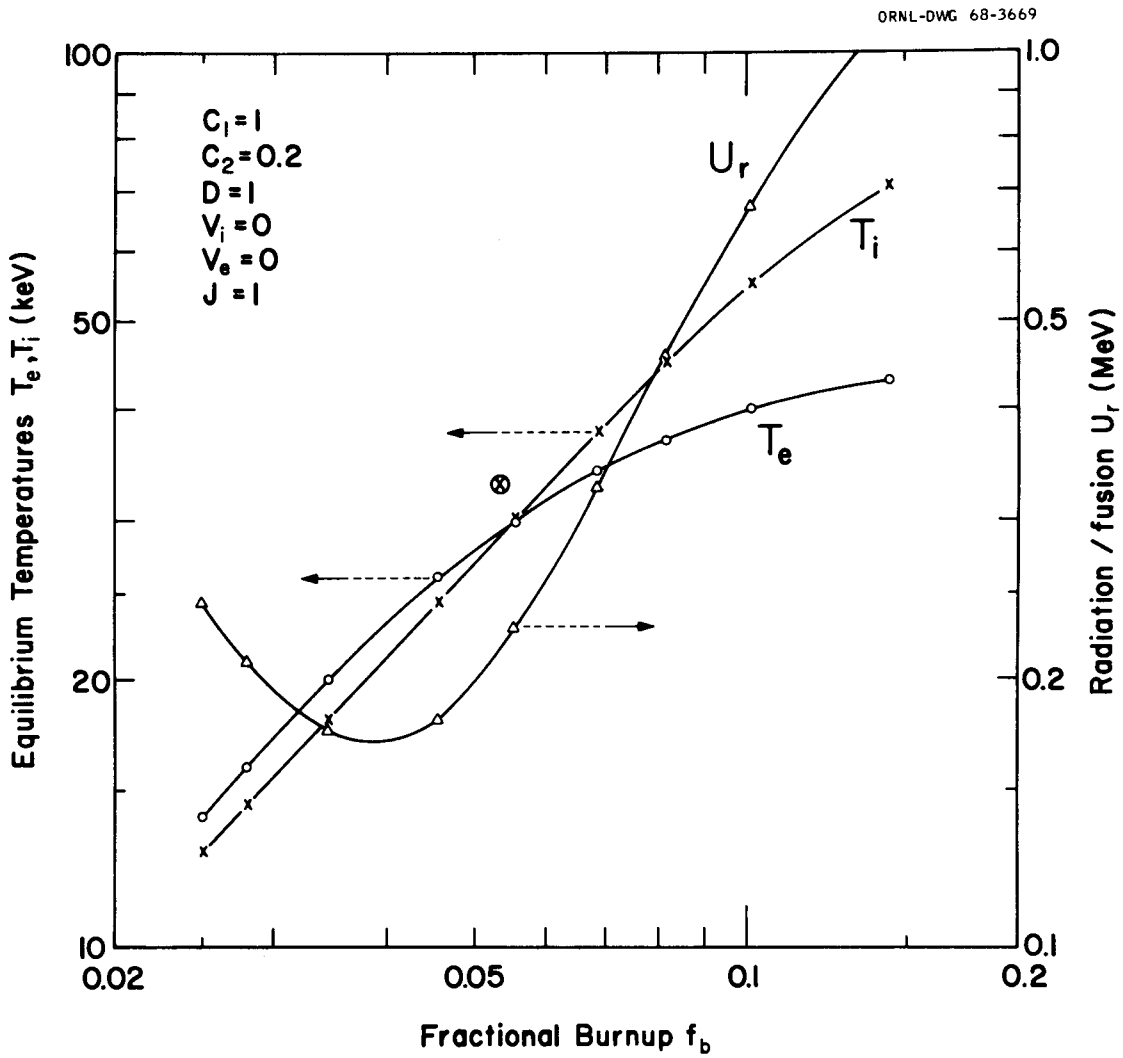

Fig. 3.6. Ion and Electron Temperatures, and Radiation/Fusion vs Fractional Burnup in a Self-Heated Plasma. Medium synchrotron radiation (C_2 = 0.2, D = 1).

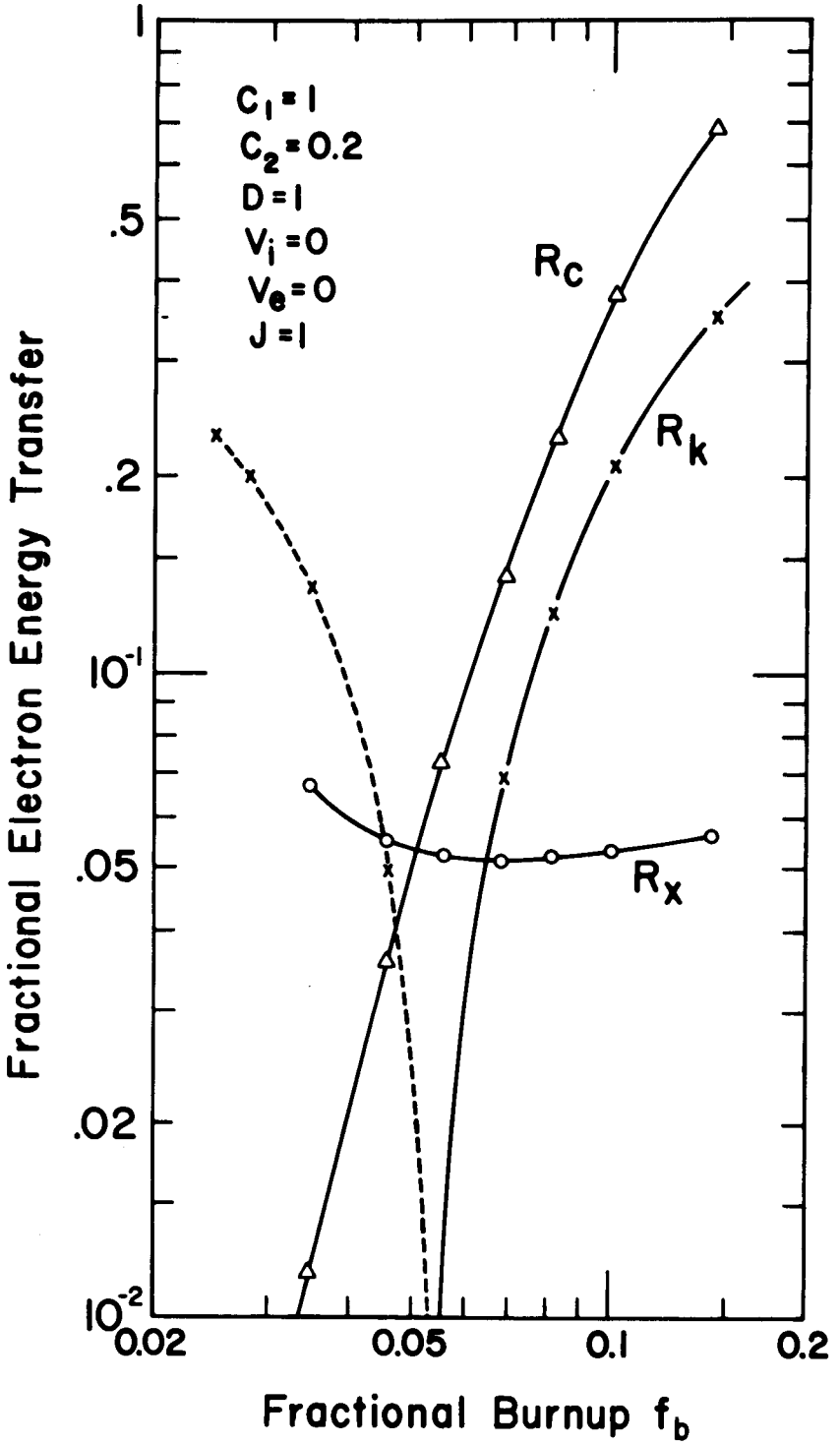

Fig. 3.7. The Bremsstrahlung (R_x), Synchrotron Radiation (R_c), and Energy Transfer from Ions (R_k), all Expressed as Fractions of the Electron Energy Gained from α-Particles. Self-heated plasma, same as Fig. 3.6. The dashed R_k curve indicates electrons lose energy to ions.

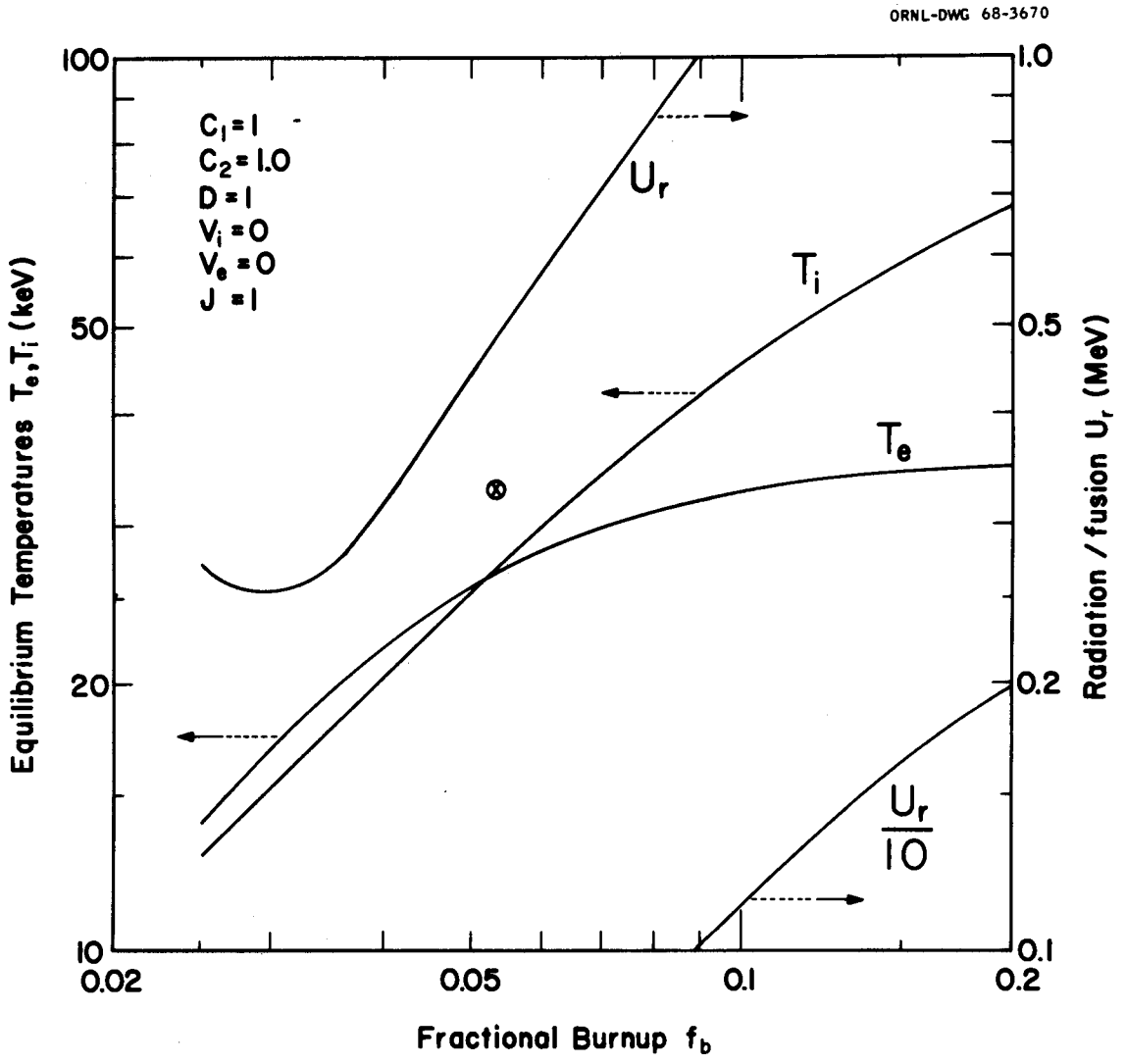

Fig. 3.8. Ion and Electron Temperatures, and Radiation/Fusion vs Fractional Burnup in a Self-Heated Plasma. Large synchrotron radiation (C_2 = 1.0, D = 1).

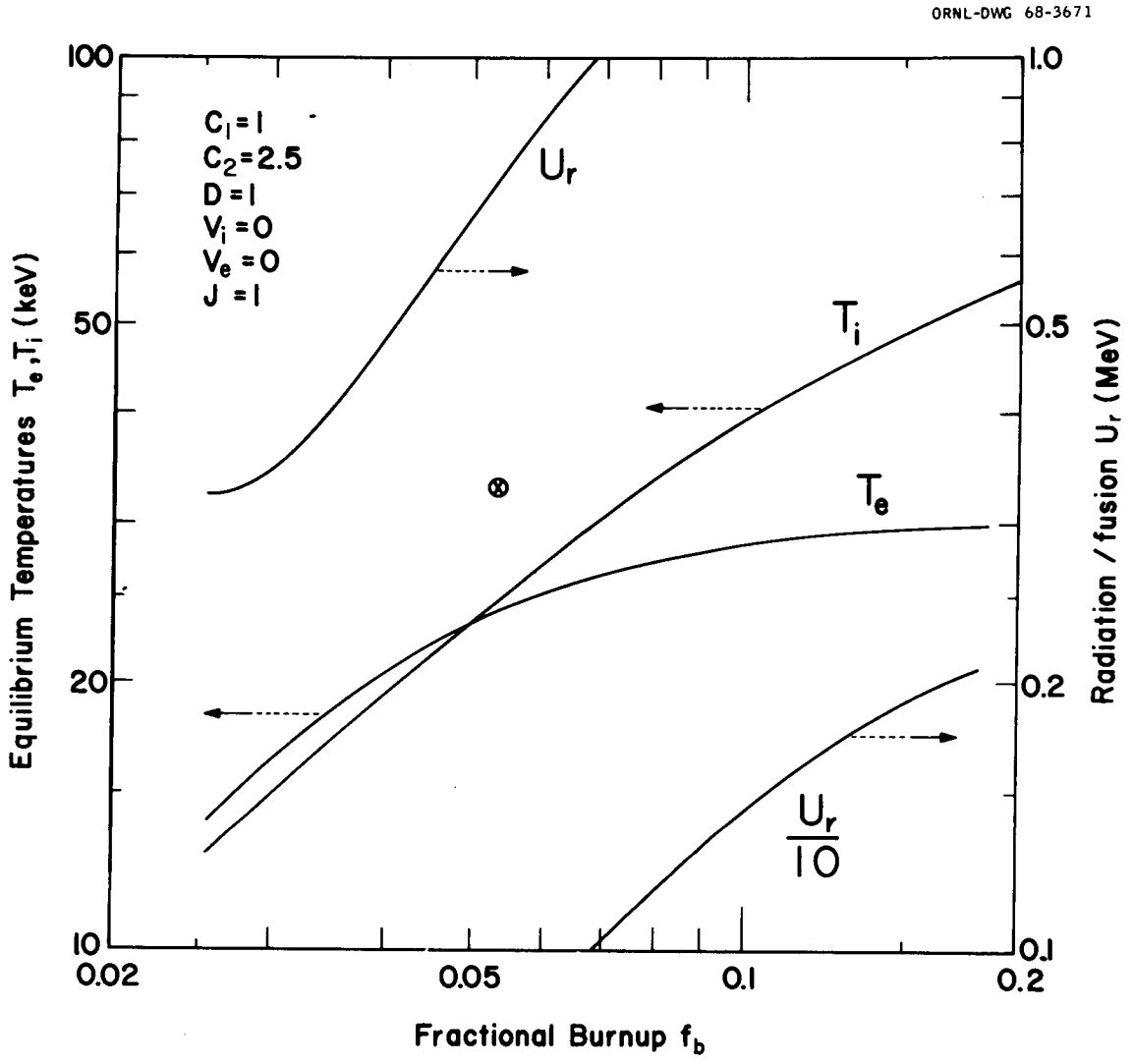

Fig. 3.9. Ion and Electron Temperatures and Radiation/Fusion vs Fractional Burnup in a Self-Heated Plasma. Very large synchrotron radiation ($C_2 = 2.5$, $D = 1$).

This latter effect is seen in Fig. 3.7, where we plot the fate of the energy gained by the electrons from various sources. The quantity R_c is the synchrotron radiation divided by the energy gained directly from the α's; similarly R_x is bremsstrahlung; and R_k is the ratio (electron energy gained from ions)/(electron energy gained from α's directly). The dashed R_k values at low f_b mean that electrons heat ions. We see that R_x increases at very low f_b, leading to the behavior of U_r in Fig. 3.6; R_x increases slightly at high f_b, the reason for which can be seen after a little mental cross-plotting: T_i is high at high f_b, and $\langle\sigma v\rangle$ increases less fast than does $T_e^{1/2}$ as f_b goes up. Note the dominant role played by synchrotron radiation at high f_b; at $f_b = 0.10$ for example, the electrons radiate in this way about 38% of the amount they get from the α's. The actual total from Fig. 3.6 is 0.67 MeV/fusion.

Note in Fig. 3.7 that the electron-ion energy transfer may be ≈ 0.5 MeV for large temperature differences; this is to be expected, and can be a significant fraction of $U_{\alpha i}$ or $U_{\alpha e}$.

Turning now to Figs. 3.5, 3.8, and 3.9, for different synchrotron radiation conditions, we find generally similar situations, with U_r increasing rapidly as more radiation escapes. Note for instance in Fig. 3.9 ($C_2 = 2.5$), at $f_b = 0.174$, that $U_r = 2.05$ MeV. In fact, this exceeds the total direct gain from the α's under those conditions (1.834 MeV); the remainder came from ion cooling.

To complete the picture, Fig. 3.10 shows the largely-expected variation of ion-electron heat transfer, versus f_b, for the extreme cases $C_2 = 0$ and 2.5. Assumptions about the synchrotron radiation affect the value of f_b where $T_e = T_i$ (hence where the curves of Fig. 3.10 pass through zero),

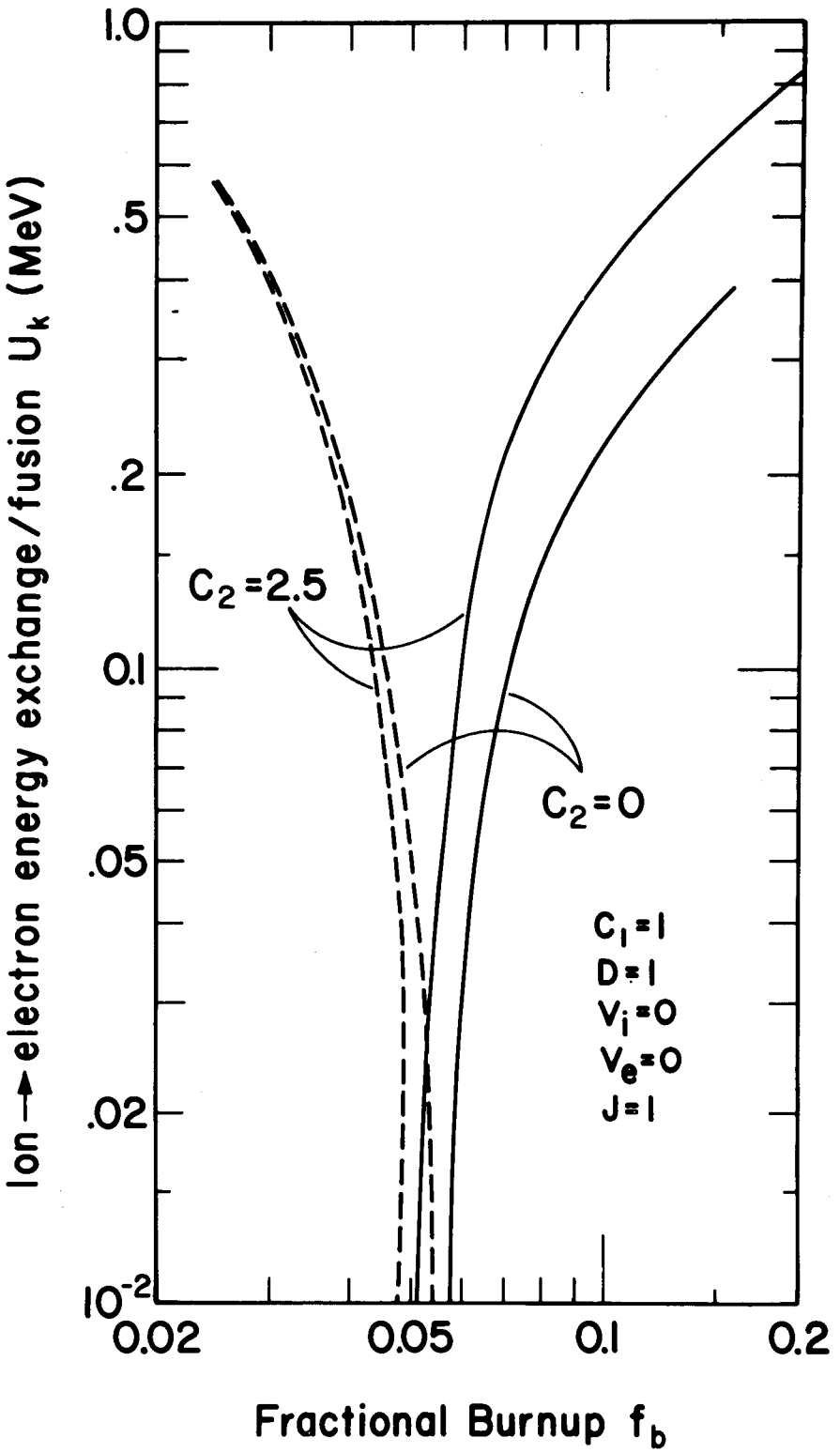

Fig. 3.10. Ion-to-Electron Heat Transfer per Fusion for a Self-Heated Plasma, for Two Synchrotron Radiation Assumptions. Dashed curves mean electrons heat ions.

and affect matters moderately at high f_b; large C_2 means low T_e, hence more ion cooling.

Several important things emerge from these calculations, to be discussed in subsequent sections. In abstract, they are:

(1) Although the curves do not demonstrate the fact, confinement time in all cases shown here (Figs. 3.4-3.10) exceeded the α-particle slowing down time (sometimes by a factor less than two). Thus at least in these systems, the α's can escape with low energy, and the analysis is thereby simplified. This will not always be the case if the ions are injected hot or heated from outside, but our calculations will show that the burnup would be uninterestingly low if the α's escape without thermalizing.

(2) The calculations of this section apply most readily to closed confinement systems (although the material and discussion are the groundwork for what follows about both open and closed systems). Because the reaction parameter is a maximum at relatively low ion temperature, Fig. 2.3, and high temperature is not needed for confinement, we should explore the lower parts of Figs. 3.4-3.10 in more detail, for closed system parameters. That is the topic of the next section. There seems to be no difficulty in finding reasonable operating conditions.

(3) At high burnup and high ion temperature, it seems almost possible to run an open-ended confinement system without plasma heating. For example, if $C_2 = 0.08$, we require $f_b = 0.17$ if $T_i = 90$ keV; this demands better ion confinement than we expect, but perhaps a modest additional ion heating will reduce f_b to an attainable value. In fact, there are many open-ended options, because both particles and energy can readily be put

in and out. Thus we have a more complicated task in evaluating open-ended plasma parameters, and in later sections will show the effect of ion heating alone, cold electron injection alone (for line tying?), both ion and electron heating, and effect of incomplete α-particle thermalization, and the effect of varying synchrotron radiation.

3.7. Closed Systems

We can explore the utility of several options, in the general range of T_e, $T_i \lesssim 30$ keV.

Figure 3.11 shows some results of ion heating, for $C_2 = 0.2$, intermediate synchrotron radiation. Both T_e and T_i rise at constant f_b as expected, and with 20 keV ion heating, we see $T_i > T_e$ over the full range of interest. The energy cost of ion and/or electron heating is conventionally judged by the quantity

$$Q = \frac{\text{Fusion power}}{\text{Injection power}} \quad . \tag{3.27}$$

Bearing in mind that the fusion power is heat, and the injection power is electric, we see that $Q = 10$ represents a large recirculation of power, $Q = 5$ represents disaster, and $Q > 20$ is reasonable. In the illustrations of this chapter, we take the fusion energy as 17.6 MeV, not the value 22.4 MeV corresponding to neutron absorption in Li^6. Thus our results will be slightly more pessimistic than some others, but not enough to make any decisive difference. Because two ions and/or electrons must be heated per fusion,

$$Q = \frac{17{,}600\ f_b}{2(V_i + V_e)} \quad . \tag{3.28}$$

Figure 3.12 is a repeat of Fig. 3.11 with contours of contant Q marked. The cost of energetic ion injection is not excessive.

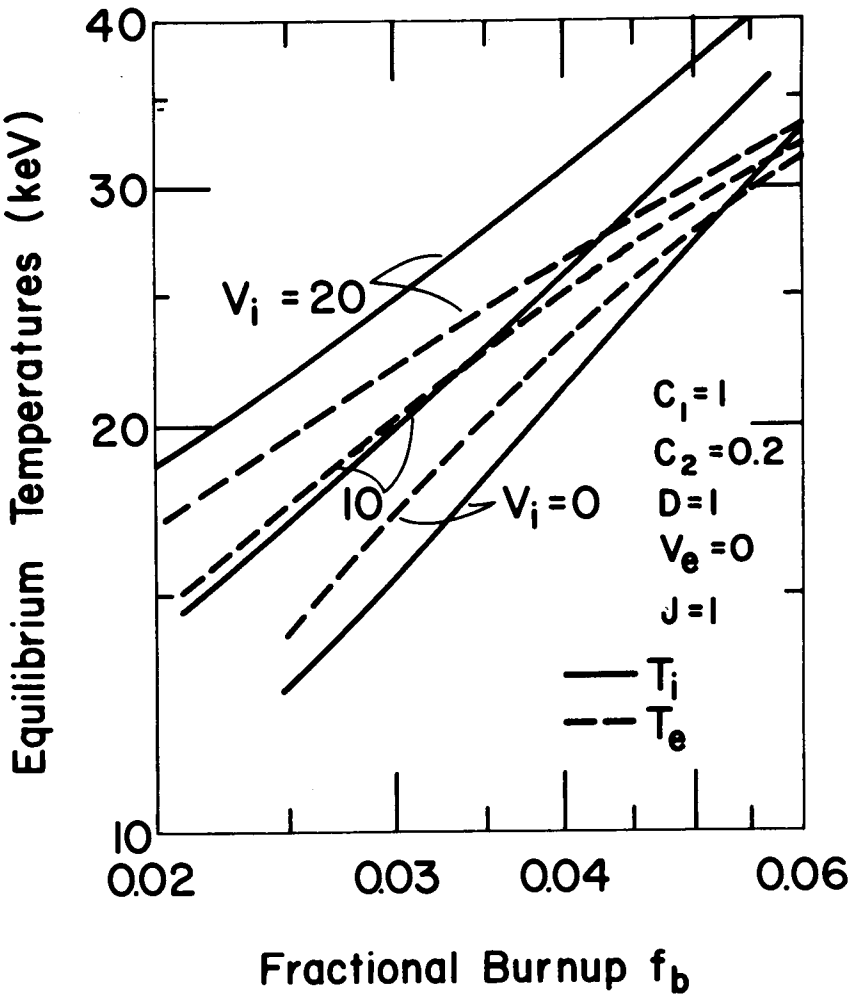

Fig. 3.11. Effect of Ion Heating (V_i = 0, 10, 20 keV), at Temperatures Characteristic of Closed Confinement Systems. Medium synchrotron radiation, normal bremsstrahlung.

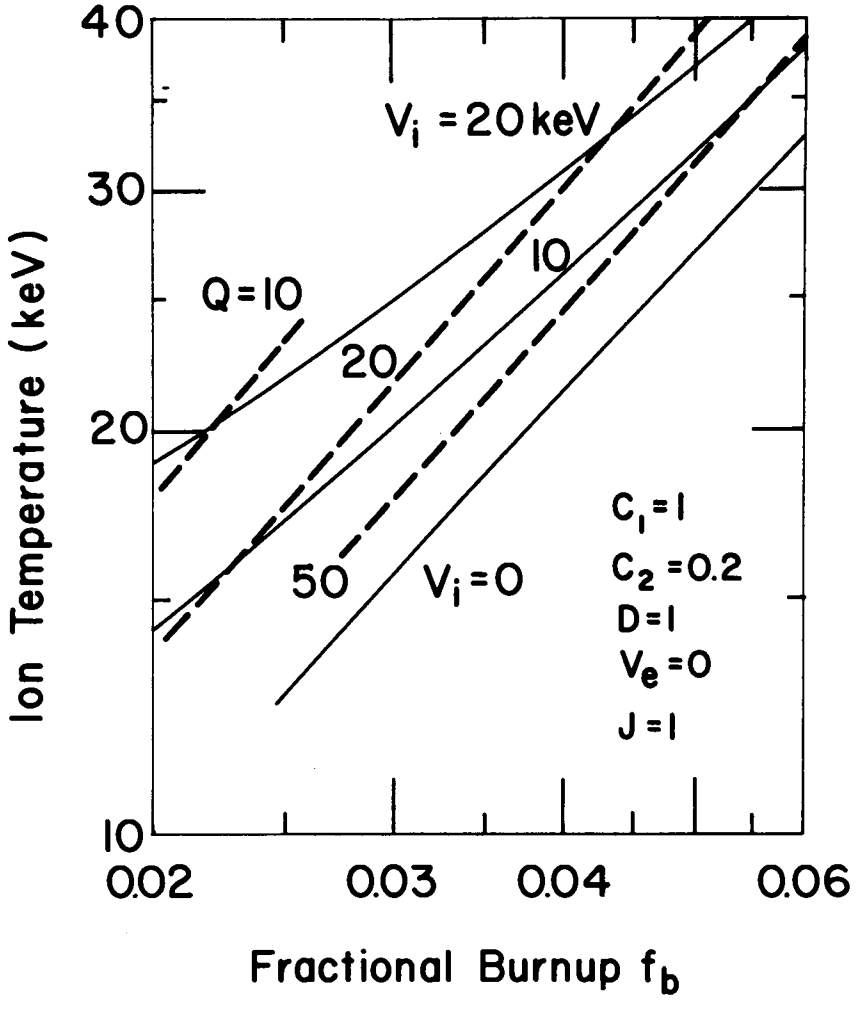

Fig. 3.12. Contours of Constant Q = Fusion Power/Injection Power, for the Conditions of Fig. 3.11, With Ion Heating.

The disadvantage of ion heating can be seen from Fig. 3.13, where the results of Fig. 3.11 are combined with the reaction parameter curve, Fig. 2.3. Ion heating actually lowers the reaction rate, over the entire parametric range. The reason is not just that T_i is rising and $\langle\sigma v\rangle/T_i^2$ decreases at $T_i > 15$ keV. More importantly, heating ions also heats electrons. This has two bad consequences: electron pressure rises, and p_α rises inordinately because the α's are more slowly thermalized.

Figure 3.14 shows that ion heating can actually reduce the radiation load on the vacuum wall. As T_i increases, $\langle\sigma v\rangle$ rises faster than does the bremsstrahlung from the warmer electrons. The effect is of little importance, because the radiation load is already small in this range of parameters.

The most desirable place to operate a closed system would appear to be at $T_i \approx 20$ keV, T_e as low as possible, and as much burnup as confinement will allow: that is, to the right of any of the curves in Fig. 3.11.

Consider first adjustments allowed in the computation code. That region would become accessible if the electrons were cooled. Flooding the system with cold electrons ($V_e = 0$, $J > 1$) seems incompatible with having a closed system. Thus we turn to radiation control.

Consider synchrotron radiation first; Figs. 3.5, 3.6, 3.8, and 3.9 show the effects of C_2. All of these, in combination with Fig. 2.3, yield maximum reaction parameters at $f_b \approx 0.025$, which surely is too low for convenient tritium gas recovery. In addition, T_e is so low that the synchrotron radiation is negligible anyway. Certainly, varying C_2 affects matters at high T_e and T_i, but there the reaction parameter is needlessly small. Thus we explore matters at intermediate values, choose $f_b = 0.05$, and see

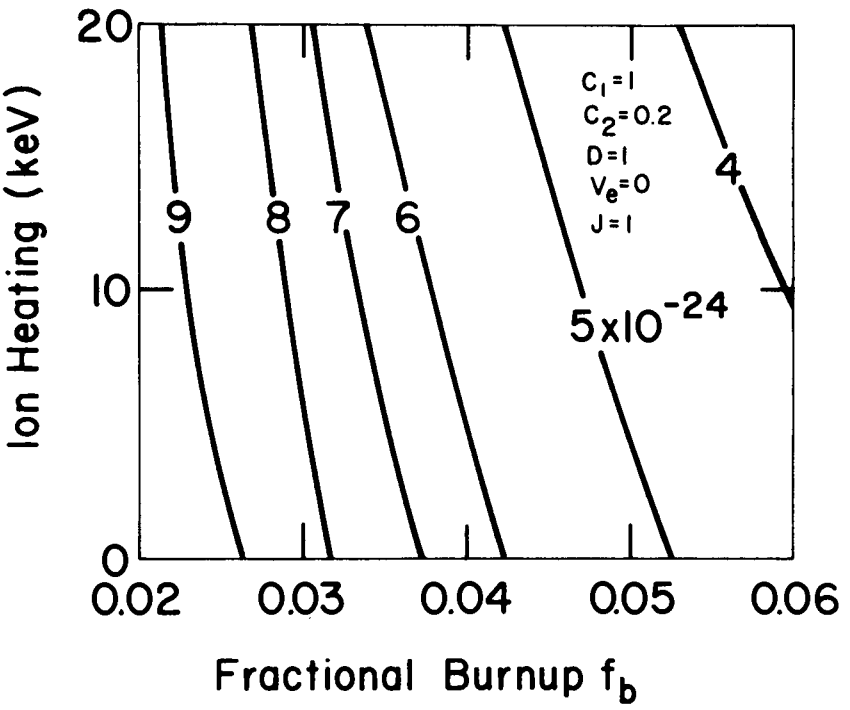

Fig. 3.13. Contours of Constant Reaction Parameter P showing the Effect of Ion Heat and Fractional Burnup, Under Equilibrium Conditions. Medium synchrotron radiation.

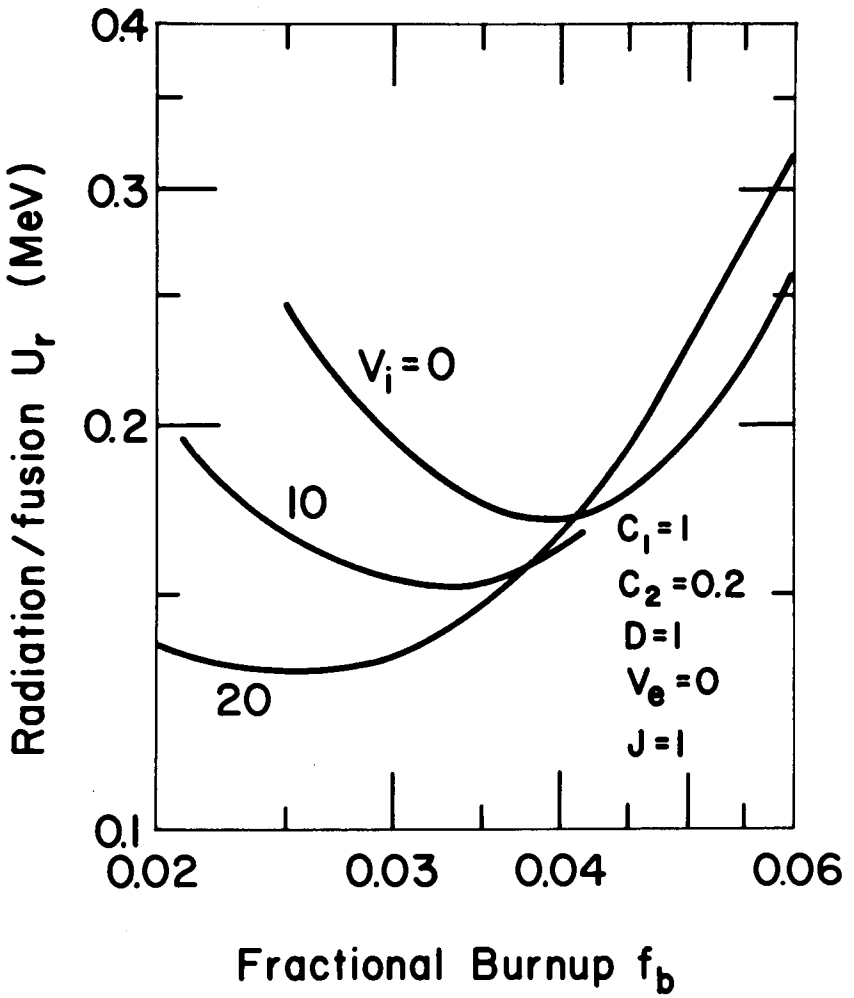

Fig. 3.14. Effect of Ion Heating (V_i = 0, 10, 20 keV) on the Radiation from a Plasma Characteristic of Closed Confinement Systems. Medium synchrotron radiation, normal bremsstrahlung.

the effect of varying C_2. Figure 3.15 shows both the reaction parameter and the radiation load. While $\langle\sigma v\rangle$ is reasonable, varying C_2 has little effect.

Next, observe the effect of enhanced bremsstrahlung, achieved by introducing a low density of heavy ions, shown in Fig. 3.16. The changes are better seen if quantities are plotted vs T_i, as in Figs. 3.17-3.20. The first of these shows T_e, f_b, and reaction parameter P for normal bremsstrahlung through the interesting range 14 keV < T_i < 28 keV; the wall radiation U_r is too small to plot. In Figs. 3.18-3.20, we see the expected large increase in radiation U_r, moderate increase in f_b and P, and drop in T_e as the bremsstrahlung rate is increased by factors 5, 10, and 15. The bend in the T vs f_b and f_b vs T_i curves for C_1 = 10 and 15 shows the approach toward a modified ignition temperature, at which fusion power equals enhanced radiation. For these radiative conditions, P is a maximum at even lower ion temperature than was investigated. For C_1 = 15 however, f_b is unreasonably high at such low T_i (Fig. 3.20). The radiation, while large, is not unreasonable; even 2 MeV/fusion only represents 12% of the total fusion energy, and will be less than the γ-ray backshine from some moderator configurations.

Finally, in regard to this matter of adjusting T_e, T_i, f_b, etc., we conclude in general that reducing α-ion and (especially) α-electron heat transfer would be beneficial. This might also be accomplished in part by adjusting the low-energy electron distribution, as was mentioned earlier. No speculation upon the feasibility of the stratagem for closed system parameters will be made.

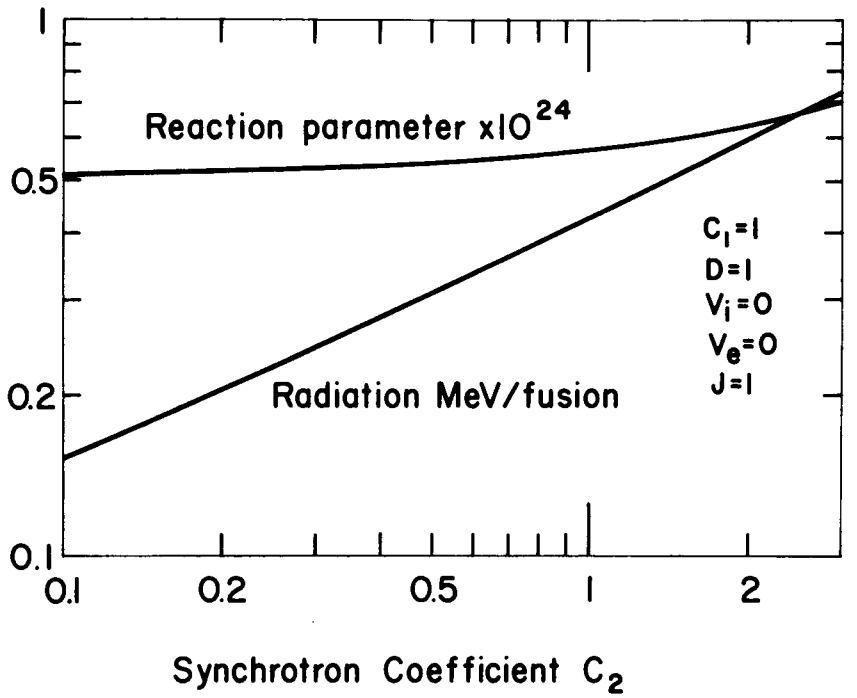

Fig. 3.15. Effect of Varying Synchrotron Radiation on Properties of a Plasma Characteristic of Closed Confinement Systems. Fractional burnup is 0.05.

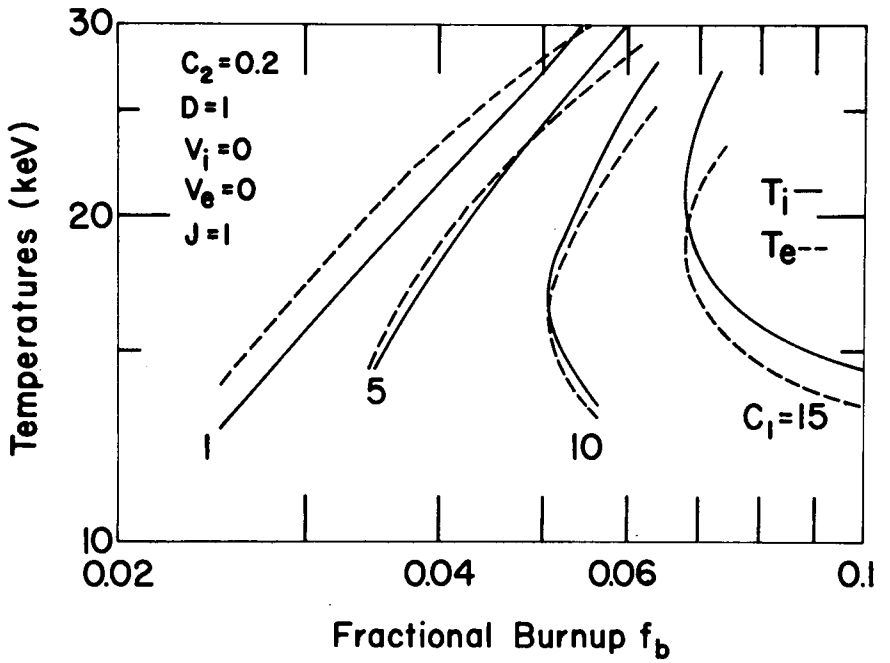

Fig. 3.16. Effect of Normal (C_1 = 1) and Enhanced (5X, 10X, 15X) Bremsstrahlung on Equilibrium Conditions in a Self-Heated Fusion Plasma.

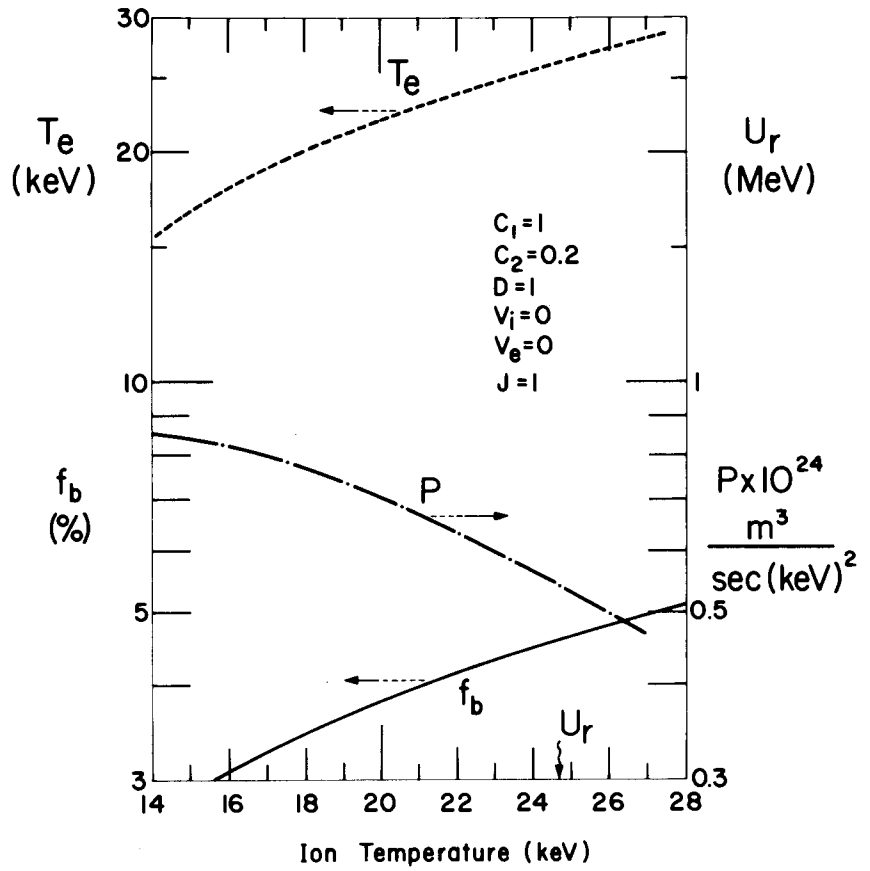

Fig. 3.17. Electron Temperature T_e, Fractional Burnup f_b, Reaction Parameter P, and Radiation/Fusion U_r vs Ion Temperature, for a Self-Heated Plasma, with Normal Bremsstrahlung.

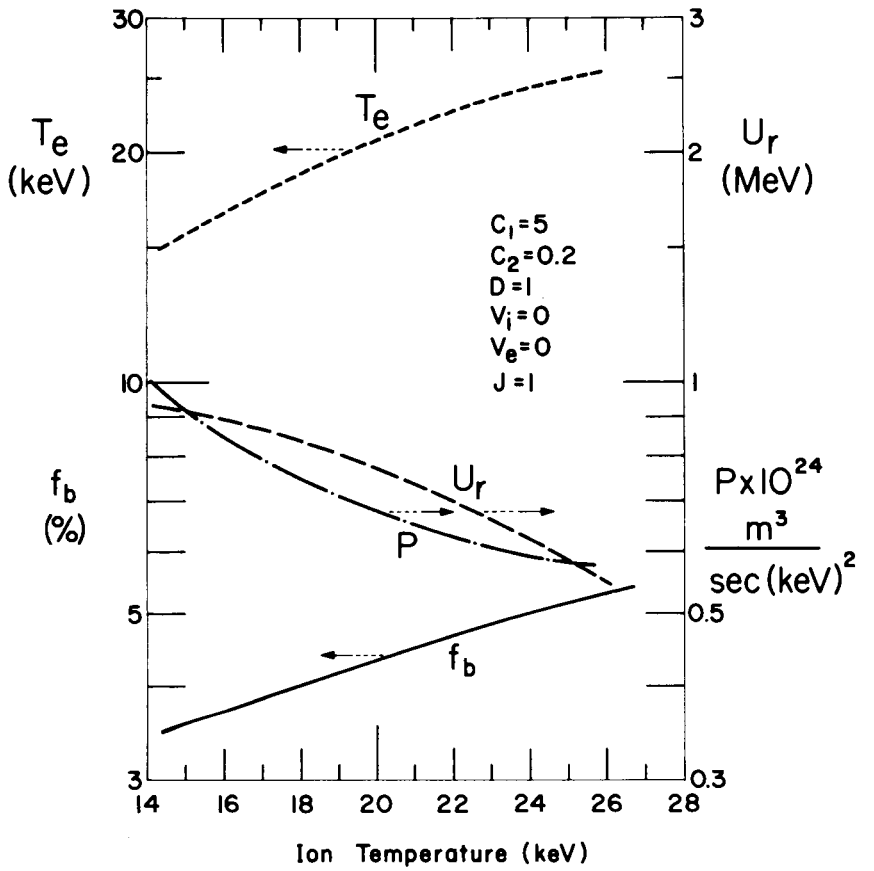

Fig. 3.18. Electron Temperature T_e, Fractional Burnup f_b, Reaction Parameter P, and Radiation/Fusion U_r vs Ion Temperature, for a Self-Heated Plasma, with 5 X Normal Bremsstrahlung.

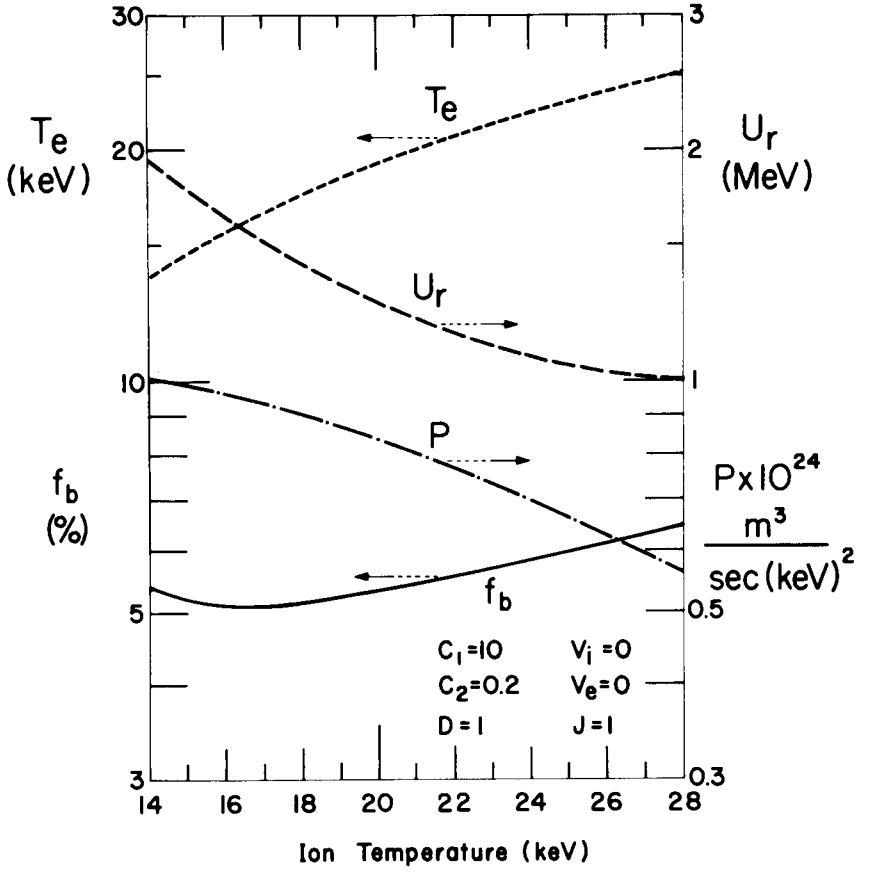

Fig. 3.19. Electron Temperature T_e, Fractional Burnup f_b, Reaction Parameter P, and Radiation/Fusion U_r vs Ion Temperature, for Self-Heated Plasma, with 10X Normal Bremsstrahlung.

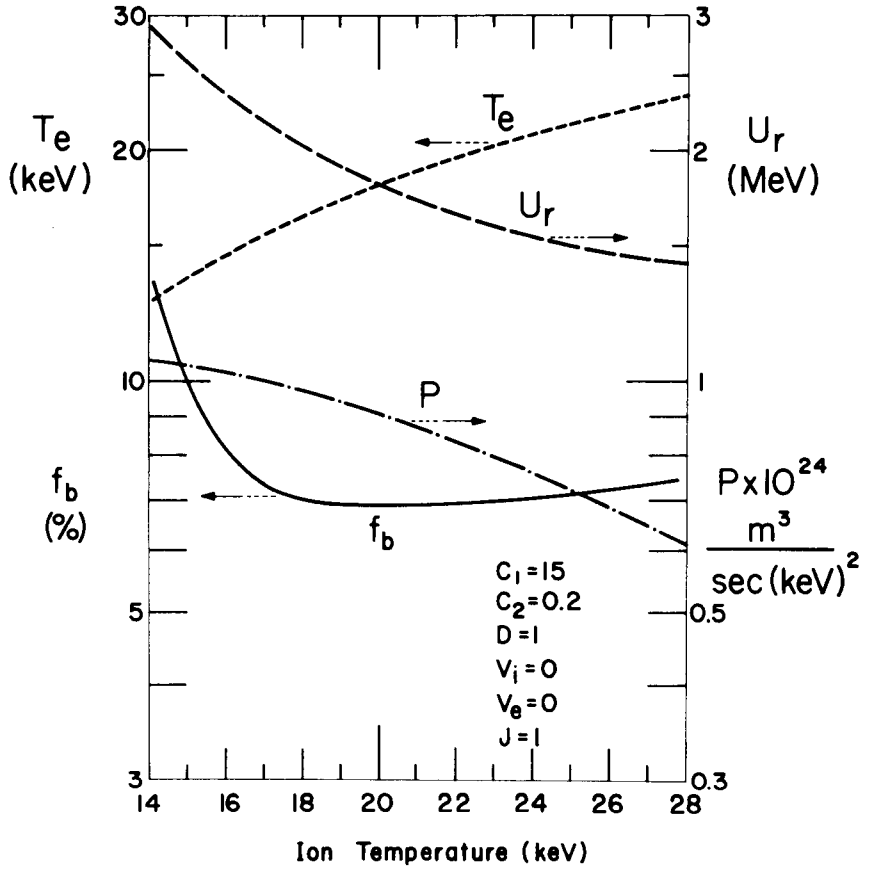

Fig. 3.20. Electron Temperature T_e, Fractional Burnup f_b, Reaction Parameter P, and Radiation/Fusion U_r vs Ion Temperature, for a Self-Heated Plasma, with 15X Normal Bremsstrahlung.

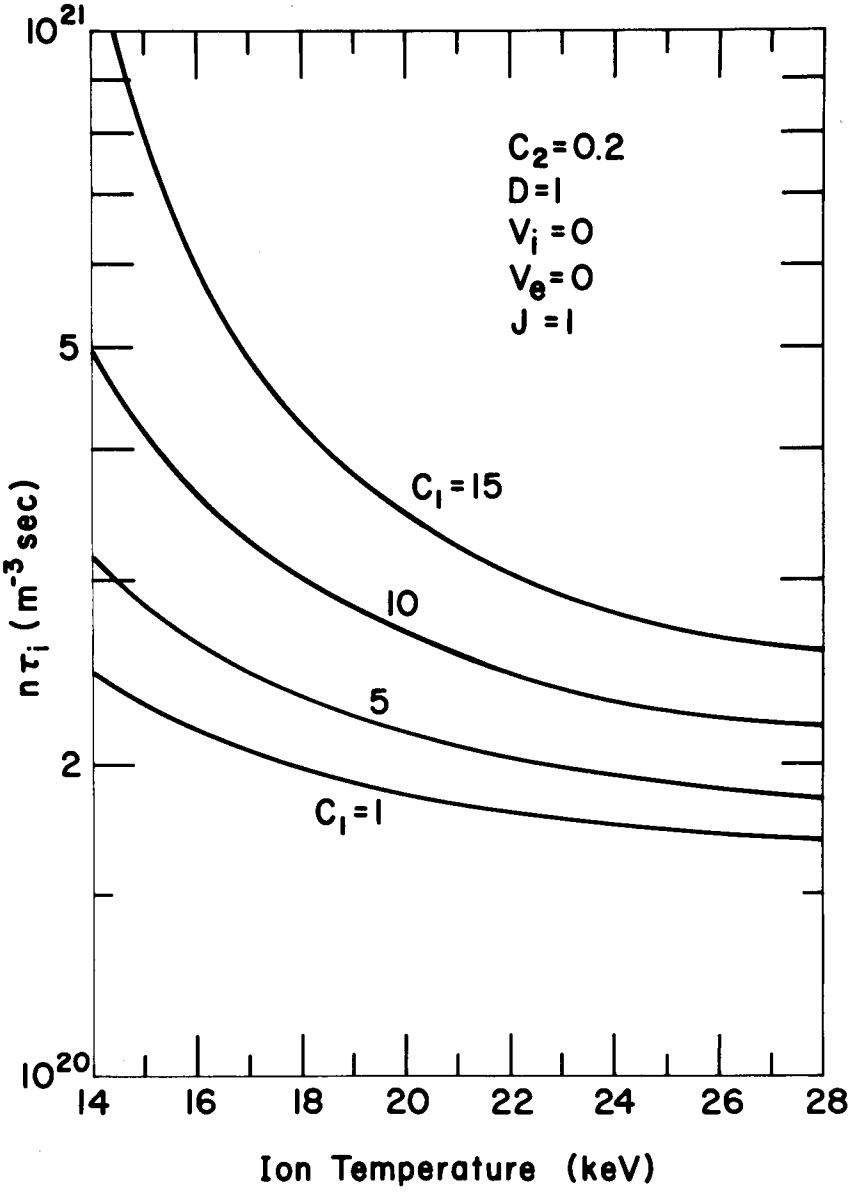

Fig. 3.21. "Containment Parameter" $n\tau_i$ for a Self-Heated Plasma, vs T_i, with Normal ($C_1 = 1$) and Enhanced Bremsstrahlung. The $C_1 = 1$ curve is virtually identical with values previously calculated by Kofoed-Hansen.[34]

It is customary to show the "containment parameter" $n\tau_i$ in analyses of this sort. Figure 3.21 shows $n\tau_i$ for the normal and enhanced bremsstrahlung cases of Figs. 3.16-3.20. The curve for normal bremsstrahlung ($C_1 = 1$) lies within 5% of the $n\tau$ curve computed by Kofoed-Hansen[34] and reported by Carruthers et al.[30] in their Figure 6.

3.8. Open-Ended Systems

Design of open-ended systems is dominated by the high scattering loss through the mirrors, in a min-B system or otherwise. We will not enter the thicket of loss rate calculation from mirrors but remind the reader particularly of references 7-13. To bypass the problem, note that specifying the ion temperature and fractional burnup is sufficient to determine the required probability ψ of ion loss per 90° effective Coulomb scatter. Figure 3.22 shows contours of constant ψ on our usual T_i - f_b plot, adapted from R & C, Chap. 13. Operation with $T_i > 100$ keV brings little benefit; in fact, we wish to operate near the low temperature end of any available parametric range. It is generally believed that $\psi = 0.3$ is possible, $\psi = 0.1$ is rather improbable, and $\psi = 0.05$ could hardly be hoped for. The curves of Fig. 3.22 will be superimposed on various T_i - f_b plots.

Our first calculation is illustrated in Fig. 3.23, for $C_2 = 0.2$, and various ion injection (or *in situ* heating) energies. Both T_e and T_i are shown. Approximately, T_i increases by 6 - 10 keV for each 20 keV ion injection energy. The marked depression of T_e and T_i at low burnup and high injection energy is caused by incomplete α-thermalization, and we see the seriousness thereof. The useful general statement can be made that the α's are thermalized in any parametric region useful for fusion.

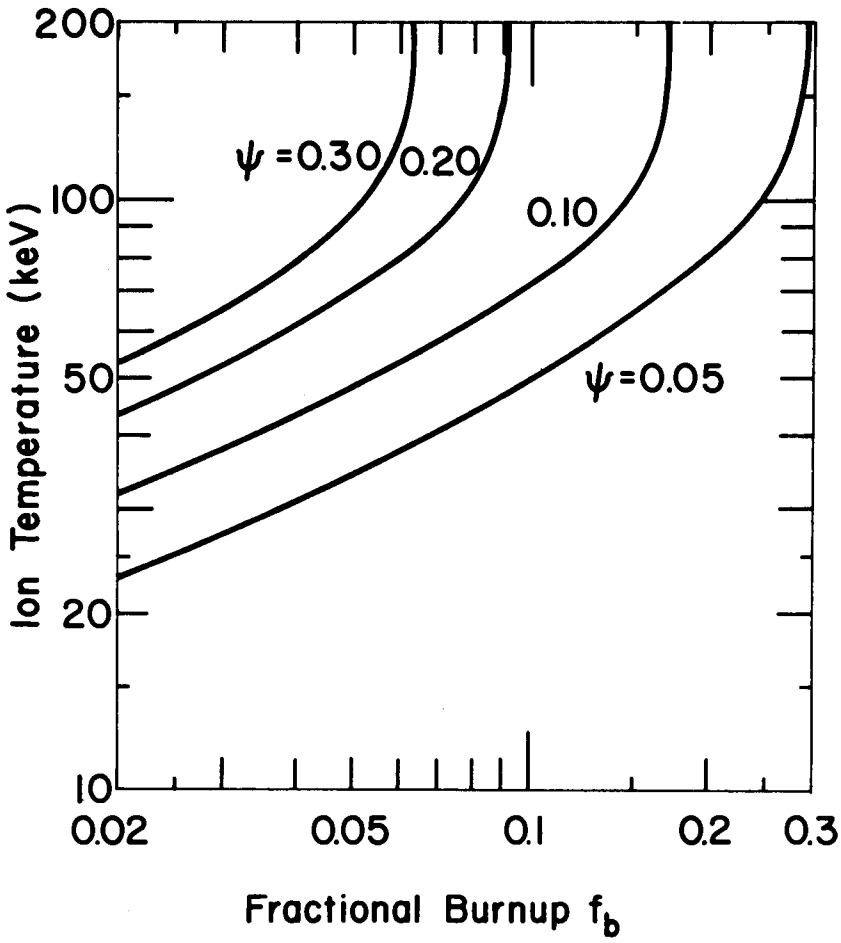

Fig. 3.22. Contours of Constant ψ = Escape Probability per Effective 90° Coulomb Scatter, on the T_i - f_b Plane.

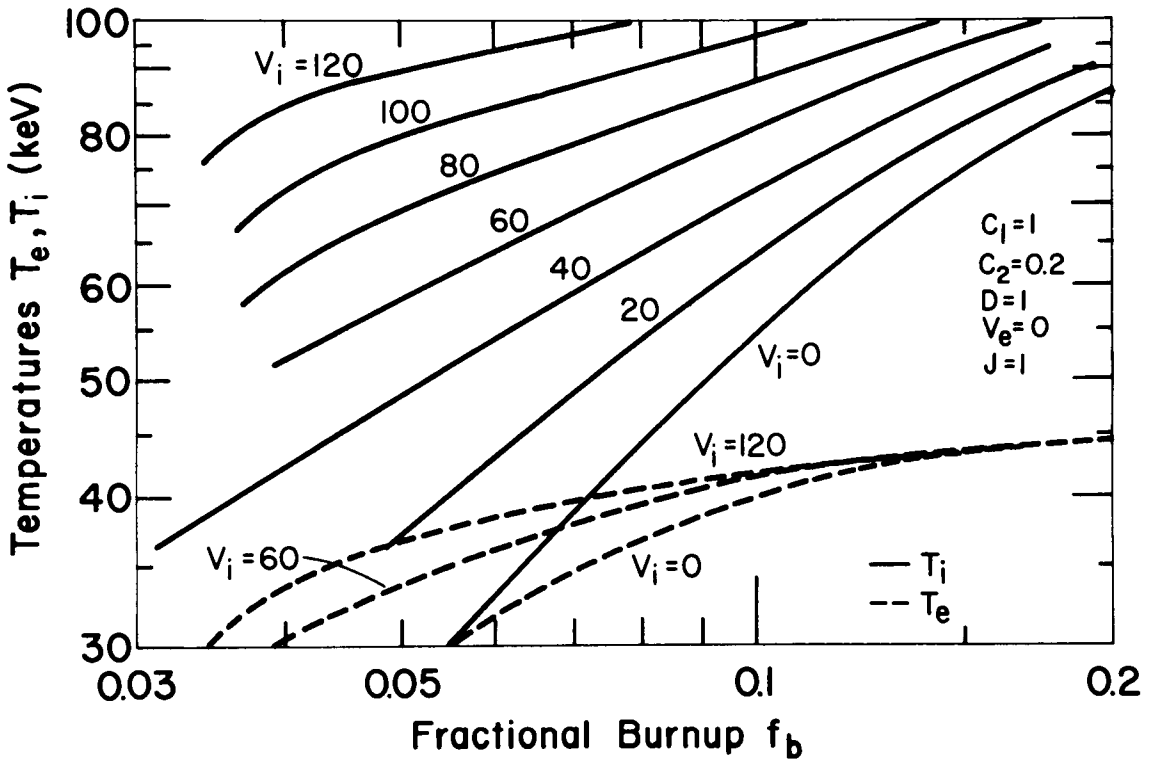

Fig. 3.23. Effect of Ion Heating (V_i = 0, ..., 120 keV) on Ion and Electron Temperatures, under Conditions Characteristic of Open-Ended Confinement Systems. Medium synchrotron radiation, one cold electron injected per ion.

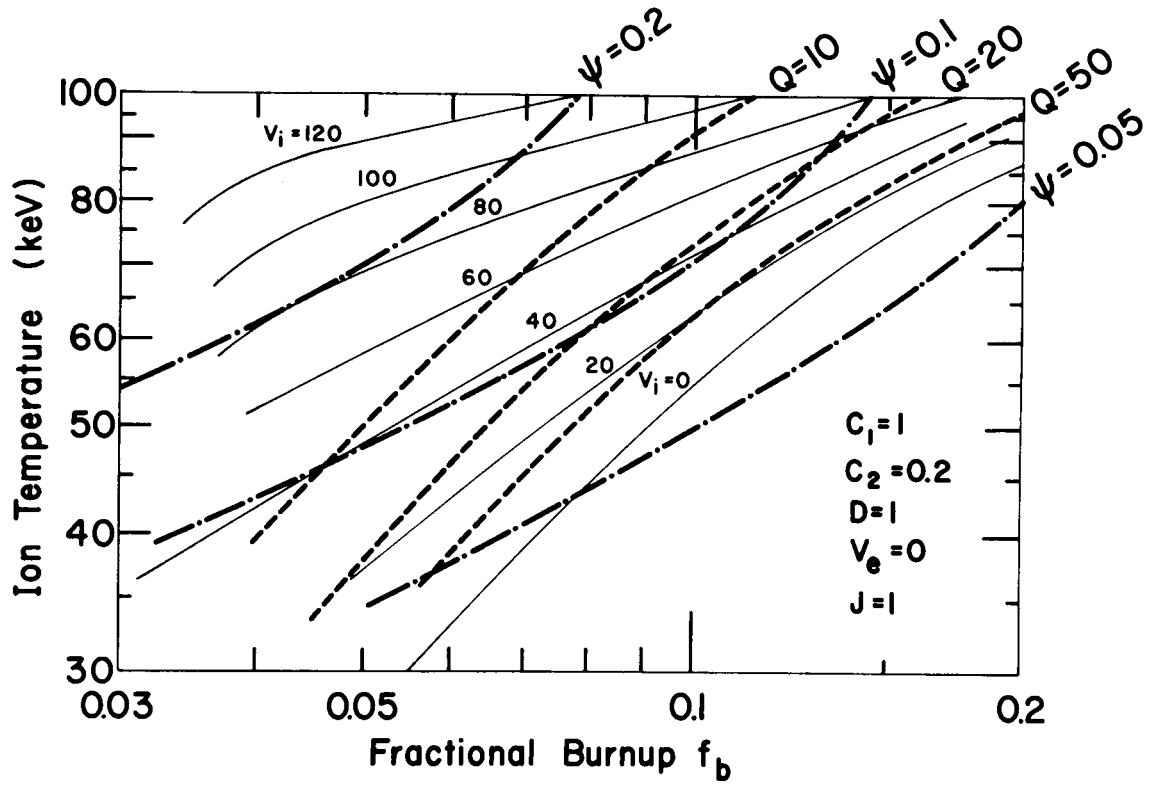

Fig. 3.24. Contours of Constant ψ = Escape Probability and Q = (Fusion Heat/Injection Energy) Superimposed on the Data of Fig. 3.23.

Figure 3.24 contains some principal results. The T_i vs f_b curves from Fig. 3.23 are repeated, with superimposed ψ-curves from Fig. 3.22 and calculated Q-curves for the specified values of V_i and f_b. In brief, we wish to operate both at large ψ and large Q. Even the lens-shaped region enclosed by $\psi \geq 0.1$ and $Q \geq 20$ is uncomfortably small. In this region, we would prefer the low temperature end (e.g., T_i = 65 keV, f_b = 0.085, $V_i = T_e$ = 38 keV), in order to maximize the reaction parameter P. In this example, $P \approx 2 \times 10^{-24}$ m^3/sec, about one-fourth the value found in the closed system examples. If ψ = 0.05 were achievable, then with no ion heating, the more desirable parameters T_i = 43 keV, f_b = 0.078, T_e = 36 keV, $P = 3.2 \times 10^{-24}$ m^3/sec could be had.

The possible parametric variations will now be tried. First is introduction of more cold electrons, necessary for line tying perhaps. To double the electron throughput, choose J = 2; then follows Fig. 3.25. The general effect can be approximately summarized as a cost of 20 keV ion injection energy. There is no longer any region with $\psi \geq 0.1$, $Q \geq 20$. The radiation/fusion on the vacuum wall is reduced from the normal case J = 1, but we do not illustrate it. Calculations also done for J = 5 are not reported here.

Electron heating also brings its penalty in energy. We do not show a separate figure, but report that adding 20 and 40 keV electron energy is equivalent to adding about 3 and 6 keV ion energy, in the presumably best operating range of Fig. 3.24. Most of the added electron energy is radiated as synchrotron radiation. Unless there are compelling contrary reasons, it is much more economical to put energy directly into the ions than into electrons.

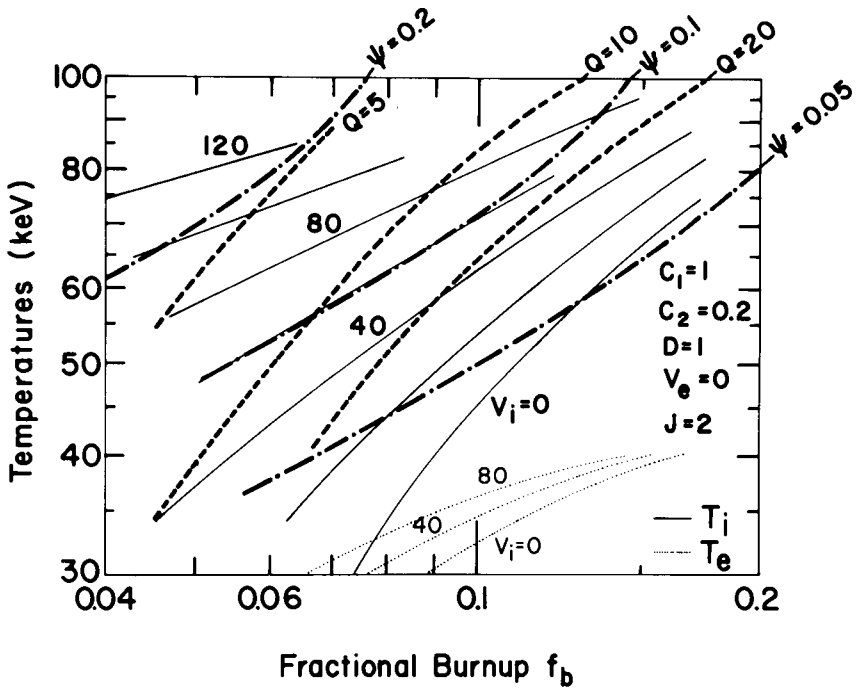

Fig. 3.25. Variation of Parameters Characteristic of an Open-Ended Confinement System. Two cold electrons are injected per ion, otherwise same conditions as Figs. 3.23 and 3.24.

Some improvement in these numbers can be had by reducing synchrotron radiation, hence increasing T_e, hence reducing ion-electron heat transfer. In Fig. 3.26, the coefficient C_2 has been reduced (from 0.2 in previous cases) to 0.08, a relatively low value. The lens between $Q = 20$ and $\psi = 0.1$ is now larger, and we can pick the point $T_i = 58$, $V_i = 32$, $f_b = 0.073$, $T_e = 39$, $P = 2.2 \times 10^{-24}$; there is more room for adjustment. Although T_e is higher, total radiation plotted in Fig. 3.27 is actually reduced.

Again, the effect of adjusting the low-energy electron population beneficially has not been explored, but the chances look brighter here than for closed systems. First T_e is already higher, not so many cold electrons are present and thermalization rates are slower. Second and more important, a 100-eV electron is faster than any ion, but slower than the α's. Thus the interesting possibility exists of reducing substantially the ion-electron heat loss (good), and lengthening modestly the α-thermalization time (also good, because confinement time is longer and there is time to spare; then a larger fraction of U_o appears in $U_{\alpha i}$), without increasing p_α excessively, or T_e hardly at all.

To end this section, we show values of the containment parameter $n\tau_i$, for the same plasma described in Figs. 3.26 and 3.27; T_i is also shown, for convenience. See Fig. 3.28.

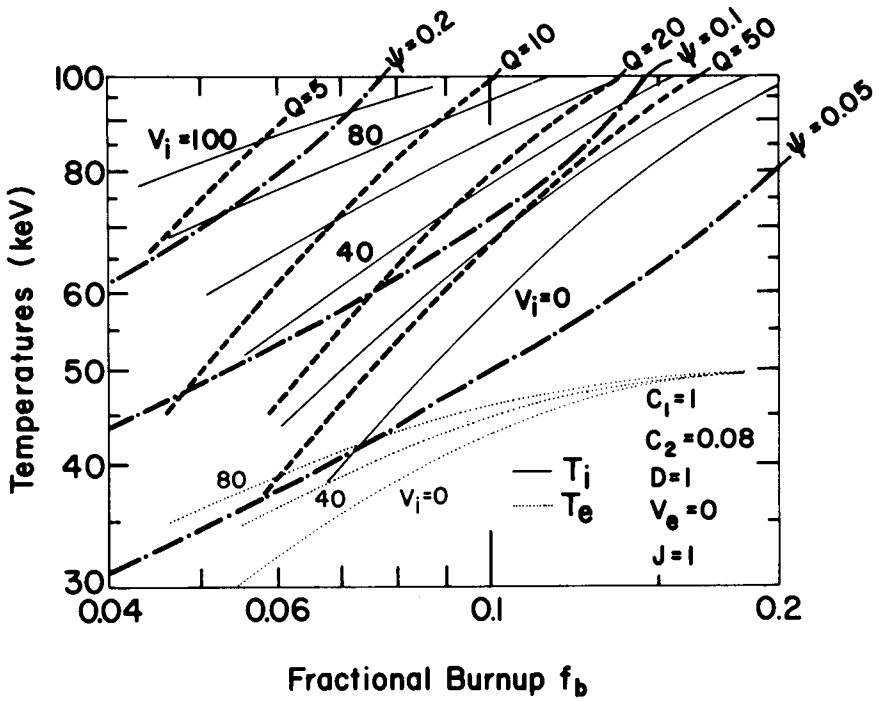

Fig. 3.26. Effect of Ion Heating, and Contours of Constant ψ and Q, for a Plasma Characteristic of Open-Ended Confinement Systems. Low synchrotron radiation, one cold electron injected per ion.

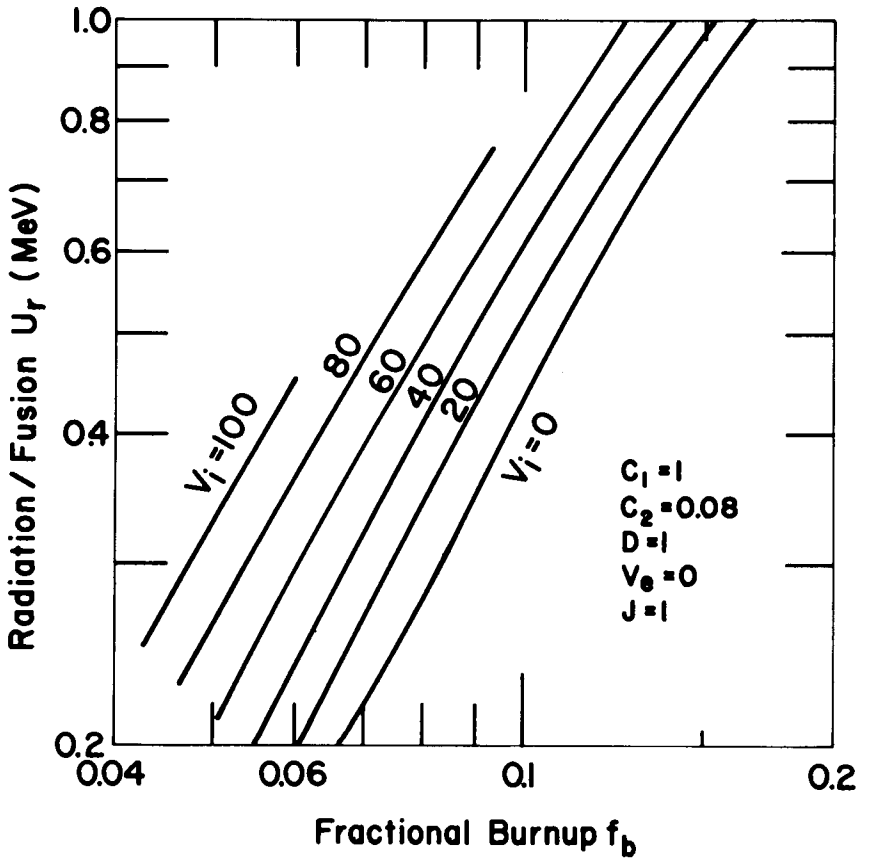

Fig. 3.27. Radiation/Fusion U_r vs Burnup for the Plasma Parameters Illustrated in Fig. 3.26.

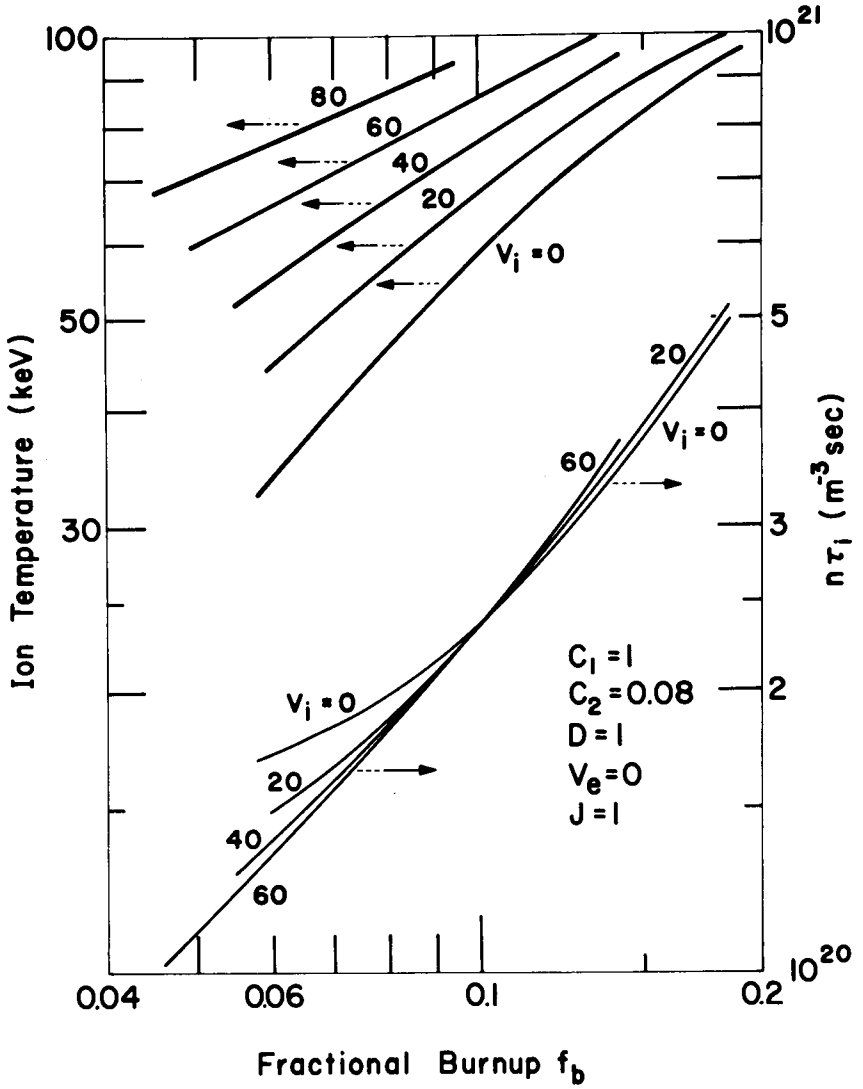

Fig. 3.28. "Containment Parameter" $n\tau_i$ for Plasmas Characteristic of Open-Ended Confinement Systems, with Energetic Ion Injection (V_i = 0, ..., 80 keV), and Low Bremsstrahlung.

4. MAGNETIC SYSTEM SCALING AND EFFICIENCY

4.1. Scaling I: Elementary Ideas

Improvements to the plasma model used for these analyses are required, whose nature we have already seen in part. But to keep a balance, attention must be given to the nature of the hardware from which a fusion system could be built.

The analysis of subsequent sections will show that the most desirable systems have minimum dimensions of the order of meters. The magnetic field windings applied to their surfaces have depths small in comparison, so the fields can be thought of as generated by surface currents. To see this, write the Biot-Savart law for field $\vec{B}$ at any interior point $\vec{r}$ as

$$\vec{B}(\vec{r}) = \frac{\mu_o}{4\pi} \int \frac{\vec{j} \times \vec{r}}{r^3} \, dv \quad , \tag{4.1}$$

where $\vec{j}$ is volume current density, and the integral is over volume. By integrating over the conductor depth, which is small compared to $\vec{r}$, we find

$$\vec{B}(\vec{r}) \approx \frac{\mu_o}{4\pi} \int \frac{\vec{k} \times \vec{r}}{r^3} \, ds \quad , \tag{4.2}$$

where $\vec{k}$ and ds are surface current density amp/m and surface area element.

Scaling these large systems from one size to another involves keeping surface current $\vec{k}$ constant at equivalent surface places to maintain $\vec{B}$ constant at equivalent volume places; the fact is evident from Eq. (4.2), where all space-dimensional quantities enter in $\vec{r}ds/r^3$, which is itself dimensionless. As a result, it is often useful to imagine the cost of magnetic material and winding as being some amount per unit area of surface, a function only of the field increment demanded across the surface.

The structural reinforcement to take up the magnetic stress will not scale so simply, however.

In considering magnetic designs, many complicated rules can be invoked to assist. For our approximate purpose, elementary ones are useful. For instance, shear and stabilizing coils can be crudely likened to a set of parallel conductors spaced a distance d apart in a plane, adjacent ones carrying opposite current. For such systems, the field falls off in direction x away from the plane as $\exp(-\pi x/d)$ for the spatial fundamental, and as $\exp(-n\pi x/d)$ for the nth spatial mode. Stabilizing effect is evidently small beyond one conductor spacing from the plane. If the stabilizing field required can be adequately described as the field at the plane itself, or at some distance from the plane measured in conductor spacings, then the magnetic material cost is independent of the conductor spacing (for closer conductors, more are required, each with proportionately less current to produce the field at shorter distance). Unfortunately, the field at some fixed distance from the stabilizers is more often required; hence cost increases as the complexity increases.

4.2. Material and Operating Cost of Magnetic Surfaces

Before taking up more complicated problems of system scaling, first consider a very basic thing: the cost of constructing a simple magnetic surface without mechanical reinforcement. To make the surface with increment B, the surface current k is B/μ_o amp/meter, which is more usefully expressed for our purpose as B/μ_o amp-m/m^2. Thus we develop the cost of magnetic surface per unit area.

(a) Superconducting Windings

The cost dollars/meter^2 for a number of things will appear, for which we choose the symbol λ, and add a subscript when the attribution is not clear otherwise.

Assume that an adjusted material cost will cover assembly as well. The cost of the surface in dollars/meter^2 will then be

$$\lambda = B(\$/\text{amp-m})/\mu_o \quad . \tag{4.3}$$

Material cost is usually expressed as mills/amp-ft; thus

$$\lambda = 2610 \left[B \frac{w}{m^2}\right] \left[\frac{\text{mills}}{\text{amp-ft}}\right] \quad . \tag{4.4}$$

The current-carrying capacity of superconducting material varies approximately as 1/B, over the useful range 3 - 10 weber/m^2. Thus take 7.5 weber/m^2 as an arbitrary standard, and write for material cost

$$\frac{\text{mills}}{\text{amp-ft}} = \zeta \frac{B}{7.5} \quad , \tag{4.5}$$

and for the surface cost

$$\lambda = 348\ \zeta \left[B \frac{w}{m^2}\right]^2 \$/m^2 \quad . \tag{4.6}$$

At present (April 1968) $\zeta \approx 3$ mills/amp-ft for material alone, giving $\$/m^2 = 1050\ B^2$. Such a number should allow also for construction costs in far future systems; surely \$26,000/m^2 at 5 weber/m^2 will permit much construction.

In this chapter, operating (refrigeration) cost of the superconducting magnet will be ignored as small.

(b) Conventional Windings

To calculate conventional winding cost, a rough analysis is required. The conductor thickness is t_c(meter), and again the surface current is B/μ_o amp/m. Costs of material, construction and operation (an equivalent capital charge) appear. The weight is 2200 t_c ρ lb/m^2, where ρ is density (Cu = 8.96, Al = 2.7). Try Cu at \$1.00/lb, winding cost proportional to B, being \$1/lb at 5 weber/m^2. The initial cost then becomes

$$\lambda = 19{,}700\ t_c \left(1 + \frac{B}{5}\right) \quad , \tag{4.7}$$

but the larger operating cost must be added. This latter is $\eta B^2/\mu_o\ t_c$ watt/m^2, where η is resistivity. For $\eta_{Cu} = 1.72 \times 10^{-8}$ Ω-m, and a 7000-hour operating year, we have

$$\frac{\text{kwh}}{\text{year}} = 76{,}300\ B^2/t_c \quad . \tag{4.8}$$

To convert Eq. (4.8) into equivalent capital cost, we require a cost of power, and interest rate. This study is concerned with the feasibility of producing $\approx$ 3 mill/kwh power, so take that number. For interest, choose a high rate — 14% — which is the most favorable for use of copper. The effective capital cost for power then is

$$\lambda = 1630\ B^2/t_c \quad . \tag{4.9}$$

The total cost is the sum of Eqs. (4.7) and (4.9), to be minimized by adjusting t_c. For these charges, the answer is

$$\lambda|_{Cu,min} = 5660\ B \left(1 + \frac{B}{5}\right)^{1/2} \tag{4.10}$$

and the very considerable thickness is $0.287\ B \left(1 + \frac{B}{5}\right)^{-1/2}$.

In large sizes, Al might be less expensive. If we take the optimistic material cost \$0.50/lb, winding cost \$0.66 B/lb (the same per unit volume as was assumed for Cu), $\eta = 2.82 \times 10^{-8}$ Ω-m, and power and interest charges as before, the cost is

$$\lambda = 2960\ t_c(1 + 1.33\ B) + \frac{2670\ B^2}{t_c} \quad . \tag{4.11}$$

The first term represents initial investment (less than for Cu) and the last represents operation. For this system

$$\lambda|_{Al,min} = 2810\ B(1 + 1.33\ B)^{1/2} \quad . \tag{4.12}$$

(c) Comparison of Superconducting and Room Temperature Windings

At fields in the vicinity of 5 w/m^2, the above costs are (if $\zeta = 3$)

$$\left.\begin{aligned} \lambda|_{supercon} &= 26{,}000,\ t \approx 0.05\ m \\ \lambda|_{Cu} &= 40{,}000,\ t \approx 1.02\ m \\ \lambda|_{Al} &= 39{,}000,\ t \approx 1.72\ m \end{aligned}\right\} \quad . \tag{4.13}$$

The disparity between the superconducting and conventional systems is larger than the apparent costs indicate; a winding thickness of 1-2 meter poses very severe construction problems and making the coil much thinner increases the operating cost substantially. Aluminum is attractive for low duty cycle devices, but not for the continuous operation we have in mind.

In the large sizes to be considered, neither superconducting nor conventional windings would be expected to take the mechanical stress. Thus a similar amount of reinforcement will be required for all systems. To be sure, suspending large amounts of material at cryogenic temperature

is more costly than supporting it at 300°K; but we will guess that the excess cost will not nullify the advantage appearing in Eq. (4.13) in favor of superconducting material.

In what follows, we assume the systems to be superconducting, and will eventually use Eq. (4.6) to compute costs.

4.3. Scaling II: Parameter Variation and System Size

In any economically attractive fusion system, a number of conditions must all be met: high heat transfer through vacuum walls, good tritium breeding, reasonable magnetic field cost, etc. The magnetic costs are high enough, and the possible configurations diverse enough, that it is useful to look at the magnetic system especially, making simple assumptions about other parts and functions of the device.

To give substance to the discussion, imagine very simple systems, consisting of plasma that produces power, and magnetic material on a peripheral surface that costs money. Space occupied by moderator, etc., is ignored, along with its cost. However, there is a limiting energy flux $\mathcal{S}$ watt/meter^2 through the wall (1 watt/m^2 = 0.318 BTU/hr ft^2). For simplicity we imagine that all the energy flows this way, even though some nuclear heat is developed in the moderator. Only part of $\mathcal{S}$ is absorbed in the wall and must be handled there, a circumstance that we kept in mind in Chap. 3, and will return to at a later time.

Some general relations are necessary. In calculating the ratio β of material to magnetic pressure, we set $T_e = T_i = T$, neglect p_α, and work with the vacuum magnetic field B_o at the place where the plasma is to be contained. Then, with $n_e = n_i = n$, we have

$$n = \frac{\beta B_o^2}{4\mu_o kT} \quad . \tag{4.14}$$

The nuclear burning rate w_n is then for the D-T reaction

$$w_n = \frac{n^2 \langle \sigma v \rangle U_n}{4} = \frac{\beta^2 B_o^4 U_n \langle \sigma v \rangle}{64 \mu_o^2 k^2 T^2} \frac{\text{watt}}{m^3} \quad ; \tag{4.15}$$

here U_n is energy/fusion.

Because the total power depends on the volume, and the magnetic cost depends on the surface, the magnetic costs, as here defined, can be made satisfactorily small if the system is large enough and other problems (e.g., heat transfer) did not supervene. The question is: how large? Size is no disadvantage if the system should be that size. Thus in the following examples, we imagine that some cost dollars per kilowatt thermal ($/kwt) can be allowed for the material described by Eq. (4.6), and calculate the necessary total power under general circumstances.

Two simple configurations can be calculated easily. The first is a sphere with plasma radius r_p, when $B = B_o$, and wall (or winding) radius r_w, where $B = B_m$. This extreme case corresponds roughly to some fat open-ended systems. The second is a long cylinder with evident parameters r_p, B_o, r_w, and B_m; the length is L, and we neglect end effects. This device, if wrapped in a circle, is the archetype of closed magnetic systems. Most configurations of interest fall between these limits; if both models give similar answers, we feel that the results will have some generality.

For both cases, from Eq. (4.6)

$$\frac{\$}{\text{kwt}} = 0.348 \, \zeta \, B_m^2 / \mathcal{S}^* \quad , \tag{4.16}$$

where $\mathcal{S}^*$ is megawatts/m^2. For the sphere, the total power is

$$W = \frac{4\pi}{3} r_p^3 w_n = 4\pi r_w^2 \mathcal{S} \quad . \tag{4.17a}$$

For the cylinder,

$$W = \pi r_p^2 \, L \, w_n = 2\pi \, r_w \, L \, \mathcal{S} \quad . \tag{4.17b}$$

In each case, the right sides of these equations can be used r_w; thus

$$r_w = \frac{3\mathcal{S}}{w_n}\left[\frac{r_w}{r_p}\right]^3 \qquad \text{(sphere)} \quad , \tag{4.18a}$$

$$= \frac{2\mathcal{S}}{w_n}\left[\frac{r_w}{r_p}\right]^2 \qquad \text{(cylinder)} \quad , \tag{4.18b}$$

and

$$W = \frac{36\pi \, \mathcal{S}^{*3}}{w_n^{*2}}\left[\frac{r_w}{r_p}\right]^6 \quad \text{Mw (sphere)} \quad , \tag{4.19a}$$

$$W = \frac{8\pi \, \mathcal{S}^{*3}}{w_n^{*2}}\left[\frac{r_w}{r_p}\right]^4 \left[\frac{L}{r_w}\right] \quad \text{Mw (cylinder)} \quad . \tag{4.19b}$$

Here all quantities are to be in megawatt units. w_n^* is now eliminated from Eq. (4.15), using suitably modified units, and the field from Eq. (4.16). The total power becomes

$$W = \frac{6.8 \times 10^{15} \, \mu_o^4}{U_n^2 \, \mathcal{S}^*}\left[\frac{k^2 \, T^2}{\langle\sigma v\rangle}\right]^2 \left[\frac{\zeta}{\beta\$/kwt}\right]^4 \left[\frac{B_m}{B_o}\right]^8 \left[\frac{r_w}{r_p}\right]^6 \text{Mw (sphere)} \quad , \tag{4.20a}$$

$$W = \frac{1.51 \times 10^{15} \, \mu_o^4}{U_n^2 \, \mathcal{S}^*}\left[\frac{k^2 \, T^2}{\langle\sigma v\rangle}\right]^2 \left[\frac{\zeta}{\beta\$/kwt}\right]^4 \left[\frac{B_m}{B_o}\right]^8 \left[\frac{r_w}{r_p}\right]^4 \left[\frac{L}{r_w}\right]$$

$$\text{Mw (cylinder)} \quad . \tag{4.20b}$$

Note the similarity in the systems.

Equations (4.20) must be put into simpler form. U_n is here measured in joules: 3.58×10^{-12} joule (22.4 MeV). The appearance of $\langle\sigma v\rangle/T^2$ shows our neglect of most of the contents of Chap. 2 for it, we take

$$\frac{\langle\sigma v\rangle}{T^2} = F \left[\frac{\langle\sigma v\rangle}{T^2}\right]_{max} , \tag{4.21}$$

where the maximum value 1.16×10^{-24} m^3 sec^{-1} keV^{-2} occurs at 14 keV. After more algebra, find

$$W = \frac{0.645}{\mathscr{S}^* F^2} \left[\frac{\zeta}{\beta\$/kwt}\right]^4 \left[\frac{B_m}{B_o}\right]^8 \left[\frac{r_w}{r_p}\right]^6 \quad Mw \text{ (sphere)} , \tag{4.22a}$$

$$W = \frac{0.143}{\mathscr{S}^* F^2} \left[\frac{\zeta}{\beta\$/kwt}\right]^4 \left[\frac{B_m}{B_o}\right]^8 \left[\frac{r_w}{r_p}\right]^4 \left[\frac{L}{r_w}\right] \quad Mw \text{ (cylinder)} . \tag{4.22b}$$

These are the working equations, pro tem; they are identical, except for a factor 9/2 and the replacement of $(r_w/r_p)^2$ by L/r_w.

These are strong and surprising dependences. An example of how they come about is helpful. Suppose there is a spherical fusion system, in which r_w/r_p has some fixed value. Then let us see what we must do if this ratio were to be doubled, keeping \$/kwt, $\mathscr{S}^*$, etc., constant. In order to preserve $\mathscr{S}^*$ we must quadruple the flux through the plasma surface, because of the fourfold area change. But this flux through the plasma surface increases linearly with radius; thus plasma radius increases fourfold, total power goes up as r_p^3, and we have a factor 2^6. Similar reasoning explains the other dependences.

As predicted, Eqs. (4.22) show that every disadvantage (poor reaction rate, poor use of field, etc.) can be overcome if the system is large

enough. Nevertheless, there are limits, and we must see what Eqs. (4.22) portend. At one extreme, choose a very pessimistic system: a low-β baseball-type mirror, approximated by a sphere, with the parameters:

$$T_i = 90 \text{ keV, so } F = 0.1$$

$$\beta = 0.25$$

$$r_w/r_p = 3$$

$$B_m/B_o = 2$$

$$\mathcal{S}^* = 5 \text{ Mw/m}^2$$

$$\zeta = 3 \text{ mills/amp-ft}$$

$$\$/\text{kwt} = 2 \text{ (we are greedy)} \quad .$$

Then Eq. (4.22a) gives $W = 3.12 \times 10^9$ Mw thermal, a factor about 10^5 too large.

But things are not all that bad. For a more optimistic design, with $\beta = 0.5$, $r_w/r_p = 1.5$, $B_m/B_o = 1.4$, \$4/kwt, and T_i and ζ the same, the total power is reduced by a factor 2^{19}, i.e., to 6000 Mwt. All this took place with moderate parameter changes.

A number of things can be learned from Eqs. (4.22) and these examples. First, and most specifically, it appears that a magnetic mirror that uses the field efficiently may be feasible (from this limited magnetic cost point of view), but an inefficient structure will not be feasible. This means moderately high β, no large mirror ratios, good occupation of the volume by plasma. The prescription is for plasmas that derive part of their stability from digging a diamagnetic hole in the confining field. But it is not the intent here to choose systems so specifically for analysis.

Second, and more generally useful, is the discovery that both spherical and cylindrical systems do not scale very differently, after assignment of appropriate dimensional ratios. Suppose mistakenly we used the cylindrical scaling law for a sphere, and set $L = 2r_w$ as a gross approximation. Upon throwing all the difference between the two equations into different field ratios B_m/B_o, we find that the two field ratios would be

$$\left[0.645(r_w/r_p)^6/0.286(r_w/r_p)^4\right]^{1/8} = 1.1(r_w/r_p)^{1/4} \quad . \qquad (4.23)$$

While the cylindrical configuration has some economic advantage, and F is expected to be desirably closer to unity in a torus than in a mirror (Sections 3.7 and 3.8), bear in mind that the torus is topologically more complicated, and the actual size may be uncomfortably large. Clearly, the systems analysis must be carried further before any such general decision can be reached.

4.4. "Magnetic Disadvantage"

We have the feeling that some properties of these magnetic configurations exist that distinguish more desirable from less desirable ones, at least as they use magnetic material efficiently. Thus we could search for some universal dimensionless parameter to differentiate them. No such quantity appears conveniently and universally in the cost calculations to be made later, but the idea is qualitatively useful: something we call magnetic disadvantage, looking for a better term.

In Eqs. (4.22), it might be the quantity $M_1 = (B_m/B_o)(r_w/r_p)^{3/4}$, for a sphere, that is raised to the eighth power; or the quantity $(B_m/B_o)(r_w/r_p)^{1/2}\ (L/r_w)^{1/8}$, for a cylinder. The difference is not large,

and the numerical factors in Eqs. (4.22) are of little account. To the extent that these quantities can be identified in real systems, we can make approximate figures of merit for them.

If the L/r_w dependence is ignored as small, the ideal standard of comparison would be a long uniform solenoid, filled with plasma, for which $B_m/B_o = r_w/r_p = 1$. For all other configurations the product is larger.

A second hopefully related figure of merit can be obtained for any real system, defined as

$$M_2 = \left[\frac{\mu_o \int jdV}{B_o \int ds_p}\right]\left[\frac{\int ds_p}{\int ds_w}\right]^n \quad . \tag{4.24}$$

The first bracket is μ_o times the number of ampere-meters ($\int jdV$) required to make unit area of plasma surface ($\int ds_p$) at the minimum interior field B_o. This quantity is unity for a simple long solenoid filled with plasma, and is very large for configurations that use field poorly. The second bracket is a partial compensation for the first: configurations for which $\int ds_p$ is small use field poorly, but some amelioration of heat transfer difficulties can be achieved because the vacuum walls of area $\int ds_w$ are remote.

The quantities M_1 and M_2 (n = 0) and M_2 (n = 1/2) have been calculated for several configurations, where minor poetic license has been taken in the assignment of typical dimensions. Some details of the calculations are given in Appendix II. The case n = 1/2 corresponds to factoring in the average plasma radius divided by the average wall radius as an advantage. Results are shown in Table 4.1, with numbers calculated in Appendix II rounded off.

We see that different ways of computing a disadvantage criterion give different results, but the trends persist.

Table 4.1.

Disadvantageous Criteria for Various Magnetic Configurations

Configuration	M_1	M_2 (n = 0)	M_2 (n = 1/2)
Simple solenoid	1	1	1
Torus, filled with plasma	1	1	1
Spherator	2.6	2.3 - 3.7*	1.6 - 2.6*
Spherator, operating as Tokamak	2.6	2.9	2.0
Simple 2.5:1 ratio mirror	2.9 - 3.2†	5.5 - 6.9†	4.5 - 5†
Strongly stabilized (4-bar) 2:1 mirror	4.5	40	14

*Depending upon whether or not area surrounding levitated wire is useful.

†Depending upon assumptions of useful volume.

If a spherator-like configuration could be made with the central conductor supported from the outside, or a quasi-steady-state min-B Tokamak could be made at all, they would apparently be quite efficient in use of magnetic material. Simple magnetic mirrors can be fairly efficient, if much of the interior volume can be utilized. In these examples, the field at the center is B_o, and the calculation pertained to using volume out to radial distance where $B = 0.75\ B_o$, or alternately $B = 2\ B_o/3$; by any standards, those are optimistic estimates of useful volume. The 4-bar stabilized mirror (and presumably also a baseball) is a very inefficient user of field, because the plasma volume out to the

last closed field magnitude contour is small. If such stabilization is indeed required, there will be severe disadvantage. Further calculations (not given here) show that reducing the stabilizing currents reduces the ampere-turn costs, but also reduces the plasma volume, so there is no marked improvement. Increasing the stabilizing bar current appreciably makes for very high field cost, with little compensating volume increase. Thus the numbers in the table are probably typical.

5. SYSTEM ENGINEERING

5.1. General Vacuum Wall and Moderator Design

The earlier designs summarized in Sec. 1.2 have been superseded. More realistic and efficient configurations are being analyzed by A. P. Fraas and D. Steiner of ORNL Reactor Division. This short chapter is a progress report; it introduces the content of Appendices III and IV, written by Fraas.

The ideal vacuum wall would have: low neutron absorption; low inelastic cross section, except for (n,2n); high heat transfer; high strength; easy fabricability; good resistance to both radiation and corrosion damage; and low cost. The moderator would have: high neutron absorption in Li^6 and little in anything else; large (n,2n) cross section and little (n,γ) etc. cross section; high heat removal capability; and low cost. Other desiderata can be imagined.

The principal difficulties with the Mo – $(LiF)_2BeF_2$ – C scheme of Sec. 1.2 are:

(1) Mo is hard to fabricate.

(2) The fluorine has large inelastic scattering, which gives [a] a large γ-ray backshine on the vacuum wall and consequent heat deposition there, and [b] a reduction in beneficial Be(n,2n)2α reactions.

(3) Heat transfer to the fused salt is fairly good, but more is desired.

The present concept is of a niobium cellular wall, probably cooled by liquid lithium flowing along field lines. See Figs. A-3.4 and A-4.7 of Appendices III and IV. Behind that is a beryllium or BeO (or Be_2C if

it can be made) pebble-bed moderator, possibly containing graphite balls also. Either $(LiF)_2$ BeF_2 or liquid lithium cools it, whence the inventory is either reduced or eliminated. Pumping power for lithium is reasonable, provided the flow path does not cross the magnetic field often. Behind these Nb-Be-Li regions are a graphite moderator, a lithium mop-up region for slow neutrons, the coil shield, and the coils. This structure will give much less γ-backshine per fusion event than any of those analyzed by Impink or Homeyer, and permits higher heat transfer from the vacuum wall. In addition, all the electromagnetic radiation will be absorbed on surfaces facing the plasma, and the backshine will mostly be absorbed on interior surfaces. Thus the vacuum wall heating has been somewhat distributed.

For this or similar designs, we take as attainable a total fusion power of 10 Mw (thermal)/m^2 incident on the wall. About 1 Mw/m^2 of this might be bremsstrahlung plus synchrotron radiation, and about 0.5 Mw/m^2 might be a combination of γ-ray absorption plus direct neutron inelastic scattering. If the plasma radiation can be reduced without penalty elsewhere, the total incident power can be correspondingly increased. A series of configurations based on Fig. A-4.7 are now being analyzed for tritium production, leakage, energy deposition, and so forth.

Cost of these vacuum wall-moderator combinations has been estimated only very approximately. The example by Fraas in Table A-3.1 comes to \$61,000/m^2, including the magnet. If the vacuum wall energy flux is 10 Mw/m^2, the total heat generation will be 12.75 Mw/m^2, because of 4.8 MeV neutron absorption in Li^6. Thus with 50% conversion efficiency, cost of this fusion system "core" would be \$9.5/kwe, a remarkably low number. We shall calculate numerical cost trends in the next chapter.

Preliminary study shows that niobium will be much superior mechanically to molybdenum, and may have as good nuclear properties. The cost of beryllium, another substantial item, is liable to decrease considerably with time.

5.2. Plasma Injection and Pumping

No simple solution either to the plasma injection and pumping problems appears, but some useful remarks can be made.

For closed magnetic systems, where we have discovered more plasma heating than we want, a simple injection scheme will almost work: throw in small pellets of frozen deuterium or tritium. For the plasma sizes to be discovered, the pellets will be evaporated before they pass through. The difficulty with the scheme comes from the fact that at 10-20 keV plasma energy, the lifetime of an atom against charge exchange is only about one-third of that against ionization by all methods. Thus the injected cold neutral atom usually becomes a cold ion, and an energetic atom leaves. The energy loss may be tolerable, even though it is ion energy: we have seen the effects of electron-ion heat transfer, and of enhancing electron radiative loss to alter the operation. More importantly, tritium might be lost into the vacuum wall, to give an intolerably large inventory there. At the operating temperatures envisaged, hydrogen (i.e., D or T) embrittlement and such classical problems do not appear serious. If the scheme is to work, it appears that the outermost wall layer must be thin, to give rapid tritium diffusion. Also the return flow of gas into the vacuum from the walls may cause problems.

Discussion of the particle flux onto the wall reminds us that sputtering by D and T fast atoms or ions can be a serious problem. Niobium

resists sputtering by low energy helium and neon ions exceptionally well, and is used for long-life gas-filled tubes on that account. Sputtering data, as well as diffusion rates through the metal and from the free surface need to be obtained for our expected operating conditions.

From systems using energetic ion injection, the results of Sec. 3.8 show that we need very efficient injectors. Reionization of a medium-energy neutral beam by the plasma appears possible, but uncertain. Lorentz ionization of excited atoms seems much less likely to be efficient.

Anent the plasma pumping problem, Fraas suggests use of a liquid lithium sheet, which absorbs deuterium and tritium very well. One of the difficulties is that a significant fraction of the fusion heat appears at the plasma pump: 20% of the heat, less the amount radiated or charge transferred to the vacuum wall. From this point of view, we see the advantage of encouraging the plasma to radiate as much energy as possible onto the large area of vacuum wall, as long as the plasma is not too much cooled thereby.

5.3. Magnetic Structure Support

Previous designs have visualized the superconducting magnets to be held in hoop tension (or some more complicated stress configuration) by stainless steel at 4°K. Fraas points out that titanium will be much better: present cost of plate is \$2/lb, and will soon be about \$1/lb. It is easier to machine than stainless steel, has two-thirds the density, and twice the working strength (10^5 psi) at 4°K. Fabricated cost of titanium will be taken as \$2/lb., which makes it about one-quarter or less the price of stainless steel, for equivalent tasks.

5.4. Radiation Damage, Tritium Recovery, Maintenance, and Other Topics

Many important topics, including the ones listed above, are now (April 1968) receiving some consideration at ORNL and elsewhere; we have nothing new to report at this time.

6. COSTS AND CONCLUSIONS

6.1 Development of a Cost Formula

The main parts of the fusion reactor "core" have been identified in previous chapters; they will be combined to form a generalized cylindrical system with parameters

Vacuum wall radius r_w meters

Coolant plus moderator thickness d meters

Vacuum field at plasma = B_o

Maximum field at windings = B

and others to be mentioned later. End effects, in case of an open-ended system, are to be ignored.

Our purpose is to combine the simplified separate parts into a formula, which is in words

$$\frac{\$}{\text{kwt}} = \frac{\dfrac{\text{cost \$}}{\text{meter length}} \text{ of [vacuum wall + moderator + magnet + support]}}{\dfrac{\text{power kwt}}{\text{meter length}}} . \qquad (6.1)$$

Consider first the numerator. Under "vacuum wall" we include all the niobium wall-like structure shown either in Fig. A-3.4 or Fig. A-4.7. In either design, the amount of niobium is about the same, for nuclear reasons: only the structural complexity differs. The material cost at \$20/lb. considerably exceeds the fabrication cost for any such system, at least for devices with vacuum wall radius $r_w < 10$ meters. For $r_w > 10$ m, analysis becomes speculative. Thus from Table A-3.1, we take the total niobium cost of \$15, 120/m^2 as a fixed wall cost/m^2, and set

$$\$/m \Big|_{\text{wall}} = 2\pi r_w \lambda_w = 95{,}000\ r_w \ (\$/m). \qquad (6.2)$$

The moderator requires division into several parts to show the cost properly, but the fact that $r_w >> d$ allows us to ignore location inside the moderator. Thus the volume/meter is $\pi\left|(r_w+d)^2 - r_w^2\right| = \pi(2r_w d + d^2)$, and consists of three parts. A fraction f_1 is filled with expensive material (e.g., Be), a fraction f_2 is filled with inexpensive graphite, and a fraction $1-f_1-f_2$ has inexpensive shielding in it. The product of specific gravity ρ and cost ($/lb) enters often enough to warrant the symbol

$$\mu_1 = \rho_1(\$/lb)_1 \tag{6.3}$$

for the material in fraction f_1, etc. In these units, it is easy to check that

$$\$/m \Big|_{moderator} = 6930(2r_w d + d^2)\,[f_1\mu_1 + f_2\mu_2 + (1-f_1 - f_2)\mu_3] \tag{6.4}$$

Typical values of μ_1 might be

BeO	45
C	1.8
$(LiF)_2\ BeF_2$	7.5
Outer Shield	2.0
Be	100 .

The magnetic material and winding cost, from Eq. (4.6), is

$$\$/m \Big|_{coil} = 2190(r_w+d)\zeta\ B_m^2. \tag{6.5}$$

To hold the magnetic stress, we assume that $B_m^2/2\mu$ acts as a bursting force to be held in by a band of material stressed to S_{psi}. For this

support material, the cost x specific gravity product is μ_s. The cost becomes

$$\$/m\Big|_{\text{support}} = \frac{8.05 \times 10^5 (r_w+d)^2 B_m^2 \mu_s}{S_{psi}} \tag{6.6}$$

For stainless steel, $\rho \approx 8$, \$/lb ≈ 2.5, and $S_{psi} = 50{,}000$, and μ_s/S_{psi} 4×10^{-4}. For titanium $\rho = 4.54$, \$/lb ≈ 2.0 and $S_{psi} = 100{,}000$; thus $\mu_s/S_{psi} \approx 9 \times 10^{-5}$, and there is a substantial advantage to using titanium.

The power kwt/m in the denominator of Eq. (6.1) will be expressed in terms of the permissible total energy flux/unit area $\mathcal{S}$ incident on the vacuum wall. The total flux is $2\pi r_w \mathcal{S}$, whence Eq. (6.1) becomes

$$\frac{\$}{kwt} = \Big\{ r_w \lambda_w + 1100(2r_w d + d^2)[f_1\mu_1 + f_2\mu_2 + (1-f_1-f_2)\mu_3] + 348(r_w+d)\zeta B_m^2 + 1.28 \times 10^5 (r_w+d)^2 B_m^2 \mu_s/S_{psi} \Big\} \Big/ r_w \mathcal{S} . \tag{6.7}$$

The plasma parameters do not enter at this stage. For a given maximum field B_m, moderator thickness d, costs μ, fractions f_1, f_2, stress S_{psi}, and wall load $\mathcal{S}$ watt/m^2, we can find the wall radius r_w for minimum cost, and the cost itself. The radius for minimum cost is

$$(r_w^*)^2 = d^2 + \frac{\Big\{ 348d B_m^2 + 1100 d^2 [f_1\mu_1 + f_2\mu_2 + (1-f_1-f_2)\mu_3] \Big\} S_{psi}}{1.28 \times 10^5 B_m^2 \mu_s} . \tag{6.8}$$

Within the limits of this model, Eq. (6.8) gives the vacuum wall radius, and Eq. (6.7) the cost of the system with minimum \$/kwt. Whether the size is reasonable or whether the plasma can be confined and questions to be asked separately.

The plasma enters this computation through the appearance of the assumed heat deposition

$$\mathcal{S} = \frac{\int_0^{r_w} 2\pi r[n_i(r)]^2 \langle\sigma v\rangle U_n dr/4}{2\pi r_w} \tag{6.9}$$

on the vacuum wall. The integral is of the burning rate, which varies with radius because n_i is a function of radius. If

$$n_i(r) = n_o J_o(2.4\ r/r_w) \tag{6.10}$$

corresponding to simple radial diffusion, then

$$\int_0^{r_w} n_i^2(r)\ 2\pi r dr = 0.269\ \pi r_w^2\ n_o^2\ . \tag{6.11}$$

We imagine being more efficient, and set the integral of Eq. (6.11) equal to $0.5\ \pi r_w^2\ n_o^2$: i.e., we can equivalently fill half the vacuum space with maximum density plasma. Equation (6.9) now becomes, with the help of Eq. (2.8)

$$\mathcal{S} = r_w\ \beta^2\ B_o^4\ P\ U_n/256\ \mu_o^2. \tag{6.12}$$

The units of these equations can be confusing. Equation (6.12) is MKS, but we wish to use P from Fig. 2.3 (m^2/sec keV^2) and assign U_n = 22.4 MeV to include the neutron absorption energy. It can be checked that the

proper form of Eq. (6.12) is

$$\mathcal{S} = 3.46 \times 10^{29}\, r_w\, \beta^2\, B_m^4 \left(\frac{B_o}{B_m}\right)^4 P^* \qquad (6.13)$$

where P^* is to be read from Fig. 2.3. The appearance of $(B_o/B_m)^4$ and our discussion about how the plasma fills the available space represents yet another way of figuring the efficiency of the confinement configuration.

The plan is to specify material parameters appearing in Eq. (6.8), plus a reasonable magnetic field, then calculate r_w^* for minimum cost. After assuming a value for $\mathcal{S}$, we find the cost from Eq. (6.7). Finally, fixing magnetic field ratio B_m/B_o and reaction parameter P fixes the required β from Eq. (6.13).

6.2 Cost Examples

In the examples to follow, we choose

$$\lambda_w = 15{,}120$$
$$d = 1 \text{ meter}$$
$$f_1 = 0.15$$
$$\mu_1 = 45 \text{ (BeO)}$$
$$f_2 = 0.4$$
$$\mu_2 = 1.8$$
$$\mu_3 = 2$$
$$\zeta = 3$$
$$\mu_s/S_{psi} = 9 \times 10^{-5}$$
$$\mathcal{S} = 10^7 \text{ watt/m}^2$$

unless otherwise specified.

Table 6.1 shows the size, cost and required β for a number of maximum field strengths B_m, under the two assumptions $B_m/B_o = 2$ or 3, and $P^* = 2 \times 10^{-25}$ m^3 sec^{-1} keV^{-2}. Besides the large size, which we discuss in a moment, the most striking thing about the results is the reduction of cost at lower field and higher β. This is an important general conclusion, and the reasons for it are simple: First, the magnet is expensive, and it is advantageous to replace high field cost by low field cost and low plasma density for a large size, to keep the wall loading constant; second the superconducting material's increased current capacity at low field accentuates this large size — low field trend. The fourth column of Table 6.1 shows this magnetic cost reduction clearly.

Consider now the size. Wrapped into a torus it is too large, but as an open-ended system it is attractive, hence our choice of P^* in calculating columns 5 and 6. If the effective system length is 1.5 times the diameter, then the 12 m radius device found here yields some 27,000 Mw thermal, which is acceptable for far future applications. Implicit in these calculations is the necessity of obtaining enough confinement time to satisfy the criteria described in and about Figs. 3.24 - 3.26. The high β case with $B_m \gtrsim 4$ weber/m^2 in Table 6.1 might satisfy the requirement of large effective mirror ratio; whether stability can be achieved is not known.

Note the effect of requiring increased field ratio B_m/B_o. For a given field B_m, cost is not affected; but the required β increases substantially and we are forced out of the low field region into considerably more expensive magnetic structures.

Table 6.1. Fusion System Parameters for Minimum Cost $/kwt

Max Field B_m weber/m^2	Vacuum Wall Radius r_w m	$/kwt	Magnet Material Fractional Cost	$\beta^\dagger$ ($B_m/B_o = 2$)	$\beta^\dagger$ ($B_m/B_o = 3$)
10	10.4	15.4	.68	.149	.336
8	10.7	11.7	.63	.230	.515
6	11.1	8.1	.51	.400	.90
5	11.6	6.7	.42	.564	-
4	12.3	5.5	.34	.857	-
3	13.9	4.6	.22	-	-

†for $P^* = 2 \times 10^{-25}$ m^3 sec^{-1} keV^{-2}

Table 6.2. Fusion System Parameters for Fixed Vacuum Radius $P = 2 \times 10^{-25}$ m^3 sec^{-1} keV^{-2}, and $B_m/B_o = 2$.

B_m	r_w = 5m		r_w = 2m	
	$/kwt	β	$/kwt	β
10	16.9	.215	20.1	.315
8	12.0	.336	13.6	.53
6	8.25	.60	9.6	.94
5	6.90	.80	7.9	-
4	5.8	-	6.4	-
3	4.7	-	5.3	-

Varying the parameters shows a number of additional important effects. The unit cost at fixed B_m increases only a little if the radius is chosen quite far from the minimum-cost value r_w^*. Table 6.2 shows the effect of choosing r_w = 5 and 2 m. Again, the penalty comes in the required value of β. For example, at constant $\beta = 0.6$, we interpolate from the tables that the cost rises from \$6.5/kwt at r_w = 11.6 m to \$8.25/kwt at 5.0 m, to \$12.5/kwt at 2.0 m, all for $B_m/B_o = 2$. Even so, this latter value is not unthinkable, and the system produces just 750 Mw thermal. If open-ended systems can operate, the penalty for demanding moderate size is not high.

In the examples just completed, the cost \$/kwt depended not at all upon the model; and the plasma parameters entered only in the choice of P. Thus for a closed system, the unit costs will be the same, but the larger reaction parameter lowers the required β; and the total power output will be larger because of the less favorable aspect ratio. Table 6.3 shows in column 2 the same unit cost as before, for a 5 m wall radius system, and in column 3 the reduced β permitted by our choosing $P^* = 1 \times 10^{-24}$ $m^3\ sec^{-1}\ keV^{-2}$.

Table 6.3 also shows the effect of allowing less nuclear heat flux per unit wall area. At constant B_m, the cost is increased in proportion; but the required β varies as $\mathscr{L}^{1/2}$ because less reaction rate is required. Observe that decreasing $\mathscr{L}$ permits operation at lower B_m for the same β, but the unit cost rises: at $\beta = 0.27$, for instance \$/kwt rises from 8.25 for $\mathscr{L} = 10^7$ to 13.8 for $\mathscr{L} = 5 \times 10^6$. The penalty is moderate.

Table 6.3. Parameters of "Closed" Systems with $r_w = 5$ m, $P^* = 1 \times 10^{-24}$, $B_m/B_o = 2$

B_m	$\mathcal{S} = 10^7$ watt/m^2		$\mathcal{S} = 5 \times 10^6$ watt/m^2	
	Cost $/kwt	β	Cost $/kwt	β
10	16.9	0.096	33.8	0.068
8	12.0	0.150	24	0.106
6	8.25	0.27	16.5	0.19
5	6.90	0.38	13.8	0.27
4	5.8	0.76	11.6	0.54
3	4.7	1.0	9.4	0.72

Table 6.4. Parameters of "Closed" Systems with $\mathcal{S} = 10^7$, $P^* = 1 \times 10^{-24}$, $B_m/B_o = 2$

B_m	$r_w = 2$		$r_w = 1$	
weber/m^2	$/kwt	β	$/kwt	β
10	20.1	0.15	25.5	0.21
8	13.6	0.24	17.9	0.34
6	9.6	0.43	12	0.60
5	7.9	0.61	9.6	0.86
4	6.4	0.95	7.7	-
3	5.3	-	6.2	-

Other variations can be made: increasing B_m/B_o is expensive for closed as well as for open systems.

For a given size and magnetic system the required β scales only as $P^{-1/2}$, which is not so serious a penalty for working at non-optimum conditions as might be imagined.

Adopting considerably smaller radius (r_w = 1 or 2 meters) leads to the higher cost — higher field systems recognizable in some earlier analyses. Table 6.4 shows some of these opportunities to build small but less attractive devices, assuming a high reaction rate parameter $P^* = 1 \times 10^{-24}$ m^3 sec^{-1} kev^{-2}.

6.3 Confinement Time

In this analysis, confinement time in open-ended systems has already appeared as a condition necessary to achieve acceptably low injection power. It now appears again, at the very end, as a requirement for both open and closed magnetic systems.

Greatest enlightenment per unit effort comes by noting that the required confinement time is

$$\tau_i = \frac{2}{n_i \langle \sigma v \rangle} \left(\frac{1}{\frac{1}{f_b} - 1} \right) \tag{6.14}$$

and the anomalous diffusion time is

$$\tau_A = 16A \, \Lambda^2 \, e \, B/kT_e. \tag{6.15}$$

Here Λ is the characteristic diffusion distance. The usual coefficient A expresses how much better the confinement is than simple Bohm diffusion.

For the two to be equal

$$A = \frac{k\, T_e\, f_b}{8\, e\, n\, \langle\sigma v\rangle\ (1-f_b)\Lambda^2\, B} \quad ; \qquad (6.16)$$

for the first time, the actual ion density appears. Equation (6.16) gives the number of "Bohm times" required. Because $\Lambda \sim r_w$, we expect these large systems to present less confinement problems.

The order of magnitude of the quantity A is important, and we choose an example from the previous work corresponding to a toroidal system with: $T_e = T_i = 15$ keV, $f_b = 0.05$ (from Fig. 3.16), $r_w = 5$ m, $B_m = 5$ weber/m^2, $B_o = 2.5$ weber/m^2, $\beta = 0.38$. The field in Eq. (6.16) will be taken as 3.75 weber/m^2, corresponding to the plasma boundary. The actual D + T ion density in this example is 1.75×10^{20} m^{-3}, from which we find A = 134. The confinement time, expressed this way, exceeds by less than a factor of 10 the confinement obtained already. For correspondingly less burnup the confinement would be reduced. For an open-ended system of (say) twice the diameter but twice the electron temperature, the confinement requirements expressed this way would be less severe.

The relatively "small" systems with r_w equal to one or two meters require very precise suppression of anomalous diffusion.

It is not clear if anomalous diffusion ideas applied here will have validity in such large systems; however, there seems little else upon which to base an extrapolation.

6.4 Conclusions

Some generally interesting things are:

(a) apart from the difficulty of achieving long-time confinement, either open or closed magnetic systems appear economically attractive;

(b) fusion systems will be electrically large and as a result will find little application during the 20th Century;

(c) the size will be physically large;

(d) achieving adequate confinement in open-ended systems will be very difficult but this conclusion is not new; certain high-β configurations (if stable) appear most promising, and work should be directed there;

(e) the magnetic fields required are moderate, and their production appear possible now.

(f) Many important problems remain that could advantageously be worked on now.

The costs in large sizes — 5 to 15 dollars per thermal kilowatt — for the reactor "core", depending upon circumstances and our degree of optimism, speak for themselves. The advantages of a plentiful neutron economy, of easy control, and of inherent safety need no discussion here at length. Pervading all thoughts are ones about stability: perhaps only moderate improvement over that now achieved is necessary.

Many areas in which work is urgently required are easy to see. First, in the plasma area, we identify:

(a) The crucial mirror-loss problem. Can the ion thermalization rate be favorably modified without too much energy expense and without depriving the plasma of α-energy?

(b) For the mirror again, the confinement problem. How small a scattering-out probability can be expected, especially at high β?

(c) For the mirror again, the confinement problem. How high can β be stably raised?

(d) For toroidal systems, the temperature balance problem. Can T_e, T_i, and f_b be beneficially adjusted by control of radiation, or whatever?

(e) For all plasmas, a better computational scheme. The present calculations require much refinement to make computed plasma conditions more believable.

(f) For all plasmas, the degree of anisotropy permitted under various realistic conditions. This is already being done in many stability studies; we have seen possibilities of benefit if the velocity distributions can be controllably non-Maxwellian.

Topics more allied to systems studies and engineering are:

(a) A minor re-study of the D-D cycle. This may seem a peculiar thing to say here but from what has been done here the role of D-D if any might finally be settled. At constant β, the burning rate does not enter alone. For instance, if diffusion can be reduced to some small fraction of "Bohm diffusion" regardless of size, then multiplying each dimension by 3.67 reduces loss rate by 13.3 and multiplies the plasma facing each unit area of wall by 3.67. The product is 50, all of which is potentially available to counteract poor burning rate. At constant heat transfer, power has increased by a factor 13.3; but that may not be disastrous, from what we have seen.

(b) Addition of fissionable or breedable material to the moderator. The disadvantages are recognizable, but the advantages of increased and more uniform power distribution throughout the moderator are real.

(c) A minor re-study of the prospects for direct conversion. In the present models, the charged particle exhaust is a nuisance, and in

some cases the removal of the charged fusion product energy is also a nuisance. This would especially be the case for a D-D reaction.

(d) Study of energy deposition and tritium regeneration in a number of proposed wall-moderator configurations. This work has started now.

(e) Investigation of the fusion cross section at low energy; it is hard to tell how accurate is our present knowledge.

(f) Diffusion of D and T in and recovery from metals of interest, from lithium, and from other materials.

(g) Design of plasma injection and pumping systems suitable for fusion (none exist now).

(h) Radiation damage under proposed fusion conditions.

(i) More comprehensive design of integrated vacuum wall-moderator configurations.

(j) Development of pumps and heat exchangers for more efficient cooling of materials in the vicinity of the vacuum wall.

(k) Design and feasibility studies of more realistic magnetic structures, including questions of support and magnetic stress.

(ℓ) New thermodynamic cycles, to see if any are better suited to fusion conditions than is a conventional simple steam cycle.

7. ACKNOWLEDGMENTS

It is a pleasure to offer thanks to Messrs. A. P. Fraas and D. Steiner of the ORNL Reactor Division for their many suggestions, some of which have appeared here; to Mrs. B. Pope, who typed the manuscript in very short time; to Mr. E. Ferguson, who arranged the numerical computations; to Mr. B. Lay, who drew every figure; to many members of the ORNL Thermonuclear Division for interesting discussions about the problem; and to my family, whom I have hardly seen during these last three months.

REFERENCES

1. L. Spitzer, D. Grove, W. Johnson, L. Tonks, W. Westendorp, Report NYO-6047, U.S.A.E.C., Washington, D. C. (1954).
2. T. Hesselberg Jensen, O. Kofoed-Hansen, A. H. Sillesen, and C. F. Wandel, Risö Report No. 2, Danish A.E.C., Research Establishment Risö (1958).
3. T. Hesselberg Jensen, Risö Report No. 6, Danish A.E.C., Research Establishment Risö (1958).
4. Risö Report No. 18, Danish A.E.C., Research Establishment Risö (1960).
5. R. F. Post, Some Aspects of the Economics of Fusion Reactors, Report UCRL-6077, August 1960, Office of Technical Services, U. S. Dept. of Commerce, Washington, D. C. (material also contained in Risö Report 18).
6. R. F. Post, Nuclear Fusion Supplement Part I, 99 (1962).
7. W. M. MacDonald, M. N. Rosenbluth, and Wong Chuck, Phys. Rev. 107, 350 (1957).
8. G. F. Bing and J. E. Roberts, Phys. Fluids 4, 1039 (1961).
9. D. J. BenDaniel, Plasma Physics 3, 235 (1961).
10. D. J. BenDaniel and W. P. Allis, Plasma Physics 4, 31 (1962).
11. G. G. Kelley, Plasma Physics 9, 503 (1967).
12. J. L. Dunlap, editor, Proc. of Intern. Conf. on Plasma Confined in Open-Ended Geometry, (Nov. 1-4, 1967), Gatlinburg, Tennessee, U.S.A. (to be published).
13. T. K. Fowler and M. Rankin, Plasma Physics 8, 121 (1966).
14. D. V. Sivukhin, Atomnaya Energiya 19, 510 (1965); English translation in Plasma Physics 8, 607 (1966).

15. R. G. Mills, Four Lectures on Fusion Power, Princeton Plasma Physics Laboratory Report MATT-145 (1962).

16. R. G. Mills, On the Initial Transient of a Thermonuclear Reactor, Princeton Plasma Physics Laboratory Report MATT-437 (March 1966).

17. R. G. Mills, Some Engineering Problems of Thermonuclear Reactors, Princeton Plasma Physics Laboratory Report MATT-548 (June 1967).

18. C. F. Wandel, T. Hesselberg Jensen, and O. Kofoed-Hansen, Nuclear Inst. and Methods 4, 249 (1959).

19. D. J. Rose and M. Clark, Jr., Plasma and Controlled Fusion, 2nd revised printing, M.I.T. Press, Cambridge, Mass. (1965), Chap. 8.

20. A. J. Impink, Jr., Neutron Economy in Fusion Reactor Blanket Assemblies, Technical Report No. 434, Mass. Inst. of Technology Research Laboratory of Electronics, Cambridge, Mass. (1965).

21. W. G. Homeyer, Thermal and Chemical Aspects of the Thermonuclear Blanket Problem, Technical Report No. 435, Mass. Inst. of Technology Research Laboratory of Electronics, Cambridge, Mass. (1965).

22. L. N. Lontai, Study of a Thermonuclear Reactor Blanket with Fissile Nuclides, Technical Report No. 436, Mass. Inst. of Technology Research Laboratory of Electronics, Cambridge, Mass. (1965).

23. G. I. Bell, Neutron Blanket Calculations for Thermonuclear Reactors, Report LA-3385-MS, Los Alamos Scientific Laboratory (Sept. 1965).

24. S. T. Cohen, The Peaceful Neutron Bomb: A New Twist on Controlled Neutron Fusion, Document from the RAND Corporation, Santa Monica, California.

25. R. A. Strehlow and D. M. Richardson, Chemistry of Tritium in Controlled Fusion Devices, in Report ORNL-3836, Thermonuclear Division Semmiann. Progress Report for Period Ending April 30, 1965.

26. S. S. Kirslis, The Interaction of Tritium with Thermonuclear Reactor Materials, unpublished thesis.

27. E. F. Johnson, Recovery of Tritium from Dilute Solutions of Lithium Tritide in Lithium, Tech. Memo. No. 25, Report NYO-6370, U.S.A.E.C. (1956).

28. D. J. Rose, W. G. Homeyer, A. J. Impink, and P. S. Spangler, Engineering Calculations for Barely Conceivable Fusion Reactors, M.I.T. unpublished document (1963).

29. L. G. Cook, H. C. Pollock, W. L. Robb, and J. E. Burke, The Thermonuclear Fusion Reactor as a Source of Central Station Electricity, General Electric Company unpublished document (~ 1965).

30. R. Carruthers, P. A. Davenport, and J. T. D. Mitchell, The Economic Generation of Power from Thermonuclear Fusion, U. K. Atomic Energy Authority Research Report CLM-R85, The Culham Laboratory, Abingdon, Berks., England (1967).

31. F. L. Ribe, T. A. Oliphant, Jr., and W. E. Quinn, Feasibility Study of a Pulsed Thermonuclear Reactor, Report LA-3294-MS, Los Alamos Scientific Laboratory (1965).

32. F. E. Dunn, Effects of Plasma Stability on the Feasibility of a Pulsed Fusion Device, S. M. Thesis, Dept. of Physics, Mass. Inst. of Technology, Cambridge, Mass. (June, 1965).

33. H. Burkhardt, Nuclear Fusion 2, 1 (1962).

34. O. Kofoed-Hansen, Reference 4, pp. 347-365.

35. Reference 21, pp. 58-59.

APPENDIX I

Plasma Thermal Balance Calculation

1. Define parameter T_e
2. Compute $\gamma = 1.43 \times 10^{-3} T_e^{3/2}$
3. Compute $h_s = 1.25 \times 10^{18} T_e^{3/2}$
4. Compute $\phi = \ell n \frac{\gamma + 1}{\gamma}$
5. Define parameter θ
6. Set rrial $\theta = \phi$
7. Compute $U_{\alpha i} = 2330 \int_o^\theta \frac{\gamma dx}{[(\gamma + 1)e^{-x} - \gamma]^{1/3}}$
8. Compute $U_{\alpha e} = 2330 \int_o^\theta [(\gamma + 1)e^{-x} - \gamma]^{2/3} dx$
9. Define parameter C_1
10. Compute $(WX) = 1.2 \times 10^{-20} C_1 T_e^{1/2}$
11. Define parameter D
12. Define parameter C_2
13. Define parameter V_i
14. Define parameter V_e
15. Define parameter $J(= h_i/h_e)$
16. Compute
$$(WC) = \frac{2.41 \times 10^{-27} C_2 T_e^{3.75} (T_e + T_i)^{3/2} (1 + \frac{T_e}{204})}{D}$$
17. Compute
$$K = \frac{4.8 \times 10^{-18} T_i (1 - \frac{T_e}{T_i})}{T_e^{3/2}}$$
18. Look up (σv) = tabular function of T_i

19. Compute

$$Q = (\sigma v)[U_{\alpha e} - 3T_e + 2V_e]$$

$$-J\left[\frac{3T_e - 2V_e}{3T_i - 2V_i}\right]\left[(\Sigma v)(U_{\alpha i} - 3T_i + 2V_i) - K\right]$$

$$+K - (WX) - (WC)$$

20. If $\left\{\begin{array}{l} Q < 0, \text{ choose large } T_i \\ Q > 0, \text{ choose lower } T_i \\ Q = 0, \text{ proceed} \end{array}\right\}$ in general

21. Compute

$$h_i = \left[\frac{6T_i - 4V_i}{(\sigma v)(U_{\alpha i} + 2V_i - 3T_i) - K}\right]$$

22. Compute $\phi_s = 3 \times 10^{-18}\, h_i / T_e^{3/2}$

23. If $\left\{\begin{array}{l} \phi_s \geq \phi, \text{ proceed} \\ \phi_s < \phi, \text{ choose new } \theta \end{array}\right.$ (but the case will probably be unfeasible for fusion)

24. Compute $f_b = \left[1 + \frac{2}{h(\sigma v)}\right]^{-1}$

25. Compute $(RK) = \frac{K}{(\sigma v)U_{\alpha e}}$

26. Compute $(RX) = \frac{(WX)}{(\sigma v)U_{\alpha e}}$

27. Compute $(RC) = \frac{(WC)}{(\sigma v)U_{\alpha e}}$

28. Compute $(RSI) = \frac{V_i}{1750\, f_b}$

29. Compute $Y = \frac{h}{h_s}$

30. Compute $UK = \frac{K}{(\sigma v)}$

31. Compute $UX = \frac{(WX)}{(\sigma v)}$

32. Compute $UC = \frac{WC}{(\sigma v)}$

Print T_e; C_1; C_2; D; V_i; V_e; J; γ; h_s; $\emptyset$; $U_{\alpha i}$; $U_{\alpha e}$; T_i; (σv); Q; h_i; h_i; $\emptyset_s$; f_b; (RK); (RX); (RC); (RSI); Y; (UK); (UX); (UC).

APPENDIX II

Calculations of M_1 and M_2

1. Simple long solenoid, filled with plasma.

Evidently, $M_1 = B_m/B_o(r_w/r_p)^{3/4} = 1$. To calculate M_2, note that the sheet current k is B_o/μ_o, and that $\int j dV = k\int ds_w = k\int ds_p$. Thus $M_2 = 1$.

2. Torus, minor radius r, major radius R, filled with plasma.

Define B_o as the field at the minor axis. Then by inspection, $M_1 = 1$.

To calculate M_2, define the total circulating current I, and the field $B_o = \mu_o I/2\pi R$. The total amp-meters is $2\pi rI$ and the area is $4\pi^2 rR$. Thus again $M_2 = 1$.

3. Spherator, as shown in Fig. A-2.1

All dimensions are expressed in terms of the levitated conductor radius a. According to Yoshikawa*, a reasonable configuration consists in placing the outer loop at radius 3a/2, placing the axial field stagnation points at $z = \pm a$ (as shown), and choosing an axial wire current I_3 twice the levitated ring current I_1. With these choices

$$\frac{I_2}{I_1} = \frac{\sqrt{2}[(3/2)^2 + 1]^{3/2}}{9} = 0.922 \quad .$$

The minimum field occurs at two rings above and below the midplane, passing through the places shown by the symbols B_o in the figure. Coincidentally, the levitated conductor alone makes a field nearly equal to B_o at the center

*S. Yoshikawa, private communication.

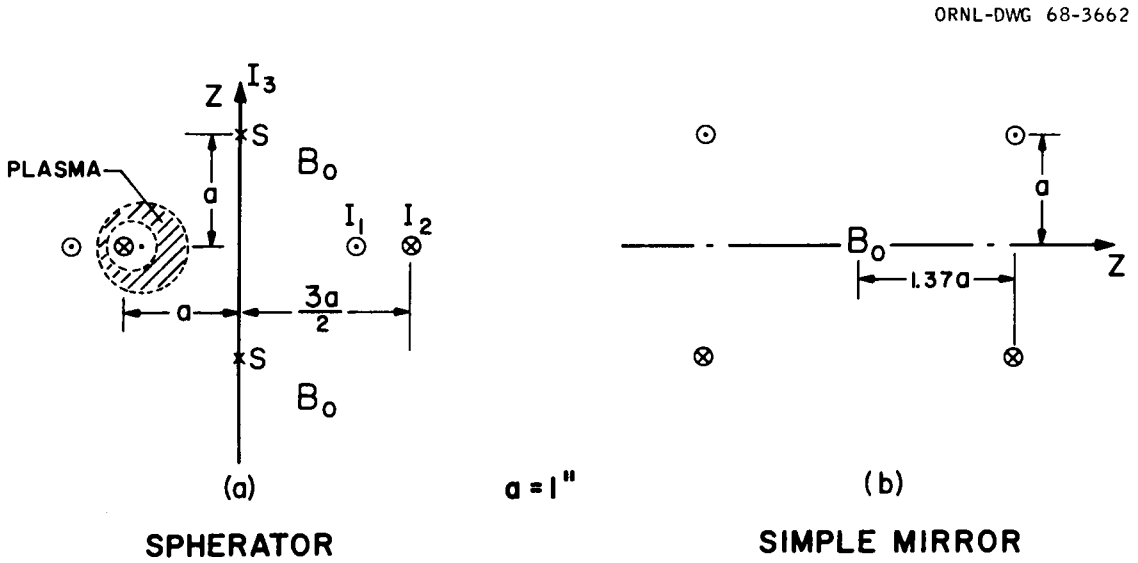

Fig. A-2.1. Schematic Confinement Systems for Magnetic Analysis.

of the system. Thus

$$B \approx \mu_o I_1/2a \ .$$

If we assume the axial current is transported radially at $z = \pm a$, and peripherally at $r = 3a/2$, the following amp-meters obtain:

Levitated Ring	$6.28\ a\ I_1$
Outer Ring	$8.7\ a\ I_1$
Axial Wire	$14\ a\ I_1$
Total	$29\ a\ I_1$

The plasma is contained in a torus whose axial length is $2\pi a$, and whose cross section area is very close to $a^2/2$, as shown; but excised from this area is an amount $a^2/6$ that contains the levitated conductor.

We judge that $r_w/r_p \approx 1.4$ in this device. The maximum magnetic field, with the conductors arranged over the largest available area, is about $2B_o$. Thus $M_1 \approx (2)(1.4)^{3/4} = 2.6$.

For the more difficult task of calculating M_2, we must make a decision about how to count areas.

(a) All currents counted, all areas counted.

Here assume that the central hole can be turned into an asset, in terms of nuclear heat removal. Find then that total area is $25a^2$, total current is $29\ aI_1$, $B_o = \mu_o I_1/2a$, as before. Thus

$$M_2(n=0) = 2.33 \ .$$

If we try $n = 1/2$, judging again $r_p/r_w = 0.7$,

$$M_2(n=1/2) = 1.62 \ .$$

(b) All currents counted, control hole not counted.

Here the area is 15.8 a^2, other quantities are the same, and we have

$$M_2(n=0) = 3.68$$

$$M_2(n=1/2) = 2.58$$

(c) Levitated wire and control hole omitted.

The device must operate as a min-B Tokamak, with the erstwhile levitated wire replaced by induced plasma current. Now area = 15.8 a^2, current cost is 22.7 aI_1, and

$$M_2(n=0) = 2.88$$

$$M_2(n=1/2) = 2.02$$

4. A Simple Mirror, as in Fig. A-1b.

We choose a mirror ratio 2.5; the configuration is shown. The field is easy to calculate, but the useful volume and equivalent radius require some aesthetic judgment. Let the reference field be B_o at the center on axis. Then we make two choices of the useful radial extent, based on the minimum permissible value of field at the midplane, off axis.

(a) $B = 0.75\ B_o$

This field is found at r = 0.675 a, z = 0. The surface excluding ends, of the figure of revolution passing through (r = 0.675 a, z = 0) has area 8.92 a^2. The equivalent cylindrical area is 17.2 a^2. Thus we set $r_w/r_p = (17.2/8.92)^{1/2} = 1.39$ and

$$M_1 = (2.5)(1.39)^{3/4} = 3.2 \quad .$$

To find M_2, we use the handy calculated fact that if a = 1 inch, current/coil = 1000 amp, then B_o = 101 gauss. From this

$$M_2(n=0) = 6.9$$

$$M_2(n=1/2) = 4.95$$

(b) $B = 2\,B_o/3$

Ths contour passes through (r = 0.795, z = 0), area = 11.42 a_o^2, $r_w/r_p = 1.23$,

$$M_1 = 2.9$$

$$M_2(n=0) = 5.5$$

$$M_2(n=1/2) = 4.5$$

5. A Stabilized Mirror.

We choose a model calculated at ORNL*, which has minimum field on axis at the center of B_o = 3950 gauss, made from mirror coils at z = $\pm$ 13 cm, r = 11 cm, each carrying 128,000 amp. The four bars are at r = 14 cm, carry 150,000 amp each, and we consider the current in each bar to be magically terminated at z = $\pm$ 13 cm.

For this device axial mirror ratio is 2, the maximum closed |B| contour is at B = 4550 gauss, the plasma surface area is 267 cm^2 (which can be well approximated by a sphere 4.6 cm radius), and the winding area is about 2280 cm^2, arbitrarily excluding the mirror holes. The equivalent r_w/r_p is $(8.5)^{1/2}$ = 2.92, a very wasteful number.

From all these numbers, find

$$M_1 = (2.0)(2.93)^{3.4} = 4.5$$

$$M_2(n=0) = 40$$

$$M_2(n=1/2) = 13.7$$

---

*I am indebted to C. E. Parker for these calculations.

APPENDIX III

Parameters for a Series of Reference Designs of Thermonuclear Reactors

A. P. Fraas

In the course of extending the work on conceptual designs for thermonuclear reactors, it has appeared desirable to set up a series of reference designs to help point up the engineering problems.

Description

The two basic reactor configurations of Figs. A-3.1 and A-3.2 were considered, that is, a torus and a cylinder with magnetic mirrors at the ends. In both cases the diameter of the vacuum shell containing the plasma was taken as approximately 10 meters. Additional cases for vacuum shell diameters of 7 and 13 meters were also considered to show the effects of moderate changes in the plasma diameter. The major diameter of the torus, i.e., the diametral distance across the torus from plasma centerline to plasma centerline, was taken as three times the minor diameter, that is, the ID of the vacuum shell. The length of the cylindrical machines was taken as 1.5 diameters. Actually, as indicated in Fig. A-3.2, the latter would probably not be a constant diameter cylinder but rather would be keg-shaped with substantially smaller diameters at the ends than at the middle.

Probably the most severe engineering problems in this series of machines are posed by the vacuum wall. For good power plant thermal efficiency the shell and inner reflector must be operated at a high temperature. The temperature must be held reasonably uniform in the face of

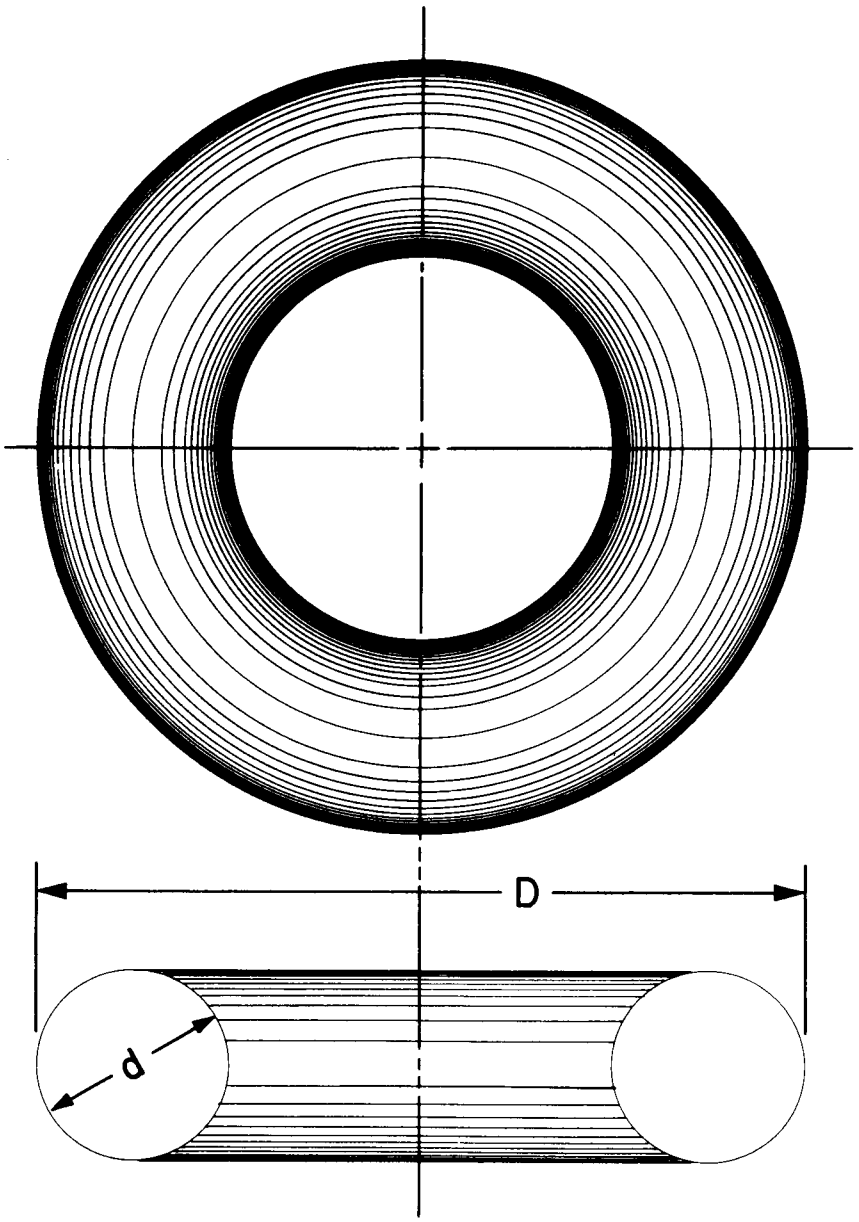

Fig. A-3.1. Basic Proportions for the Toroidal Configuration.

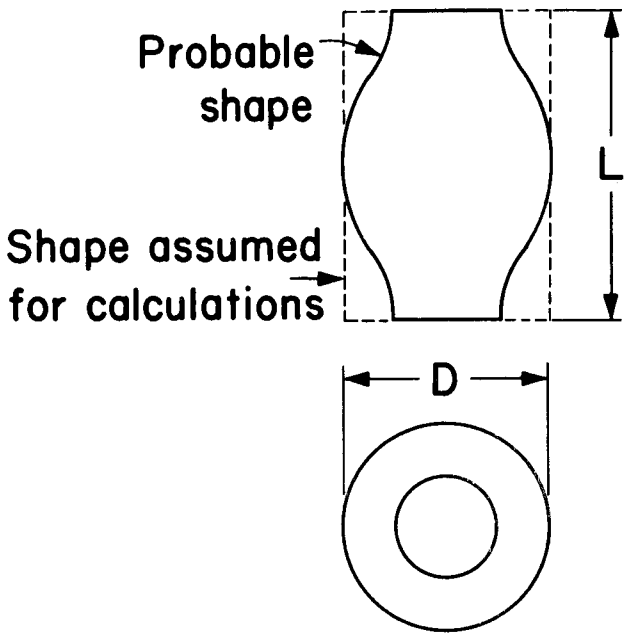

Fig. A-3.2. Basic Proportions for the Cylindrical Configuration.

a very high heat flux, hence a high performance cooling system is required. At the same time, the relatively thin vacuum wall is subject to a substantial external pressure and hence must be designed to withstand severe buckling loads. A 2 cm thick vacuum wall on a 10 m diameter would have a wall thickness-to-diameter ratio 1/5 that of an eggshell. To improve the structural stability it is highly desirable to employ a cellular structure similar to that shown in Fig. A-3.3 with a system of radial ribs of bulkheads between concentric shells. This construction serves to satisfy the structural requirements and also provides a good set of coolant passages.

The bulk of the energy of the reactor is released as heat in the reflector, the composition of which is shown in Fig. A-3.4. Although the heat flux from the inner vacuum wall to the coolant is very high, the fast neutrons that pass through the vacuum wall are slowed down over a fairly substantial depth of material in the reflector region, and hence the local power density there would generally be less than 50 w/cm^3. This makes it possible to employ a molten salt-cooled pebble bed region made up of spheres or cylindrical slugs of metallic beryllium or beryllium oxide. The pebble bed arrangement will make it easy to replace the beryllium or BeO when required by radiation damage. The thickness of this region will be determined by neutron economy considerations balanced against the high cost of the beryllium or beryllium oxide. These spheres or slugs would have to be canned in niobium to avoid attack by the molten salt. The next region as one moves radially outward will consist of graphite blocks designed and installed to contribute to the strength of the structure. These graphite blocks would form ribs extending through the pebble bed region to contribute to the support of the inner vacuum shell and help prevent

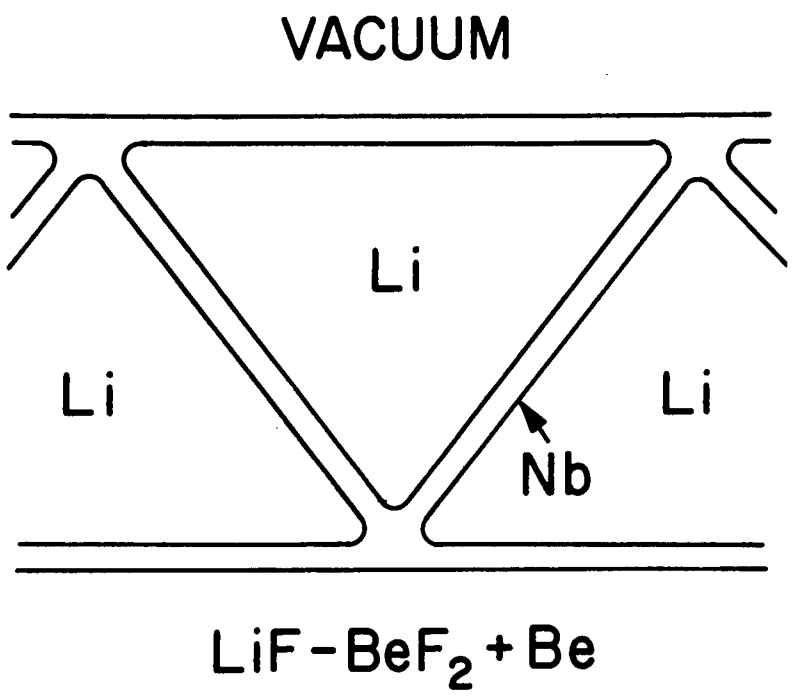

Fig. A-3.3. Section Through a Vacuum Wall Showing the Cellular Construction.

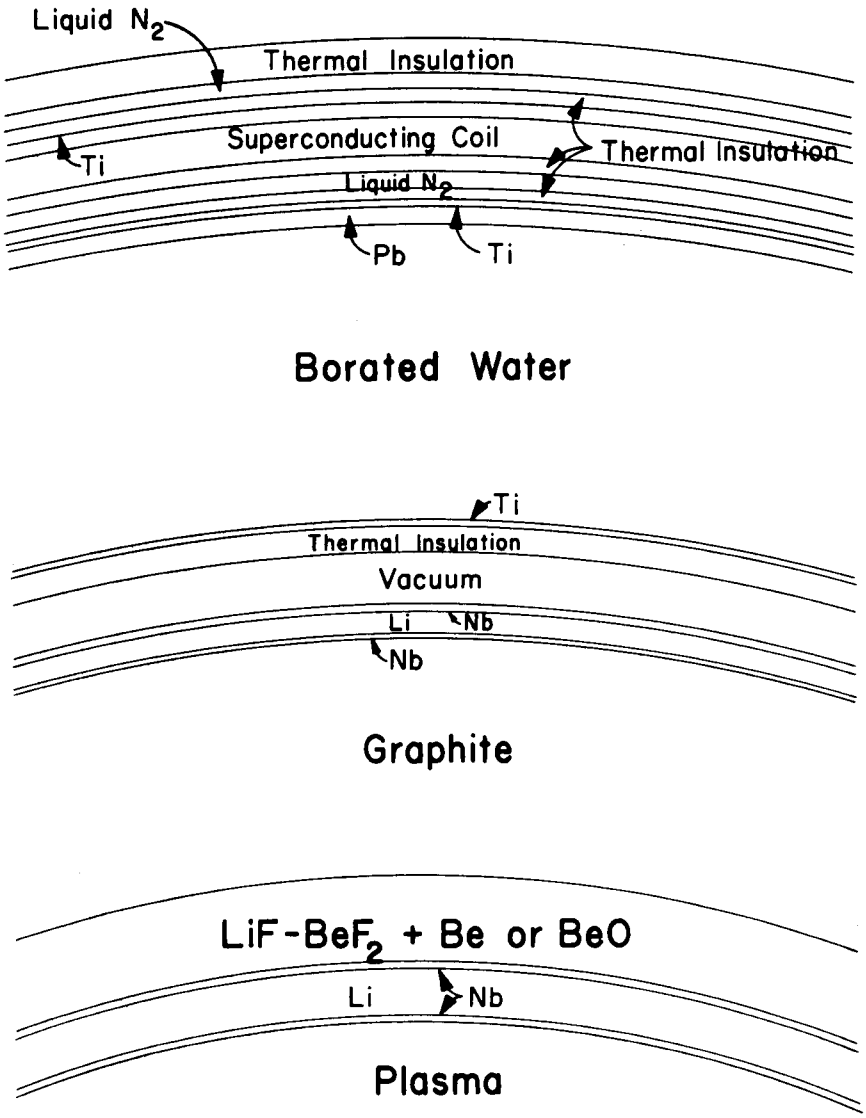

Fig. A-3.4. Section Through the Reflector Region.

general buckling. The outer niobium shell surrounding the graphite will be lithium cooled and will be of a double-wall ribbed construction similar to the inner shell both for good structural stability and for good cooling of the shell. The thickness of the lithium region will be determined by neutron economy considerations because neutrons thermalized in the BeO and graphite regions should be absorbed in ^{6}Li to produce tritium.

The bulk of the energy from the plasma will be absorbed in the inner high-temperature zone of the reflector enclosed by the niobium shells as described above. Surrounding the high-temperature region will be a water and lead shield. This will serve to reduce the investment in graphite as well as provide a nearly room temperature zone between the high-temperature reflector region and the superconducting coils. The shield region will consist of concentric titanium tanks filled with borated water and provided with a lead lining just inside the outer tank wall. Thermal insulation on either side of the water shield region would keep heat losses from the hot zone to the water and from the water to an intermediate liquid nitrogen buffer zone to a modest level. A substantial space must be provided between the hot reflector region and the water shield in the torus configuration because of the large amount of differential thermal expansion between them. The niobium shell will move radially outward approximately 10 cm in going from room to operating temperature.

The superconducting coils will be placed outside the water shield region and will be surrounded by double layers of thermal insulation with liquid nitrogen cooled plate coils between the layers. This arrangement will minimize the heat load on the helium cryogenic system required to maintain the superconducting coils at 4° K.

Provisions for differential thermal expansion complicate the problem of supporting the hundreds of tons of material in the cylindrical configuration or the thousands of tons of material in the torus configuration. For the reference designs considered here the water shield and superconducting coils would be segmented into discrete rings perhaps one or two meters long. The support structure envisioned would be attached to the titanium tanks for the water shield. The superconducting coils would be mounted on the water shield in such a way that at operating conditions the coils would shrink down onto the outer titanium shell of the water shield. The molten salt for cooling the hot reflector region would pass radially inward between alternate pairs of superconducting coil-water shield rings and would flow outward at the intermediate gaps. Similarly, shafts to drive the lithium circulating pumps would also pass through these gaps between adjacent rings of the water shield and superconducting coils.

The heat exchangers employed to remove heat from the lithium for the thermodynamic cycle could be cooled by the molten salt to minimize the pumping power losses associated with passing liquid streams through a strong magnetic field. A more attractive approach from the overall power plant standpoint might be to employ a potassium-steam binary vapor cycle with potassium boilers located in the lithium circuit inside the water shield. Potassium vapor would be expanded through potassium vapor turbines and then condensed in heat exchangers that would serve as steam boilers that would supply high pressure steam at 1000^{o}F to conventional steam turbines. This arrangement will make possible a thermal efficiency of around 60%. Sufficient work[1] has been carried out with small potassium vapor systems to show not only that the concept is feasible but also to

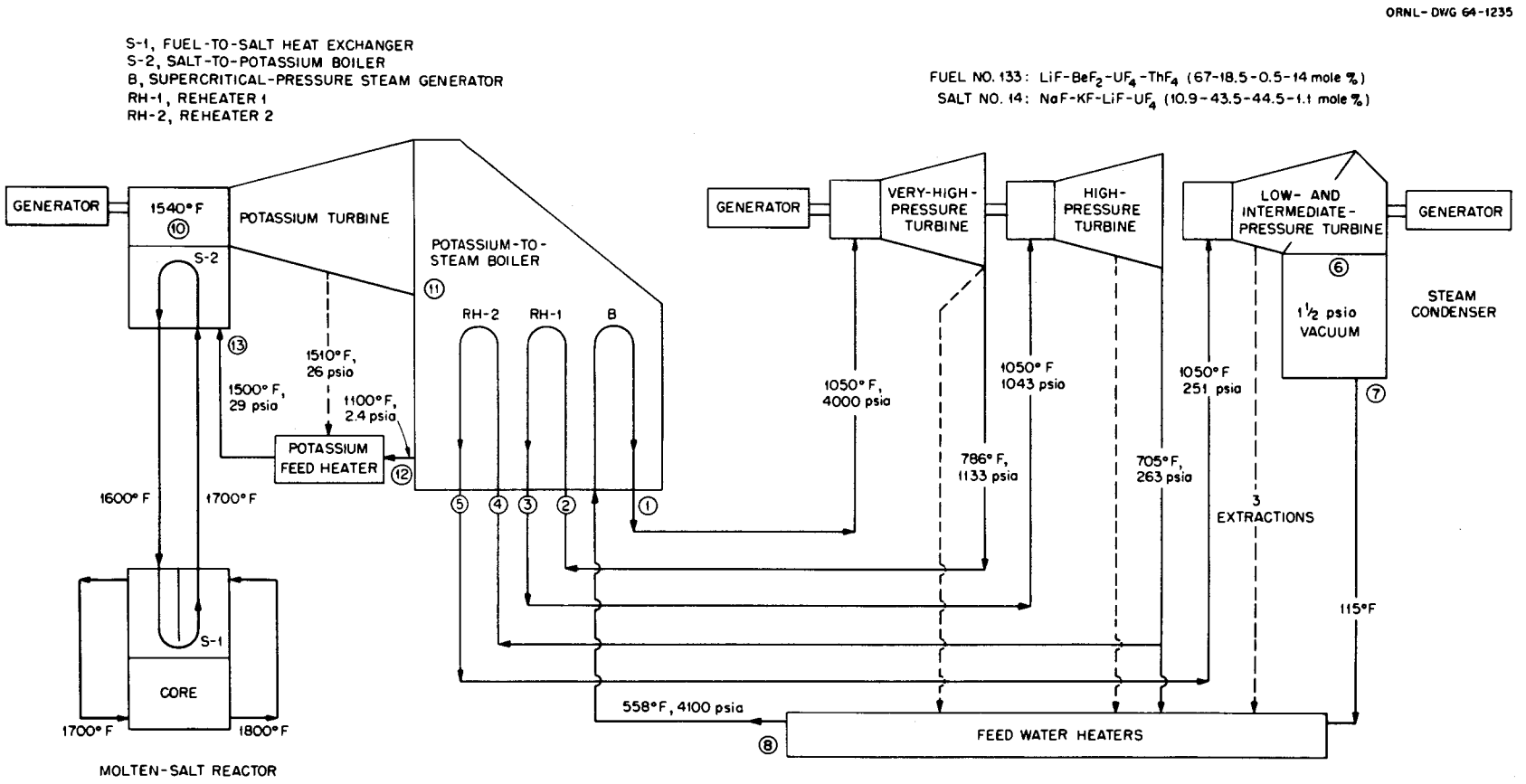

Fig. A-3.5. Flow Diagram for Binary-Vapor-Cycle Power Plant.

provide sufficient data to proportion the major component such as boilers, turbines, and condensers with confidence. A flow sheet for the thermodynamic cycle is shown in Fig. A-3.5 for a typical set of potassium and steam conditions.

Size, Weight, and Cost Effects

The large size of these machines leads to feasibility questions associated with the large masses of material required and their cost. To provide some perspective on these problems Table A-3.1 was prepared to show the weight and cost of the material in each of the regions of Fig. A-3.4 per square meter of surface of the vacuum shell. Table A-3.2 was then prepared to show the effects of the principal dimensions on the area of the vacuum shell and on the total weight and cost of the materials required. Data are given in Table A-3.2 for three different diameters of the vacuum shell for both the toroidal and the cylindrical configurations. A column at the right of Table A-3.2 gives the thermal power output for each case assuming a value of 10 Mw/m^2 of the vacuum shell. This coupled with the assumption of a 60% overall thermal efficiency gives a cost of about \$12/kw of electricity for the basic structure considered here. The cost of heat exchangers and pumps would certainly be much less than this, hence this figure compares favorably with \$50/kw which is the usual cost of boilers for conventional coal-fired steam plants.

Reference

1. A. P. Fraas, Trans. ASME Journal of Engineering for Power 88 Series A, 355 (1966).

Table A-3.1. Sequence, Thickness, Weight, and Cost of the Various Layers Through the Reflector-Shield-Superconducting Coil Region

Layer	Material	Thickness	Weight (Kg/m^2)	Cost ($/lb)	Cost ($/$m^2$)
Vacuum wall	Nb	2 cm	172	20	7,560
Lithium coolant	Li	10	53.4	5	495
BeO	BeO	15	450	15	14,830
Graphite	C	40	640	1	1,410
Lithium coolant	Li	5	27	5	297
Outer Nb wall	Nb	2	172	20	7,560
Thermal insulation	Al_2O_3	5	5	1	25
Water tank	Ti	1	58	2	260
Neutron shield	H_2O	60	600	0	0
Gamma shield	Pb	2	200	1	440
Water tank	Ti	1	58	2	260
Thermal insulation	$Al+Al_2O_3$	2	5	1	100
Plate coil	SS	3	40	3.40	300
Thermal insulation	$Al+Al_2O_3$	2	5	1	100
Plate coil		3	40	3.40	
Superconducting coil	Cu+(Nb-Zr)	7	630	($26,000/$m^2$)	26,000
Ti loop		2	120	2	530
Thermal insulation		2	5	1	100
Plate coil		3	40	3.40	300
Thermal insulation		5	12	1	25
		1.69 m	1778		60,892
			3292		

Table A-3.2. Effects of Vacuum Shell Size and Shape on the Cost and Weight of the Shell-Reflector-Shield-Superconducting Coil Assembly and on the Power Output for 10 Mw/m^2 of Vacuum Wall

Plasma Goemetry	Vacuum Shell (ID~m)		Vacuum Shell Area (m^2)	Cost ($ x 10^{-6})	Weight (lb x 10^{-6})	Power [Mw(t)]
		Torus (Major) Diam. - m)				
Toroidal	7	21	1455	88.7	10.5	14,550
Toroidal	10	30	2970	181	21.5	29,700
Toroidal	13	39	5010	305	36.3	50,100
		Cylinder (Length - m)				
Cylindrical	7	10.5	232	14.1	1.68	2,320
Cylindrical	10	15	471	28.7	3.42	4,710
Cylindrical	13	19.5	777	47.3	5.63	7,770

APPENDIX IV

ENGINEERING PROBLEMS OF THE VACUUM WALL AND REFLECTOR

A. P. Fraas

Introduction

The vacuum wall of a thermonuclear reactor presents some very difficult engineering problems. It must operate at high temperature if the heat generated by the reactor is to be used effectively, the structural metal must be thin (of the order of 2 cm) for good neutron economy, it must be large in diameter, it must withstand an external pressure which will tend to cause inward buckling, and the large amount of heat deposited in it by radiation must be removed without generating any serious thermal stresses or thermal distortion. As a matter of fact, the effectiveness with which it can be cooled will place an upper limit on the overall output of the reactor per unit of vacuum wall surface area, and hence there is a strong incentive to employ the highest performance wall cooling arrangement that can be devised consistent with neutron economy considerations.

Buckling Considerations

The buckling of thin-walled shells at elevated temperatures where creep plays an important role has been given relatively little attention. Fortunately, this problem has proved important at ORNL both under the ANP program and under the gas-cooled reactor program so that a substantial amount of experience is readily at hand on the creep buckling problems of both cylindrical and spherical shells. It is believed that the critical buckling pressures for the doubly curved surfaces of the toroidal and keg-shaped shells of interest here will fall somewhere between the critical buckling loads for spheres and cylinders.

Much of the ORNL work on spheres was carried out with copper at 400°F[1] while the work on cylindrical shells was carried out with stainless steel at 1200°F.[2] This is fortunate since it happens that the creep strength and modulus elasticity of these two materials are roughly the same as for niobium at 1700°F, which is in the temperature range in which it would be desirable to run the vacuum wall.

Theoretical analyses indicate that the critical buckling pressure for a thin-walled shell is directly proportional to a function of the modulus of elasticity and Poisson's ratio multiplied by the cube of the ratio of the thickness to the radius.[2] Since the elastic properties of the copper at 400°F, of stainless steel at 1200°F, and of niobium at 1700°F are much the same, for thin shells as a first approximation one can take the critical buckling pressure as directly proportional to the cube of the shell thickness-to-radius ratio. Table A-4.1 has been prepared to summarize the creep buckling test data and extend it to conditions approaching those of interest here. Some additional cases for niobium shells have been added to cover the range of current interest.

In view of the fact that the values given in Table A-4.1 are for actual collapse of the shell under external pressure, it is evident that a substantial factor of safety ought to be employed. For present purposes it appears that a factor of two may be reasonable. This leads to an unacceptably thick niobium shell for the 10^5 hr of life required for a practicable reactor. However, it appears quite reasonable to make use of a cellular structure such as one of those shown in Fig. A-4.1 to provide the desired depth of section. While no analysis has been made, it is believed that this sort of structure can be built to give something approaching

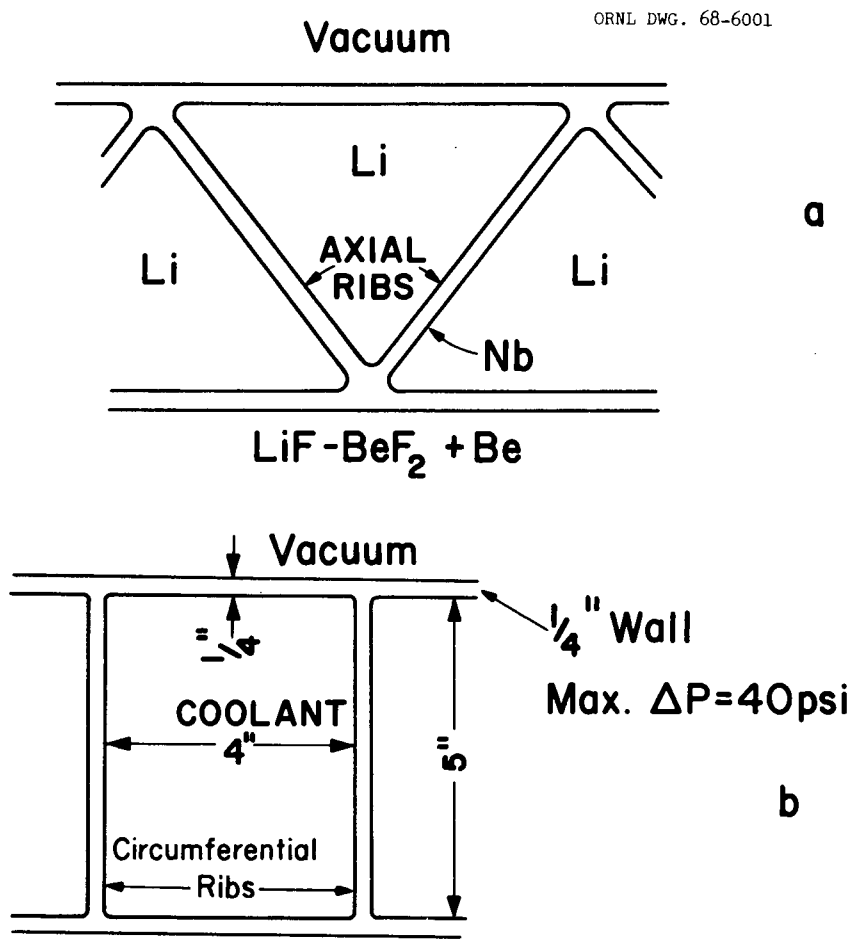

Fig. A-4.1. Sections Through Two Cellular Structures that Appear Promising for the Vacuum Wall.

Table A-4.1. Summary of Data on Buckling of Shells under External Pressure

Shell Shape	Shell Material	Temperature (°F)	Time to Buckle (hr)	Modulus of Elasticity (psi x 10^{-6})	Shell Thickness (in.)	Shell Radius (in.)	Shell Thickness-to-Radius Radius	Critical Buckling Pressure (psi)	
								Calculated	Measured
Sphere	Cu	300	200	13	0.032	6.25	0.0005	-	80
Sphere	Cu	400	1000	13	0.032	6.25	0.0005	-	28
Cylinder	SS	1200	3000	20	0.25	3.875	0.065	-	460
Cylinder	SS	1200	500	20	0.25	7.0	0.036	150	-
Cylinder	SS	1200	500	20	0.80	200	0.004	0.2	-
Cylinder	Nb	1700	1000	10	-	-	-	-	-

the same resistance to buckling as a solid wall of the same thickness for the range of conditions of interest here (where the nominal pressure stresses would be well below the creep limit for the lifetime envisioned). This, of course, will have to be checked out as the relationships are involved and subtle.

Cooling of the Vacuum Wall

The amount of heat to be removed from the vacuum wall will depend in large measure on the reactor power output per square meter of vacuum wall and the fraction of the incident energy flux in the form of x-ray and soft gamma radiation. For purposes of this memorandum it will be assumed that the power output of the reactor will be 10 Mw/m^2 and that 15% of this power will appear as heat in the vacuum wall as a consequence of the absorption of x-rays and soft gammas. This corresponds to a heat flux of 470,000 $Btu/hr \cdot ft^2$, a formidable figure.

The principal candidates for cooling the vacuum wall are a molten fluoride salt and metallic lithium. Heat transfer coefficients for these two fluids are presented in Figs. A-4.2 and A-4.3 for flow through the inside of circular passages. Both analyses and tests indicate that substantially the same heat transfer coefficients will prevail in rectangular or triangular passages having the same hydraulic radius (i.e., the same equivalent diameter). These heat transfer coefficients were calculated from the physical properties presented in Table A-4.2 and Fig. A-4.4. If one assumes a 15 m long flow channel with a 10 cm radial gap between the plates of a configuration such as that of Fig. A-4.1, the temperature rise in traversing the channel, the coolant pressure drop, and the film temperature drop can be plotted as a function of the fluid velocity as in Fig.

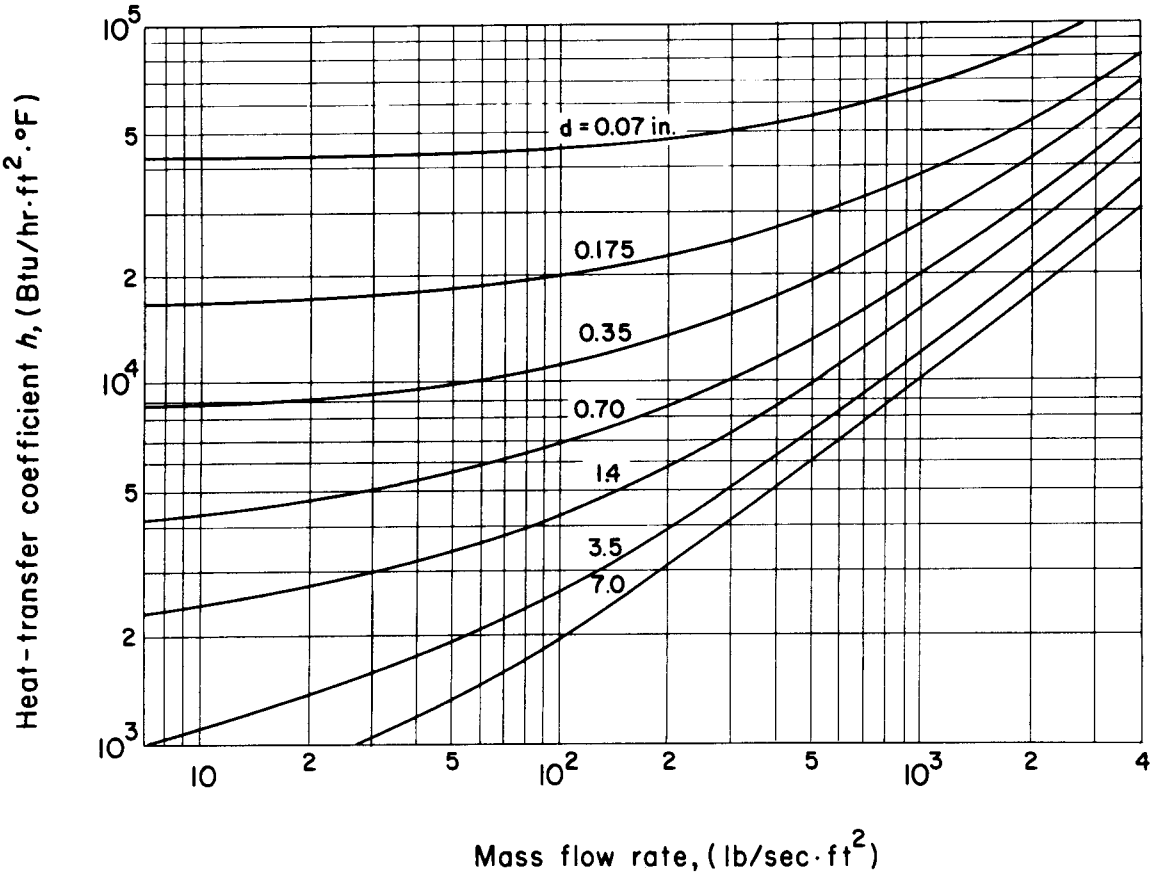

Fig. A-4.2. Heat-Transfer Coefficient for Liquid Lithium Flowing in Round Tubes.

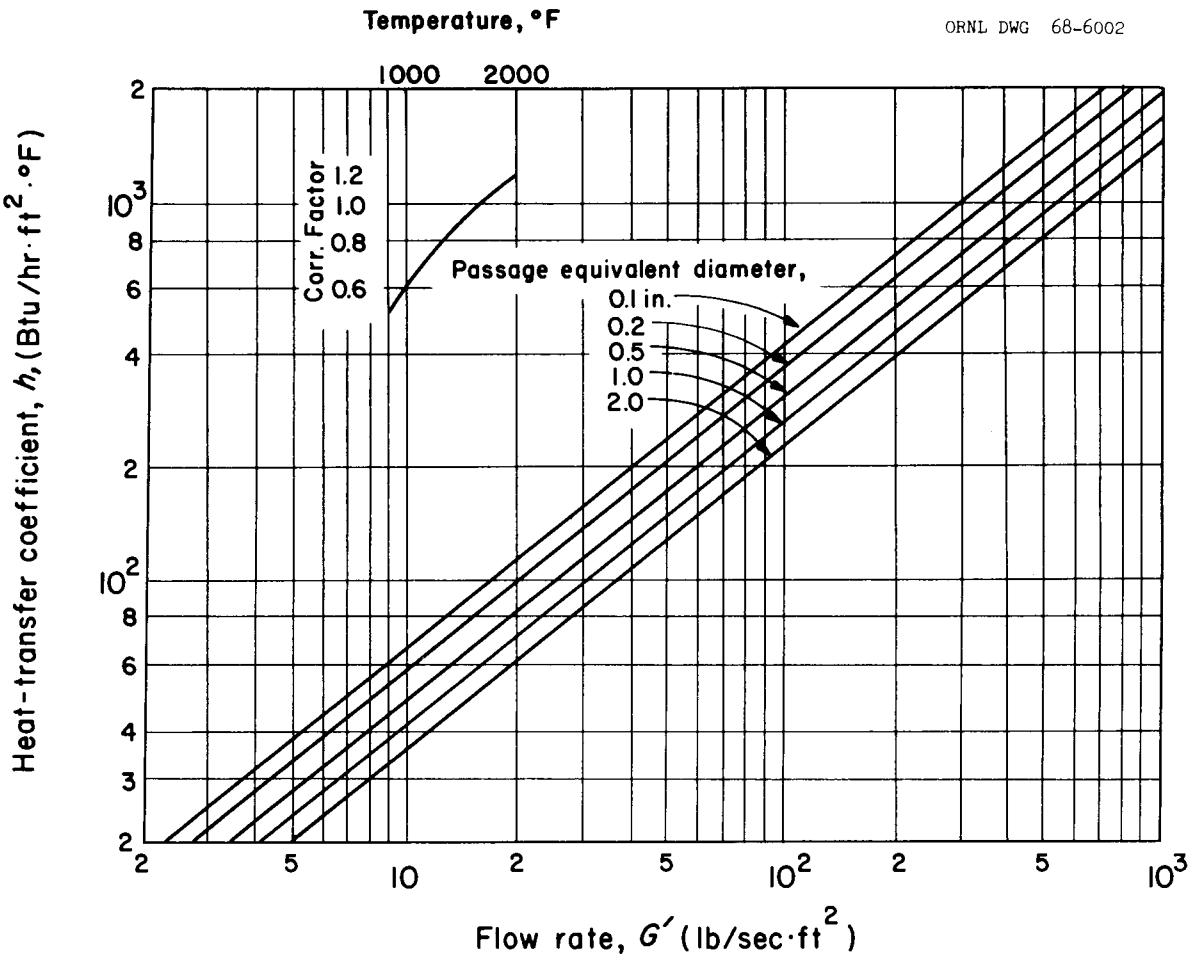

Fig. A-4.3. Heat-Transfer Coefficients for LiF (67 mole %) - BeF_2 (33 mole %) at 1500°F under Turbulent Flow Conditions.

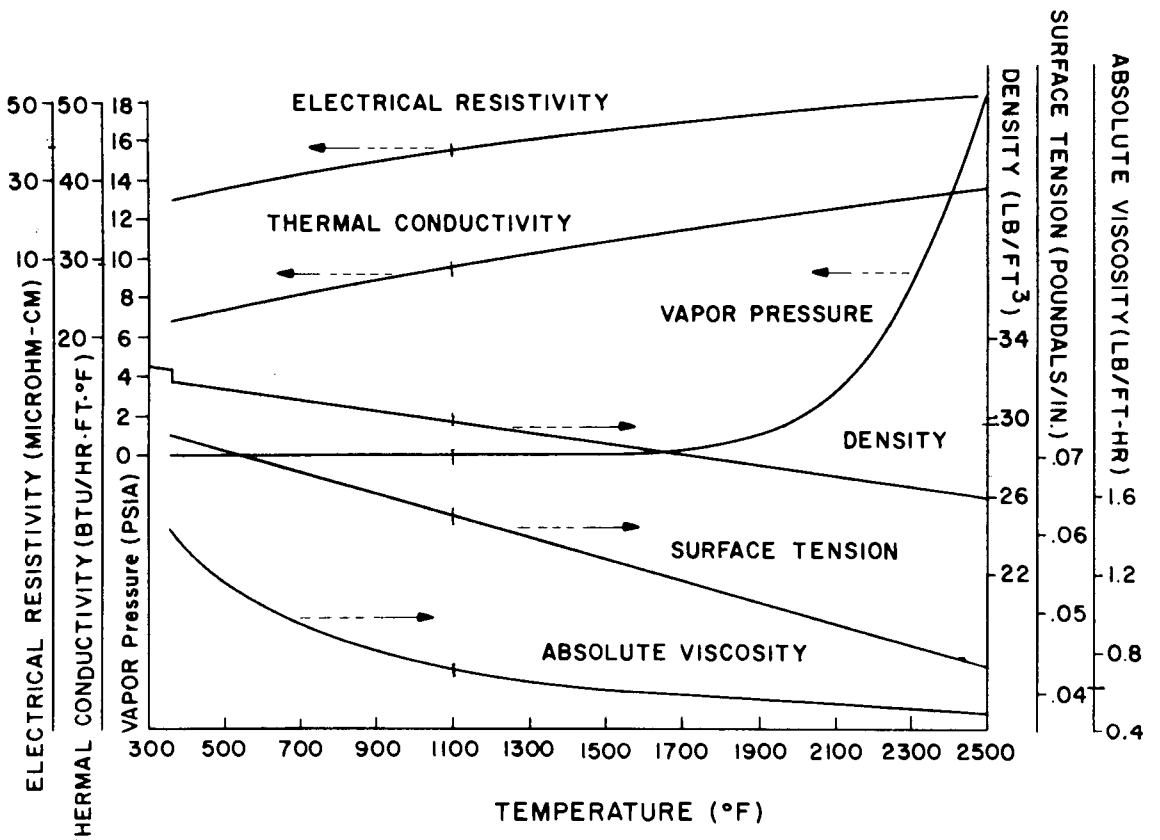

Fig. A-4.4. Physical Properties of Lithium.

Table A-4.2. Physical Properties of a Molten Salt, LiF (67 mol %) BeF_2 (33 mol %)

Melting point, $^{\circ}F$	850	($455^{\circ}C$)
Density @ $1200^{\circ}F$, lb/ft^3	122	($2.214 - 4.2 \times 10^{-4}$ t) (in g/cm^3 for t in $^{\circ}C$)
Viscosity @ $1200^{\circ}F$, lb/hr·ft	14	($0.116\ e^{3755/T}$) (cp for T in $^{\circ}K$)
Specific heat @ $1200^{\circ}F$, Btu/lb·$^{\circ}F$	0.57	($\pm$ 20%)
Thermal conductivity @ $1200^{\circ}F$, Btu/hr·ft·$^{\circ}F$	0.578 $\pm$ 10%	(0.010 w/cm·$^{\circ}C$)

A-4.5. It is desirable to keep the thermal stresses within the elastic range, which implies that the temperature rise should be kept to approximately 200°F and the film temperature drop to about the same level. It is evident in Fig. A-4.5 that lithium is much superior to a molten salt for cooling the vacuum wall. This fact is also shown in another fashion by Fig. A-4.6. This again shows the film temperature drop from the wall to the coolant, the temperature rise in the coolant stream, and the pressure drop, but this time as functions of the wall heat flux. In addition, the temperature drop through several representative thicknesses of niobium wall are shown on the same coordinates together with the temperature rise in the coolant stream for a pumping power loss equal to 1% of the total heat input to the stream. (This does not include electromagnetic pumping losses for the lithium - only conventional turbulence losses are included). Two horizontal dashed lines have also been drawn across Fig. A-5.6, one for a conservative limit from the thermal stress standpoint and the other for a possible upper limit that would have to be validated by testing of models, and would depend a great deal on the extent to which local stress concentrations become important.

Perhaps the most important point shown by Fig. A-4.6 is the fact that the lithium film temperature drop is less than 1/3 that for the molten salt. As can be seen in Figs. A-4.2 and A-4.3, the heat transfer coefficient for a liquid metal is not a sensitive function of the velocity as is the case for a molten salt, and hence there is much less tendency for local hot spots to develop as a consequence of irregularities in the local velocity distribution in a channel under turbulent flow conditions. Because of hot spot considerations, the practicable power output obtainable from a thermonuclear reactor with lithium-cooled walls will run at least three and

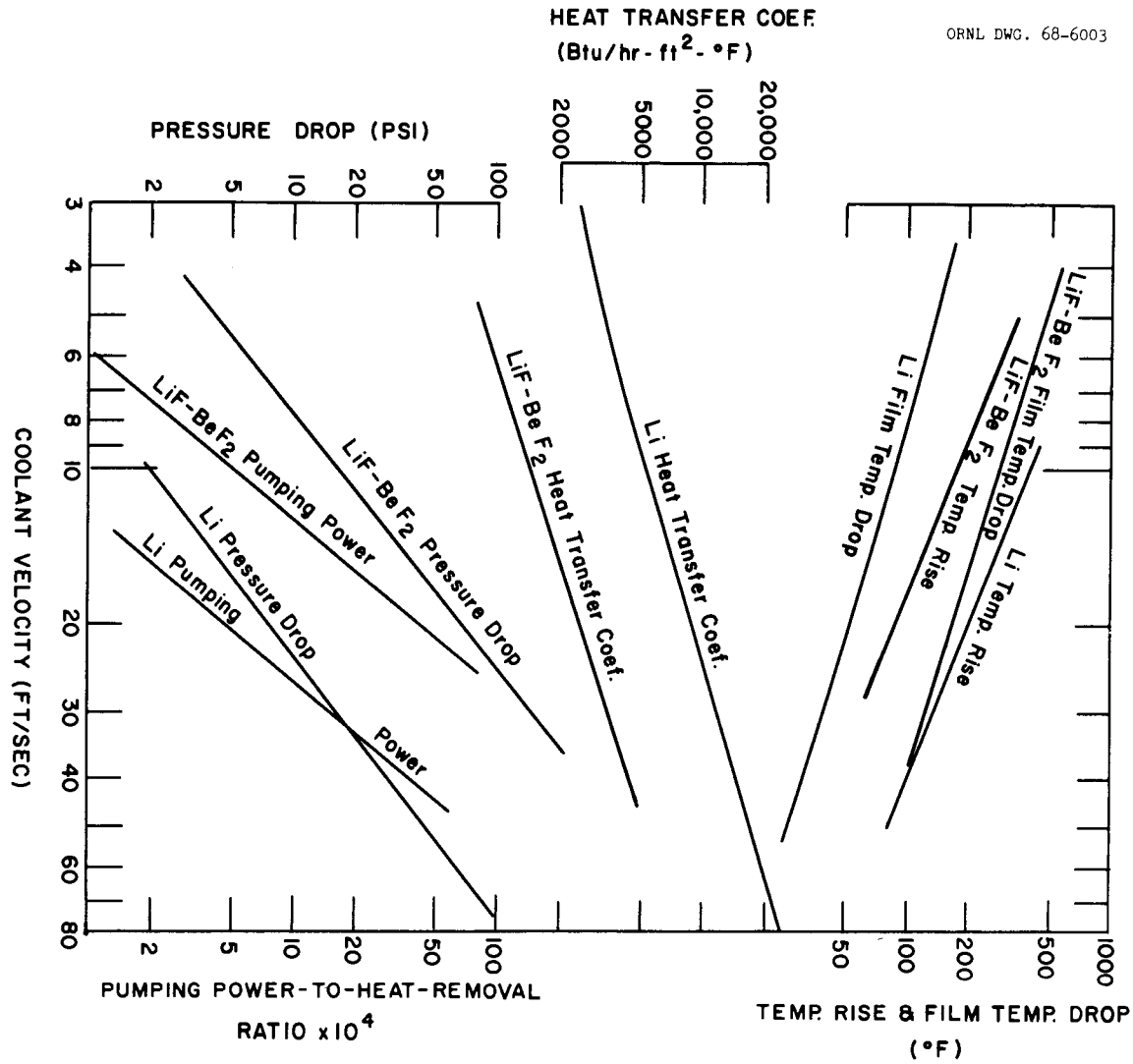

Fig. A-4.5. Effects of Coolant Velocity on Heat Transfer Parameters for a 50 ft long Loop having a Heat Flux of 470,000 Btu/hr-ft^2 (15% of 10 Mw/m^2) and an Equivalent Passage Diameter of 5 Cm.

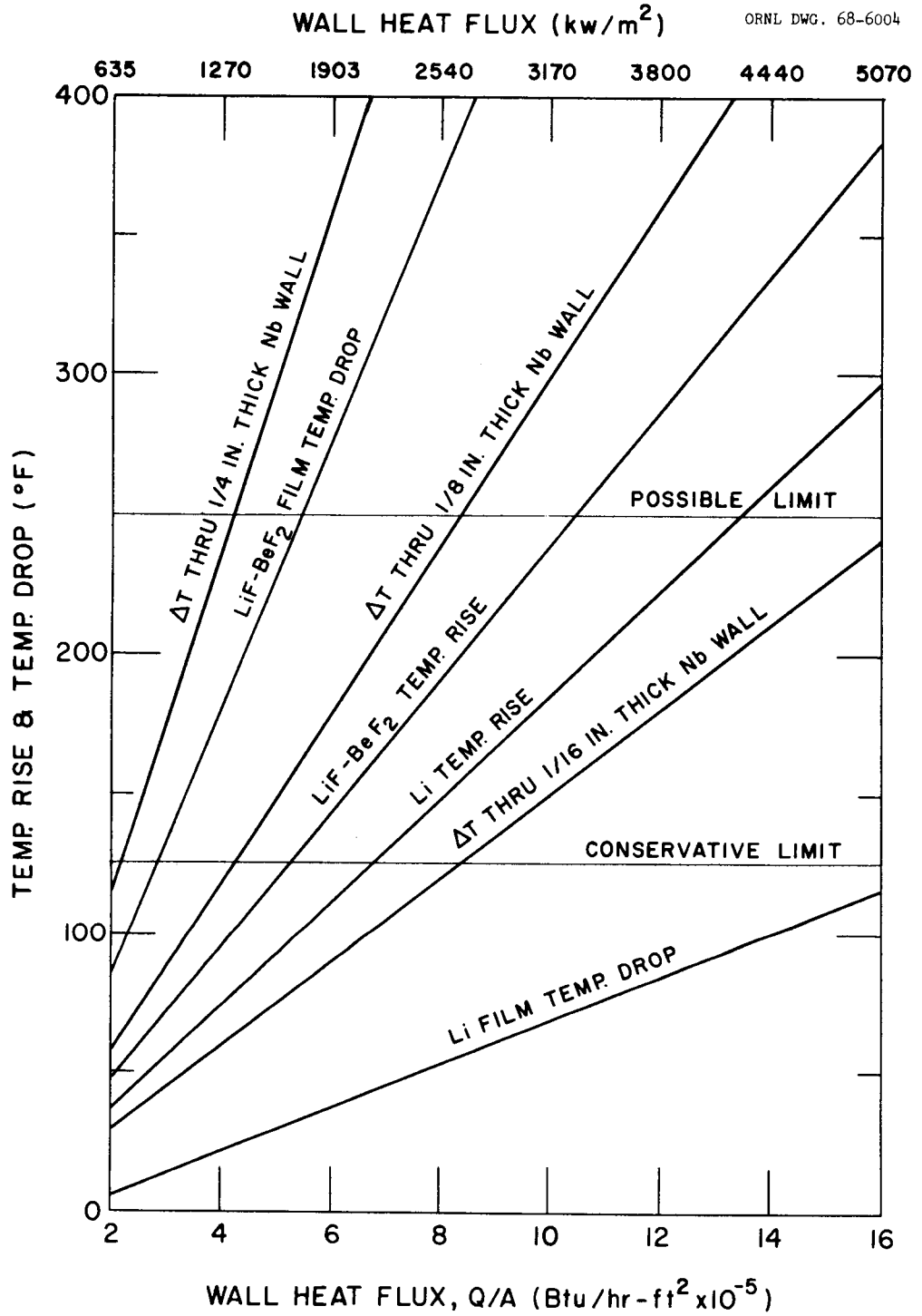

Fig. A-4.6. Effects of Heat Flux on Temperature Drops and Temperature Rise in Coolant for 40 psi ΔP in Coolant Loop 50-ft long and 2 in. in Diameter.

possibly five times as high as could be obtained from the same unit with a molten salt as the coolant for the vacuum wall. However, to take advantage of this high heat transfer coefficient it would also be necessary to make use of a rather thin niobium wall or otherwise the temperature drop through the wall will be excessive. Figure A-4.7 shows a structure in which the vacuum wall would be formed by elements of cylinders stressed in simple hoop tension. The grid to which they are attached would provide the structure to resist general buckling. This configuration would permit the use of a thin vacuum wall.

Electromagnetic Resistance to Flow

The pumping power associated with forcing a liquid metal stream through a strong electromagnetic field would be prohibitively high unless the flow path were made parallel to the lines of magnetic flux. It appears that this can be arranged, but it has the disadvantage that it fixes the planes in which the ribs between the inner and outer shells must lie. It is for this reason that the triangular construction of Fig. A-4.1a is favored for lithium rather than circumferential ribs with a box-type structure such as that of Fig. A-4.1b which would be superior from the structural standpoint. In the latter, shear loads induced by bending of the double-walled shell under external buckling loads would be carried through the web in shear, and the structure can probably be made stiffer than if the loads must be carried in tension and compression of diagonal struts as in the structure of Fig. A-4.1a. Time has not permitted a detailed evaluation of these effects.

The power required to pump a liquid metal through a magnetic field is given by

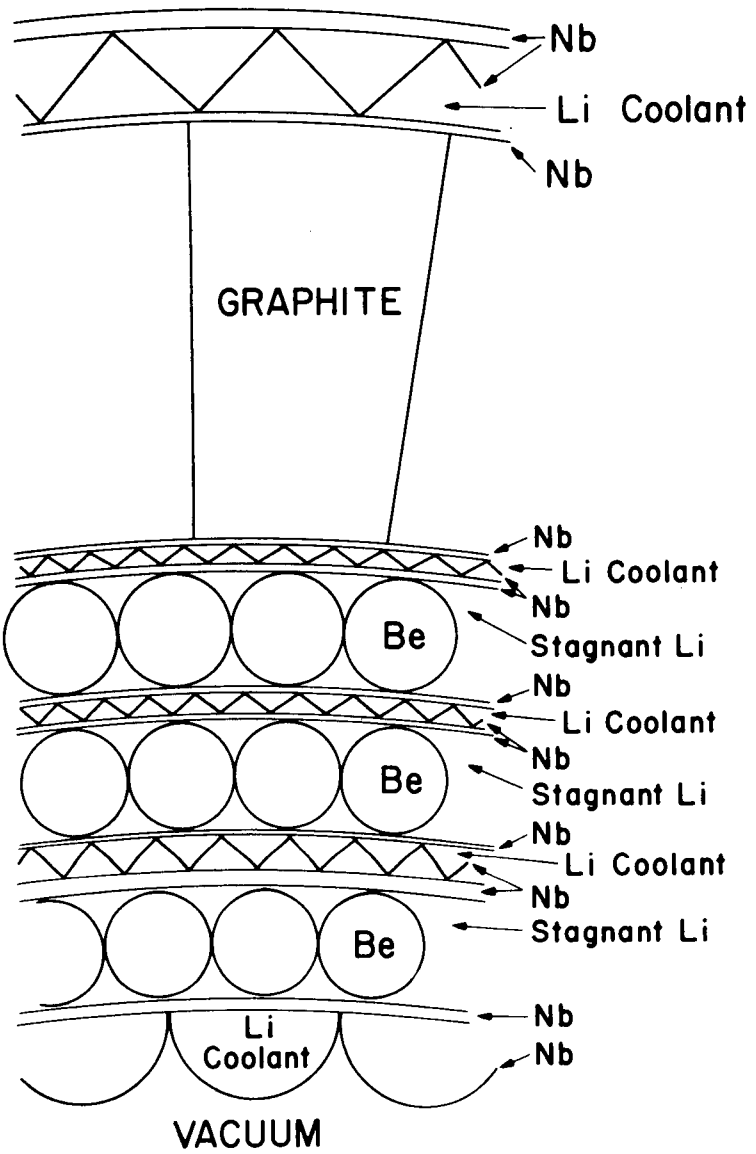

Fig. A-4.7. Transverse Section Through Cellular Reflector Region.

$$P = \frac{K^2 A_2 Q^2 \phi^2}{\rho \ell A_1^2}$$

where

ρ = electrical resistance of fluid stream, ohm·cm (38.5 $\mu\Omega$ cm for Li),

ℓ = path length across magnetic field, cm,

A_1 = flow passage area, cm^2,

A_2 = area normal to flow of electrical current, cm^2,

K = constant, 10^{-8},

Φ = magnetic field strength, Gauss,

Q = fluid flow rate, cm^3/sec,

P = power, watts.

The lithium flow rate required to remove all of the power output of a 10,000 Mw thermal reactor with a 200°F temperature rise is given by

$$\text{Li flow rate} = \frac{10^7 \times 28{,}316}{200 \times 30} = 4.72 \times 10^7 \text{ cm}^3/\text{sec} \quad .$$

For a thermonuclear reactor operating with a magnetic field of 50,000 Gauss, the lithium coolant flowing axially through an annulus 10 cm thick and 10 m in diameter, and a flow path length across the lines of flux of only 10 cm to provide for a simple 180 deg flow reversal at each end, and a mean flow path length for the electrical current of 10 cm, the electromagnetic pumping power for both ends becomes

$$P = \frac{2 \times 10^{-16} \times 10^4 \pi \, (4.72 \times 10^7 \times 5 \times 10^4)^2}{38.5 \times 10^{-6} \times 10(10^4 \pi)^2} = 92 \text{ Mw} \quad .$$

This ideal pumping power is equal to only about 1.2% of the thermal power output, or, with allowance for pump and cycle efficiencies, about 2.4% of the net electrical outputs, and hence does not represent a serious power

loss. On the other hand, it is evident from the above calculations that to keep the pumping power this low will require great care in the design of the lithium flow passages to minimize the distance through which the lithium would flow across the lines of force of the magnetic field. This in turn will require that an actual pump must be located in a portion of the magnetic field in which the flux intensity is much reduced, and the flow passages must parallel the lines of magnetic force except where the flow reversals occur at the ends of the loop. Thus the bulk of the electromagnetic resistance to flow will stem from cutting lines of force where they diverge, and this power will be equivalent to that for the simple idealized case assumed above. To meet this requirement it will probably be necessary to compromise other aspects of the design.

Cooling of the Reflector

About 75% of the power output of the reactor will appear as heat in the hot zone of the reflector as a consequence of slowing down fast neutrons. For good neutron economy the inner portion of the reflector ought to be largely beryllium or BeO to take advantage of the (n, 2n) reaction. In view of the inherently high cost of beryllium it is advantageous to keep the thickness of this region to a minimum consistant with neutron economy considerations, that is, 10 to 20 cm. Graphite is a good choice of material for the balance of the reflector because it will thermalize the neutrons degraded in energy by the beryllium, and will cause very little absorption. Further, it is structurally strong and can be installed in such a way as to contribute substantially to the structural strength of the complete assembly.

There is reason to believe that radiation damage to niobium will

develop much less rapidly than damage to beryllium or graphite. Assuming that this will prove to be the case, the beryllium or BeO can be installed in the form of spheres or cylindrical slugs to provide a pebble bed that can be drained from the reactor when radiation damage becomes a problem. The thickness of the beryllium layer can be proportioned so that the radiation damage to the graphite will not be serious throughout the life of the plant.

Corrosion and mass transfer present problems in high temperature reactor systems. For this reason it would be desirable to cool the reflector region with helium. However, analyses indicate that to remove the heat from a beryllium or BeO pebble bed with a reasonable pumping power would require that the helium be at a pressure of at least 300 psi. This would introduce an unacceptably severe external pressure on the vacuum wall tending to cause it to buckle inward, hence gas cooling of the reflector does not appear attractive because the resulting compromises would lead to important reductions in permissible power density in the reactor. The irregular flow of a molten metal through a pebble-bed would lead to very high pumping power losses because of electromagnetic effects. This could be avoided by using a molten salt such as the beryllium-lithium fluoride employed in the molten salt fission reactor. The salt will give adequate heat transfer performance with modest pumping power requirements, but the fluorine makes it less desirable from the physics standpoint.

One way to introduce beryllium into the inner region of the reflector and cool it with lithium without either serious electromagnetic pumping losses or the poisoning effects of fluorine would be to make use of alternate passages for the lithium coolant and the beryllium pebble bed. One

means of accomplishing this is shown in Fig. A-4.7. The niobium structure would resemble stacks of corrugated cardboard with the corrugations orthogonal in adjacent layers. The lithium coolant flow passages would run parallel to the lines of force in the magnetic field. The passages carrying the beryllium balls would run approximately circumferentially around the reactor, and would constitute much the greater fraction of the total volume of the region. To minimize the amount of structure, the circumferential webs in all but the innermost of the ball regions might be spaced at intervals of perhaps 50 cm. This would also permit close packing of the balls to yield a higher volume fraction of beryllium. If metallic beryllium balls were employed, it would be necessary to fill the interstices between the balls with lithium to provide a sufficiently good thermal conduction heat flow path from the beryllium to the lithium coolant passages so that the beryllium would not melt. If beryllium oxide balls were used, it might be thought possible to depend on a combination of thermal radiation and conduction through a static or gently flowing helium stream to remove the heat from the balls to the lithium coolant, but rough estimates indicate that this would give a ball surface temperature of about 2000°C.

The graphite region of Fig. A-4.7 might be cooled by a coolant stream of either helium or a molten salt. Lithium could not be permitted to contact the graphite, and individual thin-walled niobium cans would not only have adverse effects on both the neutron economy and the capital investment, but would also be subject to cracking as a consequence of thermal stresses. However, by laying the graphite blocks so that there is no more than one radial gap between graphite blocks along a radius in the region between the inner and outer cooled walls of Fig. A-4.7 it will probably be

possible to design for operation with no cooling passages in the graphite.

Pebble Design

Because of corrosion considerations it will be necessary to enclose either beryllium or beryllium oxide pebbles within a niobium can. There will be no problem of chemical interaction between beryllium oxide and a niobium can, but beryllium will tend to form intermetallic compounds with the niobium, and hence it would be necessary to employ a diffusion barrier. It seems likely that this could be done by anodizing the metallic beryllium to provide a thin, adherent oxide film.

There are test data available from in-pile tests to indicate the effects of thermal stress on beryllium oxide under a range of temperatures from 100°C to 1200°C. At the power densities contemplated, severe thermal stresses would tend to crack up the beryllium oxide and the large internal ΔT might even lead to melting of the beryllium oxide at the center of the ball. The situation appears analogous to that in UO_2 fuel elements which seem to function quite well in spite of center melting and severe fracturing of the sintered UO_2 matrix in the cooler region close to the capsule wall.

The pebble bed might be made up of cylindrical slugs rather than spheres. This would have the advantage that a higher volume fraction of beryllium or beryllium oxide might be obtained, and the cylinders would probably be cheaper to fabricate. Beryllium could be extruded in the form of cylindrical bars and cut to length. The best way to fabricate beryllium oxide is by cold pressing and sintering in the form of cylindrical slugs. It would probably be possible to deep-draw niobium cups which could be used with an enclosure that might be electron beam welded as indicated in Fig. A-4.8.

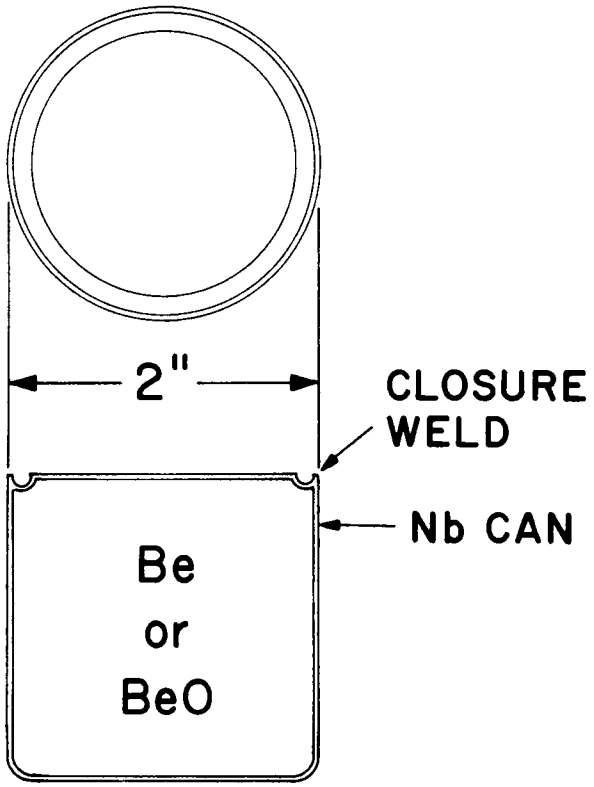

Fig. A-4.8. Cylindrical Slug of Be or BeO Canned in a Deep-Drawn Cup of Nb.

The larger the diameter of the balls employed the lower the fabrication cost. On the other hand, increasing the diameter will increase internal temperature drops and thermal stresses. Preliminary estimates indicate that a good compromise would be spheres or cylinders 4 or 5 cm in diameter.

Radiation Damage Considerations

The fast neutrons from the plasma will strike the vacuum wall at a rate such that the total integrated flux will run about 2×10^{23} in the course of 20 yr for a reactor output of 10 Mw/m^2 of wall. This intense fast neutron flux through the vacuum wall and the inner portion of the reflector makes radiation damage a limiting factor in the design. The temperature of the material is an important factor influencing the character and rate of radiation damage to be expected. Although no data are available for fast neutron dosages to niobium higher than 10^{20} nvt, studies by solid-state physicists indicate that niobium is likely to be more resistent to radiation damage than the iron-chrome-nickel alloys. A number of specimens of niobium are currently being irradiated in the EBR-II at 425°C. Test work on these should be completed in 1 or 2 yr with the target for exposure of a few times 10^{22} nvt. This, of course, will give doses at a mean neutron energy of around 1 Mev. There does not appear to be any way short of operation of a thermonuclear reactor to obtain doses of 10^{23} nvt with 14 Mev neutrons. No particle accelerator is available to give a sufficiently intense neutron source to yield the desired radiation dose in anything like a reasonable period of time.

A substantial amount of data are available on in-pile fast neutron irradiation of materials such as beryllium oxide, magnesium oxide, aluminum oxide, and graphite. These data indicate that exposure to fast

neutron irradiation at temperatures of around 800 to 1000°C leads to substantial amounts of radiation damage at neutron doses of a little more than 10^{21} nvt. Further, the data show that, because of annealing effects, the temperature range around 1100°C gives close to the minimum rate of damage for beryllium oxide.

The bulk of the data on metallic beryllium have been obtained at much lower temperatures. However, some of the work has entailed annealing the beryllium after irradiation, and these data indicate that swelling from helium production in the beryllium will be a problem at an integrated flux of around 10^{20} nvt. A volume increase of about 1% occurs when the beryllium is irradiated at 700°C to a fast neutron fluence of 2×10^{20}. The swelling was found to be much less than 0.5% in irradiations at 600°C to a fast neutron fluence of 8×10^{20}. The situation for beryllium or BeO is different from that for niobium in that the much higher neutron energies in the thermonuclear reactor should be expected to lead to much more severe damage than has been found in fission reactor irradiation at around 1 MeV because of the much higher incidence of (n, 2n), and (n, α) reactions. As a consequence, extrapolation of the available in-pile irradiation tests for design purposes will entail substantial uncertainties. In brief, it appears that, through the use of a moderately porous cold pressed and sintered BeO structure, it will be possible to obtain beryllium oxide bodies that will be much more resistent to fast neutron irradiation than would be the case for metallic beryllium in the temperature range desired, that is, around 1000°C, but that in any case radiation damage will require reprocessing of the BeO many times during the course of the life of the plant.

If radiation damage to both beryllium and beryllium oxide proves to be so severe that the cost of frequent reprocessing of the pebble bed

becomes excessive, it will be quite possible to sacrifice something from the neutron economy standpoint by eliminating the pebbles entirely and simply using a layer of beryllium-lithium fluoride molten salt.

References

1. K. N. Tong, Buckling and Creep Buckling of Spherical Shells Under Uniform External Pressure, Report No. ME992-764S, Syracuse University Research Institute, July 1964.

2. J. M. Corum, An Investigation of the Instantaneous and Creep Buckling of Initially Out-of-Round Tubes Subjected to External Pressure, USAEC Report ORNL-3299, Oak Ridge National Laboratory, Jan. 16, 1963.

3. M. Kangilaski, The Effects of Neutron Radiation on Structural Material, REIC Report No. 45, Batelle Memorial Institute (NASA), June 30, 1967.

INTERNAL DISTRIBUTION

1. I. Alexeff
2. W. B. Ard
3. C. F. Barnett
4. S. E. Beall
5. C. O. Beasley
6. M. C. Becker
7. C. W. Blue
8. R. L. Brown
9. J. F. Clarke
10. D. L. Coffey
11. R. J. Colchin
12. F. L. Culler
13. J. S. Culver
14. R. A. Dandl
15. R. C. Davis
16. S. M. DeCamp
17. R. A. Dory
18. J. L. Dunlap
19. H. O. Eason, Jr.
20. P. F. Edmonds
21. R. S. Edwards
22. A. C. England
23. J. C. Ezell
24. W. M. Farr
25-26. A. P. Fraas
27. J. E. Francis
28. W. F. Gauster
29. H. Grawe
30. G. E. Guest
31. W. Halchin
32. G. R. Haste
33. W. J. Herrman
34. J. L. Horton
35. R. P. Jernigan, Jr.
36. W. D. Jones
37. G. G. Kelley
38. M. O. Krause
39. D. M. Kroeger
40. N. H. Lazar
41. G. F. Leichsenring
42. M. S. Lubell
43. J. N. Luton, Jr.
44. J. F. Lyon
45. H. G. MacPherson
46. J. R. McNally, Jr.
47. O. D. Matlock
48. O. B. Morgan
49. R. V. Neidigh
50. C. E. Parker
51. A. M. Perry
52-68. H. Postma
69. J. A. Ray
70. R. G. Reinhardt
71. M. Roberts
72-99. D. J. Rose
100. I. A. Sellin
101. E. D. Shipley
102. D. J. Sigmar
103. J. E. Simpkins
104. A. H. Snell
105-106. D. Steiner
107. W. L. Stirling
108. R. F. Stratton
109. R. A. Strehlow
110. A. M. Weinberg
111. E. R. Wells
112. W. L. Wright
113. O. C. Yonts
114-115. TD Library
116-117. CR Library
118. Document Reference Sec.
119-121. Laboratory Records
122. ORNL-RC
123. ORNL Patent Office

EXTERNAL DISTRIBUTION

124. P. L. Auer, Advanced Research Projects Agency, The Pentagon, Washington, D. C.

125. M. Benedict, Massachusetts Institute of Technology, Cambridge, Massachusetts 02139

126-130. A. M. Bishop, Division of Research, U. S. Atomic Energy Commission, Washington, D. C.

131. L. M. Branscomb, Joint Institute Laboratory of Astrophysics, Boulder, Colorado

132. S. J. Buchsbaum, Bell Telephone Laboratories, Murray Hill, N. J. 67971

133. G. Bekefi, Massachusetts Institute of Technology, Cambridge, Mass. 02139

134. R. Carruthers, Culham Laboratory, Culham, Abingdon, Berks., England

135. Librarian, Culham Laboratory, Culham, Abingdon, Berks., England

136. N. Christofilos, University of California, Lawrence Radiation Laboratory, P. O. Box 808, Livermore, California 94551

137. S. O. Dean, Division of Research, U. S. Atomic Energy Commission, Washington, D. C.

138. T. H. Dupree, Massachusetts Institute of Technology, Cambridge, Mass. 02139

139. J. E. Drummond, Boeing Scientific Research Laboratories, P. O. Box 3981, Seattle, Washington 98124

140. B. J. Eastlund, Division of Research, U. S. Atomic Energy Commission, Washington, D. C.

141. O. C. Eldridge, Dept. of Physics, University of Tennessee, Knoxville, Tenn.

142. T. K. Fowler, University of California, Lawrence Radiation Laboratory, P. O. Box 808, Livermore, California 94551

143. W. A. Fowler, California Institute of Technology, 1201 E. Calif. Blvd., Pasadena, California 91109

144. M. B. Gottlieb, Princeton University, P. O. Box 451, Princeton, N. J. 08540

145. W. C. Gough, Division of Research, U. S. Atomic Energy Commission, Washington, D. C.

146. R. W. Gould, California Institute of Technology, Pasadena, Calif. 91109

147. R. Hancox, Culham Laboratory, Cluham, Abingdon, Berks., England

148. E. G. Harris, Dept. of Physics, University of Tennessee, Knoxville, Tenn.

149. H. W. Lewis, Physics Dept., University of California, Santa Barbara, California 93106

150. L. M. Lidsky, Massachusetts Institute of Technology, Cambridge, Mass. 02139

151. R. G. Mills, Princeton University, P. O. Box 451, Princeton, N. J. 08540

152. C. E. Nielsen, Dept. of Physics, Ohio State University, Columbus, Ohio

153. R. S. Pease, Culham Laboratory, Abingdon, Berks., England

154. J. A. Phillips, Los Alamos Scientific Laboratory, P. O. Box 1663, Los Alamos, N. M. 87544

155. R. F. Post, University of California, Lawrence Radiation Laboratory, P. O. Box 808, Livermore, Calif. 94551

156. F. L. Ribe, Los Alamos Scientific Laboratory, P. O. Box 1663, Los Alamos, N. M. 87544

157. M. Rosenbluth, Institute for Advanced Studies, Princeton University, Princeton, N. J.

158. R. Scott, Dept. of Physics, University of Tennessee, Knoxville, Tenn.

159. T. H. Stix, Princeton University, P. O. Box 451, Princeton, N. J. 08540

160. R. F. Taschek, Los Alamos Scientific Laboratory, P. O. Box 1663 Los Alamos, N. M. 87544

161. T. J. Thompson, Massachusetts Institute of Technology, Cambridge, Mass. 02139

162. J. L. Tuck, Los Alamos Scientific Laboratory, P. O. Box 1663, Los Alamos, N. M. 87544

163. C. M. Van Atta, University of California, Lawrence Radiation Laboratory, P. O. Box 808, Livermore, Calif. 94551

164. S. Yoshikawa, Princeton University, P. O. Box 451, Princeton, N. J. 08540

165. T. O. Ziebold, Massachusetts Institute of Technology, Cambridge, Mass. 02139

166. Research and Development, AEC, ORO

167-181. DTIE, AEC